CHALMERS

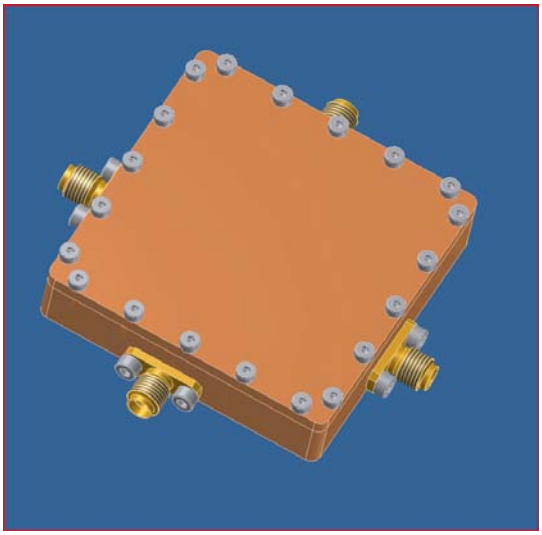

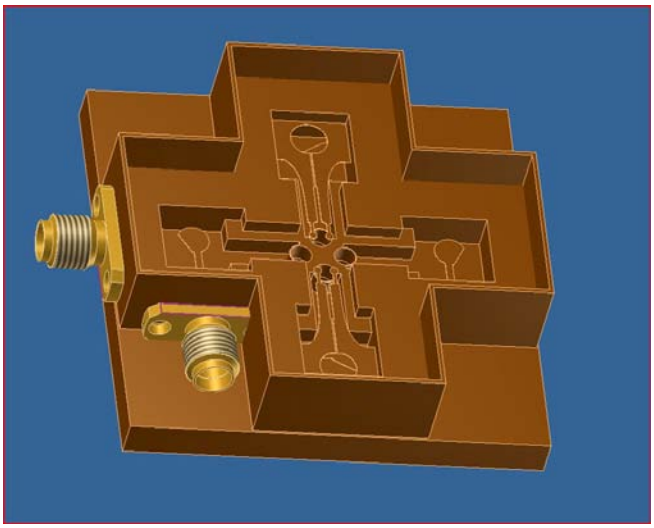

Design of Ultra WideBand Power Dividers and 180^0 Hybrids for Use With the Eleven Antenna for VLBI2010 and SKA Applications

Master of Science Thesis in the program Radio & Space Science

Abolghasem Zamanifekri

Antenna Group, Department of Signal & Systems

CHALMERS UNIVERSITY OF TECHNOLOGY

Göteborg, Sweden, April 2010

REPORT NO.2010/xxxx

Design of Ultra Wideband Power Dividers and 180^0 Hybrids for Use With the Eleven Antenna for VLBI2010 and SKA Applications

Abolghasem Zamanifekri

Antenna Group, Department of Signals & Systems
CHALMERS UNIVERSITY OF TECHNOLOGY
Göteborg, Sweden 2010

Abolghasem Zamanifekri

Design of Ultra Wideband power dividers and 180^0 hybrids for use with the Eleven antenna for VLBI2010 and SKA applications

© 2010 by Abolghasem Zamanifekri

Examiner: Prof. Per-Simon Kildal

Antenna Group, Department of Signals & Systems
Chalmers University of Technology
SE-412 96 Göteborg
Sweden
Telephone + 46 (0) 31-772 1000

Abstract

This report deals with numerical design of the new descrambler board for the Eleven feed antenna for application in future wideband radio telescopes, especially in the Square kilometer array project (SKA) or very long baseline interferometry (VLBI2010) . it mainly focus on designing a new passive solution for Eleven feed as well as reducing number of ports from eight to four ports. In brief, current descrambler board is discussed and also three passive solutions for this purpose have been discussed. A new wideband passive Balun and an ultra wideband power divider have been introduced in this report. The advantages and disadvantages of the new board are then discussed.

Keywords: Ultra wideband Balun, ultra wide band power divider, eleven feed, descrambler board, center puck

Acknowledgments

First I would like to thank Professor Per-Simon Kildal for giving me the chance to work on this project and for all the help and support he has given me along the way. I would also like to thank my supervisor Jian Yang for his invaluable and expert scientific guidance during my thesis. I would like to extend my appreciation for his patience guidance in various problems in my thesis. I would also like to express my gratitude to Miroslav pantelov and Lief Helldnar who have supported me with excellent comments during the thesis. Finally I would like to thank all the members of the antenna group for always being supportive and helpful.

Preface

This report is the master thesis for the Radio and space science program at the Chalmers University of Technology in Gothenburg, Sweden. It was conducted at the Antenna group in the Department of Signal and System under the supervision of Dr Jian Yang. The work was done from mid June through February in the winter of 2010.

The examiner for this master thesis project is the professor Per-Simon Kildal. The project is the collaboration between Antenna group, microwave electronic laboratory and Onsala Space observatory in Chalmers. The final results for this work will be presented at the IEEE APS symposium in Toronto, in July 2010.

The work is, in part, a continuation of the work done in antenna group to develop 2-14 GHz Eleven feed for reflector antennas in future wideband Radio Telescopes. This work suggests a new passive solution for the Eleven feed antenna. Simulations in this work have been done by Commercial EM solver CST MS.

Contents

Chapter I

INTRODUCTION

1.1 Why build the square kilometer array?

In the history of astronomy research, optical astronomy was the dominant field of study for many years. The main reason can be explained by this fact that there are only two frequency bands which are visible from the surface of the earth. First one is from 3000 A to 10 000 A (the optical / near-infrared window) and the second one is from few mm to tens of meters (the radio window). So, in order to research in other wavelengths it is essential to put the telescopes outside the earth's atmosphere and therefore most of these new astronomies have become possible after the advent of space technology. Nowadays there is growing interest for research in this visible frequency band. In fact using these radio telescopes, fantastic discoveries has been made like pulsars, radio galaxies and the cosmic background.

Chronological study of radio astronomy shows that radio astronomy was started in 1923 by Karl Jansky, when he discovered that his antenna was receiving radiation from outside the earth's atmosphere. Further observations from Karl Jansky considered this radio sources as the center of the galaxy. Next milestone in history of radio astronomy marked during the Second World War when many scientists were working on projects related to radar technology. One of the main discoveries in this field was made by scientists who were trying to identify the source of jamming radar signals when they figured out that the sun is the strong time variable emitter of radio waves. Next important phase started in 1946 with the introduction of technique called astronomical interferometry. The idea can be explained using the concept of resolution. The angular resolution of a telescope is given by

$$\theta \sim \lambda / D$$

Where, D defines the aperture size. So, the need for higher angular resolution deals with two problems

- Development of instruments with larger size
- Development of instruments which operate at smaller wavelength

To achieve high angular resolutions at meter wavelengths, one needs telescope with aperture size equal to hundreds of kilometers which is obviously impossible in practice for single dish radio telescopes. Instead radio astronomers solved the problem using a technique called aperture synthesis. Complete study of aperture synthesis technique can be found in but, the basic idea is based on this fact that the correlation of the voltages from any radio antennas which are widely separate from each other allows the measurement of single Fourier component of the source brightness distribution.

Using sufficient number of measurements and inverse Fourier transform give the source brightness distribution. The well known concept of 'map' in radio astronomy is the derived image of the sky after sufficient number of measurement in this step. In order to improve the quality of derived image lots of works have been done since the first practical realization of this technique and many different fields of

science benefit from this, for example cosmology, astrophysics and fundamental physics. We are, however, unfortunately on the brink of the capabilities of the existing radio telescopes and because of this, the main question which is received lots of attention from the scientists in this field is what the next logical step for radio astronomy is.

The general opinion is that a new radio telescope with as much as two order of magnitude more sensitivity than existing telescopes would lead to great scientific advances. The Square Kilometer Array (SKA) is the next generation of radio telescope aiming to attain one square kilometer of collecting aperture. The main characteristics can be summarized as below:

- 0ne square kilometer of collecting area which makes it 50-100 times more sensitive than today's best radio telescope
- Cover the frequencies 0.15 to 30GHz (2 m to 1 cm wavelength)
- Support 100 pencil beam instantaneously

Since the first meeting in 1997, at the SKA technical workshop in Sydney several suggestions have been made. The suggestion that we will focus has been prepared by the US-SKA (United States Square Kilometer Array) consortium. The US-SKA proposal shows great promise and is planned to meet all the goals set in the Sydney. The basic idea is to use many stations (100-1000) and each station is consists of small diameter antennas. Although this large number small diameter structure (LNSD) offers some advantages over other suggestions like multi beaming capabilities, instantaneous and flexibility but the main reason behind this especial diameter is economical.

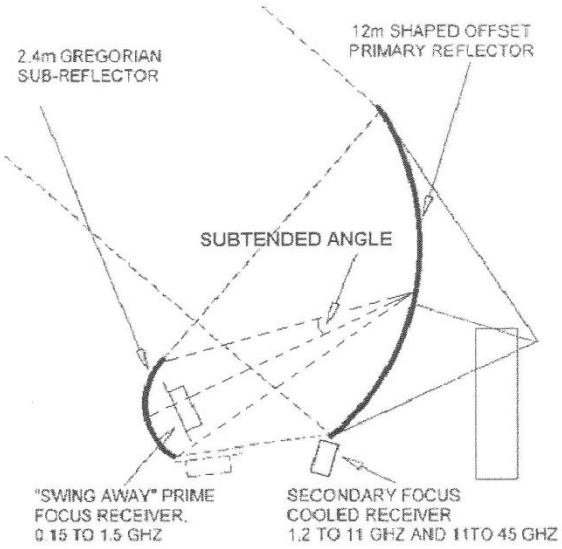

Figure 1.1: one antenna as proposed by the USSKA Consortium [1]

1.2 Square Kilometer array (engineering perspective)

In order to cope with large frequency band that has been mentioned above, each antenna makes use of three Gregorian feeds. It means that, three decade bandwidth feeds are sufficient to cover the whole frequency range. It should be mentioned that the main goal of this thesis is to design a feeding network for one of these feeds. The parameters of interests for US-SKA proposal are shown in Table 1.1.

Parameters	Value
Frequency range	0.15 to 34 GHz
NO. of elements	4400
Primary reflector radius	12 m
Secondary reflector radius	2.4 m
Subtended angle	42

Table 1.1:- The Square Kilometer Array Specification

The positioning of the elements is critical in terms of a performance and also economical point of view. The suitable solution which meets the requirements has been suggested by US-SKA. The idea is to have one compact array with 50% (2320 elements) of the elements within 35 km from the center. One intermediate array with 25 % (1160 elements) of the antenna distributed between 35 and 350 km with antennas grouped into the stations and finally an extended array with the remaining 1160 elements distributed between 350 and 3500 km, also with the elements grouped into stations. One possible configuration has been shown in figure 1.2. The reason for spiral shape related to the better UV coverage (see chapter 2 in [1]) which can be achieved by this special configuration of the elements.

The reason for placing most of the elements close to the center of the array is that it gives good surface brightness sensitivity. Having elements far from the center is useful gives better angular resolution. Although it is difficult to find a performance related reason for having groups of elements after 35 Km, but on the other hand it has many practical advantages. It makes finding and purchasing appropriate land much easier and reduces cost of constructions; also it will be useful in terms of operation and maintenance cost. The main characteristics of feeds according to the US-SKA proposal can be summarized as below:

- Compact and low loss
- Cool able to reduce the effects of thermal noise
- Ability of integrating with some sort of container (Dewer)
- Cheap and simple for manufacturing

In section 1.4 we will study in detail about all potential candidates feeds for SKA projects according to the US-SKA proposal [2].

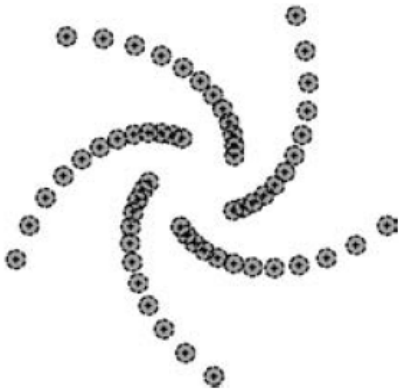

Figure1.2: one possible configuration [2]

1.3 VLBI 2010 (Very Long Baseline Interferometry)

Very long baseline interferometry (VLBI) is the geometric technique which is based on the time difference between arrival of two earth based antennas of a radio signal emitted by distant quasar. Using the large numbers of these time difference measurements makes it possible to determine the inertial reference frame which is defined by the quasars and also the precise location of the antennas. And then after post processing (e.g calculating Relative changes in the antenna locations) of a series of these measurements, geodetic properties like tectonic plate motion, regional deformation, and local uplift or subsidence can be achieved. VLBI has played and continuous to play an important role in providing the high precession geodetic data, having improved measurement accuracy and precision from meters in 1970's to millimeter at the turn of century. However, the existing worldwide VLBI system has now reached the limits of its capabilities and requires major renewal in order to provide 1 mm accuracy demanded in next few years.

In 2001, a review of existing programs and observing programs was carried out by the IVS working group which clearly defined the goals for next generation VLBI system [3]. The parameters of interests for VLBI 2010 are shown in table 1.2.

parameters	**Value**
Frequency range	1-14 GHz
Primary reflector radius	10-12 m
polarization	Dual polarization; Low cross polarization leakage

Table 1.2: VLBI 2010 Specification

The most critical component in realizing this broad frequency range is the feed system. Currently there are a few candidates for feed that will be explained in more details in section 1.4.

1.4 Different candidates for SKA and VLBI (2010) (Feed characteristics and comparison)

There are only a handful of ultra wideband feed systems that meet low noise characteristics which are required for astronomical use. In this section we will compare characteristics of these Feeds.

1.4.1 The ATA FEED

In the ATA project a non-planar, log-periodic feed is used. That is, four arrays are placed symmetrically around a ground Pyramid at 90 degree intervals. Prototypes of such feeds are shown in figure 1.4. An important advantage for this feed is the very good matching efficiency (better than -14 dB) in whole frequency range and also -10 dB beam (about 43 degree) width which meets the subtended angle requirement in US-SKA proposal. On the other hand, large aspect ratio which is determined by the low frequency end, consider as main drawback for this wideband feed. An important factor for wideband feeds which are used in radio astronomy is the constant phase center in whole frequency range. The location of phase center for ATA feed varies with the frequency . In fact it is not possible to achieve highest sensitivity in whole bandwidth without using mechanical device to move the antenna back and forth (it is not possible in practice!).

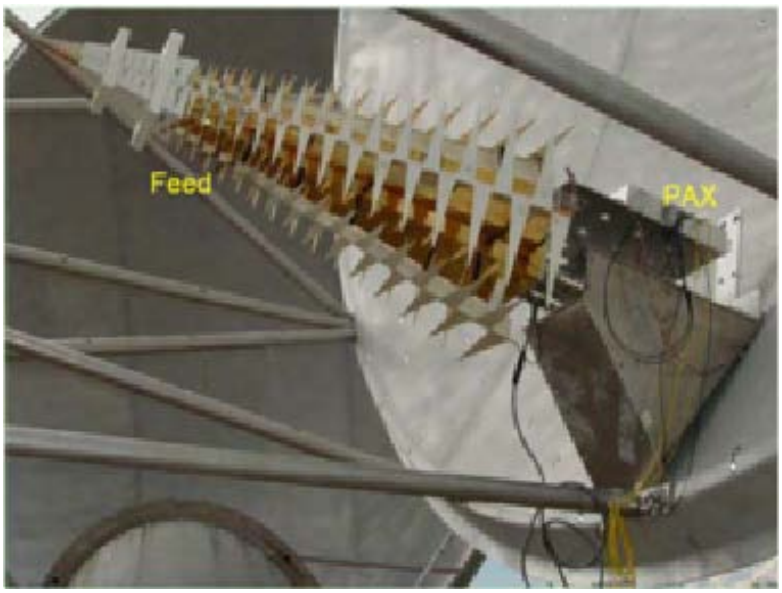

Figure 1.3: ATA Feed [4]

1.4.2 The Quad-ridge Lindgren Horn

Another ultra wideband feed which fits in general characteristics of US-SKA proposal is Quad-ridge Lindgern horn. Although this feed is very promising in terms of bandwidth (relative bandwidth is about 1:7) with reasonable size (length of feed is around 1.2 λmax), but the performance suffers from

poor matching efficiency (varying between -6 dB and -8 dB). Furthermore, both of the phase center and beam width are functions of frequency .An integration of a 2.2 to 15 GHz Quad-ridge Lindgren feed has been done in Caltech [5]. Photo of the feed and cryogenic Dewar has been shown in figure 1.5.

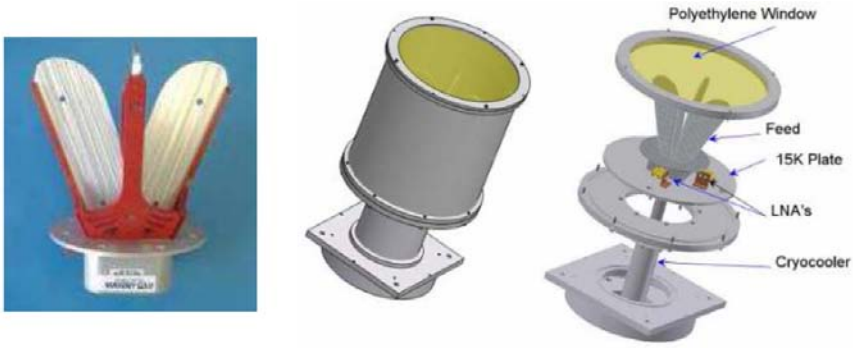

Figure 1.5: Quad-ridge Lindgren Horn [6]

1.4.3 The Eleven Feed

We will have complete study of eleven feed antenna in chapter II

Chapter II

Eleven antenna: basic theory and the pervious works which have been done by others

This chapter will review the basic theory and electrical design of Eleven feed Antenna and also current descrambler board. It should be mentioned that all the works that have been presented here have been done by the Antenna group in Chalmers University of technology previously. Electrical design section is based on the previous work which was done by Rikard Olsson [7], [8], and also information about current descrambler board comes from various publications of antenna group, mainly [9].

2.1 Introduction and electrical Design

One of the major problems with the feeds that have been introduced in pervious chapter is that phase center location varies rapidly with frequency. To solve this problem, we will have to, use mechanical device to move antenna back and forth as the frequency changes or easily accept the loss of efficiency. The mechanical solution is expensive and above all unpractical. It would therefore be great if we could find an antenna that meets the performance demands and has a constant phase center.

The idea is to use the fact that the phase center of a dipole above a ground plane is locked to the ground plane. It is also a known fact that two adjacent dipoles generate a nice boresight field pattern [10]. So the idea is very interesting and useful if we find away to add more elements working at other frequencies without causing the elements to interfere with each other in a way that degrade the performance. But first we need a background from log periodic antenna and designing rules of log periodic dipole antenna.

2.1.1 Log periodic antenna

In 1950s new type of the antenna introduced were referred to as ‘frequency independent’ antenna. In this type of the antenna, characteristics such as impedance, pattern and polarization are independent functions of frequency based on this fact that the electrical length of antenna is same in all frequency band. For example if the physical size reduced by factor of two, the characteristics of antenna will be same if operating frequency increased by factor of two.

Analytical analyses of frequency independent antenna, first started by Rumsey [11]. The idea is based on this fact that if we assume the antenna is perfectly conducting, it is surrounded by infinite homogenous and isotropic medium and its surface or an edge on its surface is defined by

$$r = F(\theta, \varphi)$$

Where, r represents the distance along the surface or edge. In this case if the antenna is to be scaled to a frequency that is K times lower than the original frequency, the antenna’s physical surface must be made K times greater to maintain the same electrical dimensions. Finally he showed that if the complete shape of the antenna can be described in terms of angle the field pattern and impedance. unfortunately antennas with this property cannot be realized according to this fact that they should be infinite in size and usually pattern is not useful. So the people started looking for good approximation of these ideal antennas that can keep the properties of frequency independent antennas, produced a

useful pattern and was practically realizable. One of the first suggestions was made by R.H.DuHamel [12] and can be seen in fig 2.1.

Log periodic antennas are basically an array of similar elements spaced in regular fashion and adapted to work at different frequencies. A log periodic antenna is characterized by its so called scaling factor τ. τ is the factor that decides which frequency are to be used as design frequencies and is defined according to

$$f_2 = \tau f_1, f_3 = \tau f_2, \dots \dots \dots \quad (2.1)$$

Rearranging and taking the logarithm on both sides we get

$$ln\frac{f_2}{f_1} = 1\ln\tau\ , \ln\frac{f_3}{f_2} = 2\ln\tau\ , \ln\frac{f_4}{f_1} = 3\ln\tau \quad (2.2)$$

Therefore it is intuitive to call this kind of antenna log periodic.

Most commonly these log periodic antennas are used in end fire mode (see figure 2.1) . The electromagnetic wave propagates between the two rod lines until it excites a resonant dipole. Thus to achieve this end fire pattern two or more arrays are used.

For many of this kind of end-fire style log periodic antennas, especially log periodic dipole antennas design rules exist. These existing design rules will be used as starting point for designing of Eleven feed. The next step will be optimization to get useful pattern.

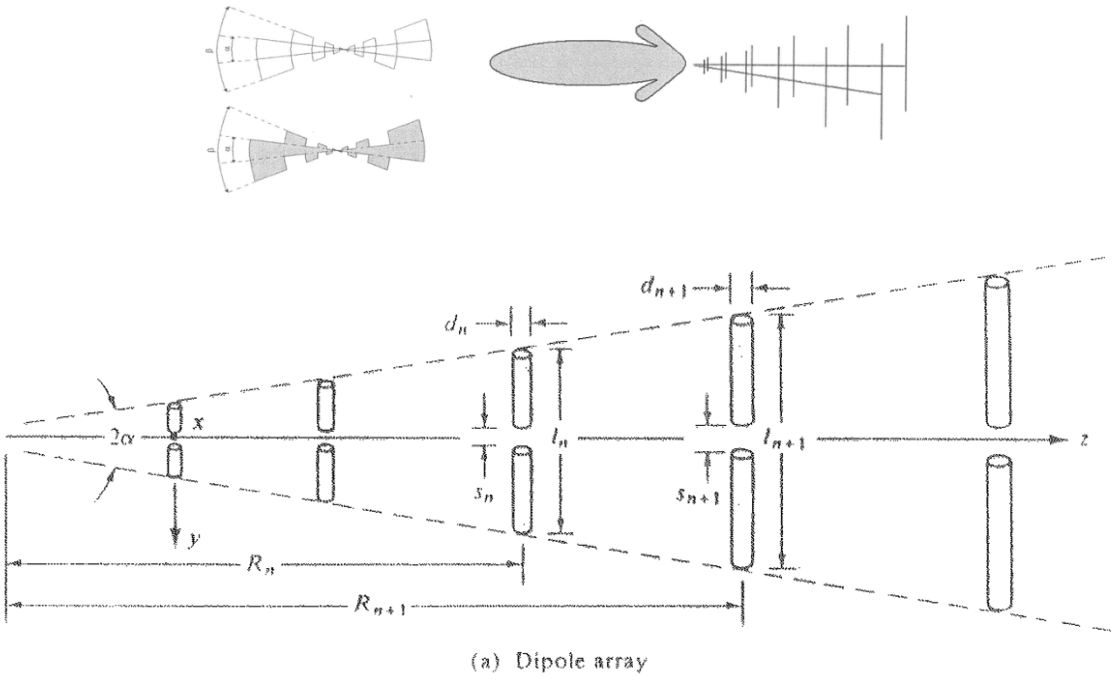

Figure 2.1: log periodic antenna as proposed by R.H DuHamel using plates and using wires (up)

Log-periodic dipole array(down) [14].

The most recognized log-periodic antenna structure is the configuration introduced by Isbell [13] . It consists of a sequence of side by side parallel linear dipoles forming a coplanar array. The three most important parameters for the dimensioning of the log periodic dipole antennas (LPDA) are the angle α, the scaling factor, see the figure 2.1.

$$\tau = \frac{x_{n+1}}{x_n} = \frac{l_{n+1}}{l_n} = \frac{d_{n+1}}{d_n} \quad (2.3)$$

And the relative element separation

$$\sigma = \frac{d_n}{2l_n} \quad (2.4)$$

The next step according to the design procedure introduced in is to determine what directive gain we want to achieve. The US-SKA proposal demands a directive gain of roughly 10 dB. We can easily get the optimal values of both the scaling factor and the relative element separation from the graph in appendix A that has been produced empirically. Then, we need to know relative bandwidth of antenna that should include real bandwidth of antenna and extra bandwidth to get rid of end effects.

How much extra bandwidth we need is called the active region bandwidth and is given by

$$B_s = B_{ar}.B \quad (2.5)$$

$$B_{ar} = 1.1 + 7.7(1-\tau^2)\cot\alpha \quad (2.6)$$

And length can be achieved by

$$L = 14\frac{K.c}{f_{min}}(1-\frac{1}{B_s})cot\alpha \quad (2.7)$$

Now we know everything but the number of elements. This is easily calculated from

$$N = 1 + \frac{\log B_s}{\log\frac{1}{\tau}} \quad (2.8)$$

2.1.2 Designing new feed

Based on the works have been done by R. Olsson [8], we can consider the data from the designing rules as the approximate values of the various geometrical parameters needed to achieve frequency independence. Since we do not actually have an array in end fire mode, these calculations will not be valid. Furthermore we should disregarded the value of the length of the array, based on this fact that according to discussion in [10] if distance between each dipole pair have to be 0.5 λ, it can be generate a nice radiation pattern. Another parameter that should be determined is the height from the

ground plane. We will place the dipoles so that the resonant radiating part of the array is 0.1 λ above the ground plane.

Another effective parameter is the height from ground plane. It should be remain at 0.1 λ. So, one useful idea is to tilt the ground plane to keep the height constant in terms of wavelength.

Due to higher impedance of folded dipole, it can be used instead of ordinary dipoles. Simulation result shows very nice aperture efficiency, also the mismatch efficiency shows much more promise than it did for the arrays of ordinary dipoles.

It should be mentioned that Different feeding networks for this kind of antenna have been suggested in [15] .

2.1.3 Complete system

The electrical design of new feed can be done based on the optimization of the above parameters. The goal of this electric design is to minimize the reflection coefficient at the input port and at the same time have a good radiation performance. The aim of avoiding strong reflection coefficient at the input port is to reduce the system noise temperature as much as possible.

There are a few analytic or quasi-analytic analyses available for the Eleven antenna and it is restricted to the basic geometry that includes only one pair of folded dipoles over an infinite ground plane [16] . Although these models can give the optimum ranges of the dimensions of each radiating dipoles pair and also derive analytic models for the impedance of single radiating folded dipole pair [17], but it is not possible to extend them to multiple cascaded folded dipoles. Therefore the optimum dipole petal geometry must be determined by the numerical analyses using a general electromagnetic solver. But the problem with these kinds of solvers is that, due to large size of log periodic dipole petals in terms of wavelength at the highest frequency it is very time consuming. Therefore a special computation approach for log-periodic geometries was developed , referred to as the partial array method.

Using the partial array method and genetic algorithm make it possible to optimize the dimensions of the dipole petals that give the lowest reflection coefficient of a linearly polarized Eleven antenna. The simulation result for reflection coefficient of the optimized linearly polarized eleven antenna in CST Microwave studio is below -9.4 dB over 2-14 GHz when referred to an input balanced port impedance of 200 ohm on both dipole petals. This 200 ohm balanced port impedance is the intrinsic input port impedance for the Eleven antenna .

The complete dual polarized 2-14 GHz Eleven antenna is obtained by adding two more dipole petals, located in the orthogonal azimuth plane compared to the first two petals.

2.1.4 System configuration

Having basic knowledge about designing and effective parameters, we can look at the configuration of the whole eleven antenna system which is represented in figure 2.2.

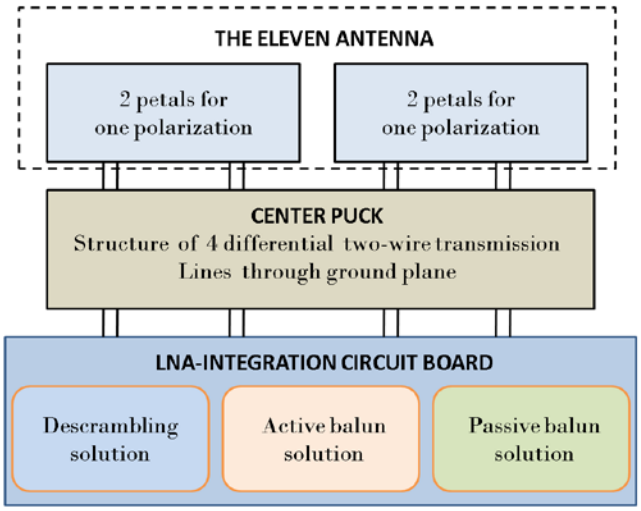

Figure2.2: system configuration of the Eleven feed [9]

The complete Eleven feed system consist of three parts: the four log-periodic dipole petals, the center puck combining the front and the rear sides of the ground plane and rear-side circuit boards for integration of LNAs and descrambling of the four ports of the log periodic dipoles. In this section we will study center puck and descrambler board separately.

2.2 Current descrambler board and center puck

The dual polarized Eleven feed has four log-periodic dipole petals, Each one with its own balanced 200 ohm port. In the first low frequency models of the Eleven feed opposite dipole medals were made of one metal piece and thereby connected on the front side of the ground plane see figure 2.3. However, this approach is not working well at high frequencies [18], which is why the center puck was introduced. The choice is to guide the four two wire lines vertically to the rear side, and there to make appropriate combinations of the ports. This gives a flexible solution that allows the descrambling and the LNA integration scheme to be changed without changing the dipole petals.

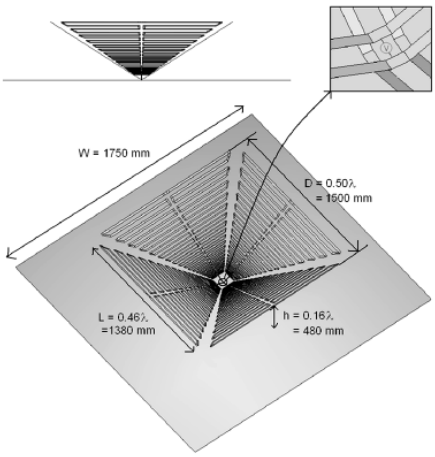

Figure 2.3: Illustration of 0.15 to 1.5 GHz dual polarized of the feed with key dimensions indicated [7]

The transition from the balanced two wire lines connecting to the log-periodic dipole arrays above the ground plane , to one single ended port per polarization below the ground plane consist of two main parts. The first is the transition of the four balanced parallel two wire lines from the front to the rear side of the ground plane, and the second is the power combining and the LNA circuitry. Each part will be explained in detail in this section

2.2.1 Center puck

Figure 2.4 shows the geometry of center puck. In this section we will calculate dimensions and impedance for each part of transition.

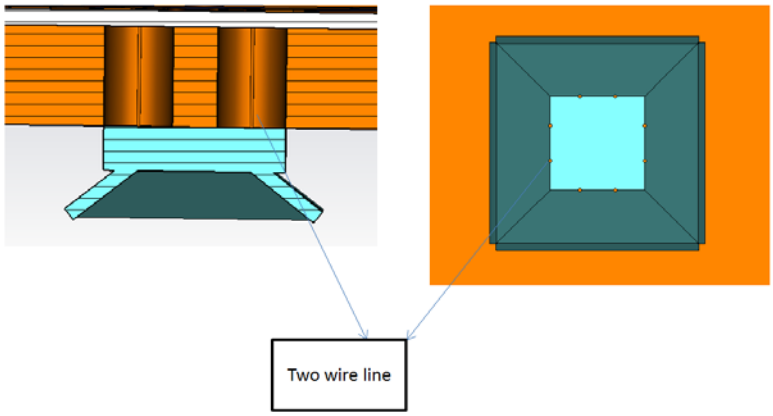

Figure 2.4: geometry of center puck

According to what we discussed in section 2.1.3 the intrinsic impedance of the Antenna is 200 ohm, therefore in first step we should transient 200 ohm differential impedance through TMM3 with constant dielectric of 3.27. The main aim of having TMM3 above the ground plane is to provide mechanical support for soldering in the connection point of LPA and twin wire lines. The distance between twin wire lines dictated by the excitation distance of dipole in highest frequency and it is not our choice. Diameter of twin wire lines is the only parameter that we can determine by considering 200 ohm impedance for parallel two wire lines in Dielectric.

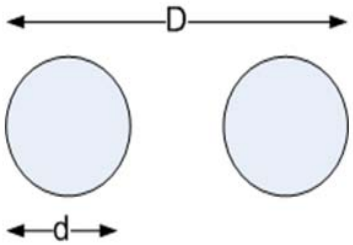

Figure 2.5: geometry of two wires in dielectric

$$Z = \frac{1}{\pi}\left(\frac{\mu_0}{\epsilon'}\right)^{1/2} cosh^{-1}\frac{D}{d} \qquad (2.9)$$

From the above calculation we get d=0.2 mm, therefore we have the diameter of twin wire lines for the next step. Now we should repeat the same calculation to get diameter of the holes in the ground plane. Considering 200 ohm for impedance, separation and diameter of wire lines will be same as before

(2.10)

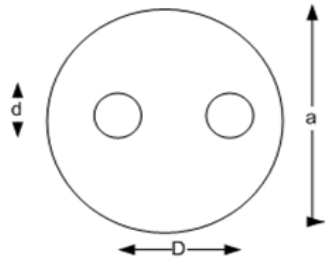

$$Z = \frac{1}{\pi}\left(\frac{\mu_0}{\varepsilon'}\right)^{\frac{1}{2}}\left[ln\left(2p\frac{1-q^2}{1+q^2}\right) - \frac{1+4p^2}{16p^4}(1-4q^2)\right]$$

Figure 2.6: geometry of shielded two wire lines

This calculation gives a=2.8 mm. it should be mention that, this is the value that gives the exact 200 differential impedance between two wire lines, but in the final step after optimization the value changes to a=3.4 mm which gives optimum performance from 2 to 13 GHz.

To verify impedance calculation we can use the waveguide port in CST microwave studio which is accurate tool for impedance calculation.

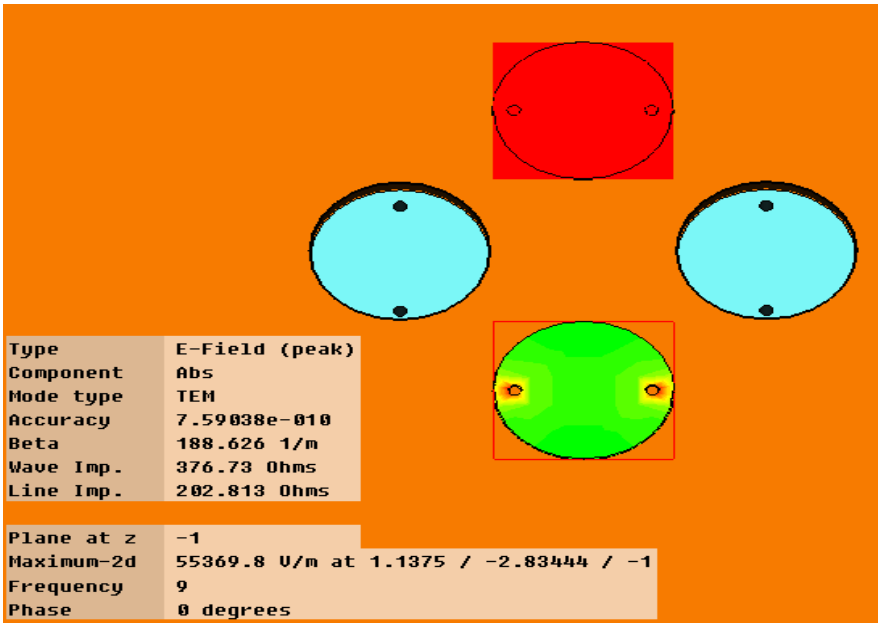

Figure 2.7: Line Impedance calculation by CST MS

After guiding the four two wire lines vertically to the rear side, the next step is to convert four pair of 200 ohm differential impedance to eight uncoupled microstrip lines which are connected to the coaxial ports. The required background from microstrip and impedance matching will be explained in chapter 2.2.1.3.

2.2.1.1 Microstrip

Now days there are growing interest for the planar structures which are suitable for using as circuit element in microwave integrated circuits (MICs) or monolithic integrated circuits (MMICs). Planar structure implies that the characteristics of structure can be described by dimensions in single plane.

For example the impedance of microstrip can be adjusted by dimensions in single plane. So, the circuit fabrication can be carried out by techniques of photolithography and photo etching. This section will explain more about theory of microstrip.

The presence of the dielectric and particularly this fact that the dielectric does not fill the air region above the strip complicates the behavior and analyses of microstrip line. In fact, the exact fields of microstrip line constitute a hybrid TM-TE wave . Using the static or quasi static solutions [19] phase velocity and propagation constant can be achieved

$$v_p = \frac{c}{\sqrt{\varepsilon_e}} \qquad (2.11)$$

$$\beta = k_0\sqrt{\varepsilon_e} \qquad (2.12)$$

Where ε_e is the effective dielectric constant of the microstrip line. The effective dielectric constant of a microstrip line is given approximately by [20]

$$\epsilon_e = \frac{\varepsilon_r + 1}{2} + \frac{\epsilon_r - 1}{2}\left(\frac{1}{\sqrt{1 + \frac{12d}{w}}}\right) \qquad (2.13)$$

The effective dielectric can be described as the dielectric constant of a homogenous medium which fills entire region. In fact this new medium replaces the air dielectric regions of the microstrip. There are some design formulas for microstrip lines that give w/d ratio for a given characteristic impedance z_0 and dielectric constant ε_r

(2.14)

$$\frac{w}{d} = \begin{cases} \dfrac{8e^A}{e^{2A} - 2}, & for\ w/2 < 2 \\ \dfrac{2}{\pi}\left[B - 1 - \ln(2B - 1) + \dfrac{\epsilon_r - 1}{2\epsilon_r}\left\{\ln(B - 1) + 0.39 - \dfrac{0.61}{\epsilon_r}\right\}\right], & for\ w/d \geq 2 \end{cases}$$

Where

$$A = \frac{Z_0}{60}\sqrt{\frac{\epsilon_r + 1}{2}} + \frac{\epsilon_r - 1}{\epsilon_r + 1}\left(0.23 + \frac{0.11}{\epsilon_r}\right) \qquad (2.15)$$

$$B = \frac{377\pi}{2Z_0\sqrt{\varepsilon_r}} \qquad (2.16)$$

More details about designing formula and loss in microstrip can be found in [21]

2.2.1.2 Impedance matching and tapering

The matching network is an ideally lossless network which is designed to solve the problem of multiple reflections in microwave discontinuities. Impedance matching network, place between load impedance and transmission line (see figure 2.8). Then reflections are eliminated on the transmission line to the left of the matching network, although there will be multiple reflections between the matching network and the load. The important reasons for using impedance matching can be categorized as below

- Maximum power is delivered when the load is matched to the line, therefore the power loss will be minimized.
- Impedance matching improves the signal to noise ratio of system. Especially in Eleven feed antenna it is important to keep the system noise temperature as low as possible.
- Impedance matching in a power distribution network will reduce amplitude and phase errors.

2.2.1.2 Different matching networks

As long as the load impedance Z_l has some nonzero real part, a matching network can always be found. Many choices are available depend on the factors like complexity, bandwidth and implementation.

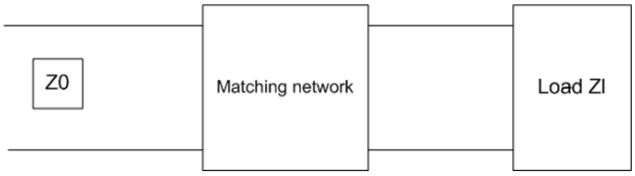

Figure 2.8: geometry of general matching network

Main methods use in matching network can be grouped as below

- matching with lumped elements
- single-stub tuning
- double stub tuning
- quarter wave transformer
- binomial multisession matching transformers
- Chebyshev multisession matching transformers
- Tapered lines

Due to the large bandwidth of tapered lines it can be used for wideband transition from four pair of twin lines to eight uncoupled Microstrip lines. Theory for this kind of tapers will be explained in section 2.2.1.4. More details for each type can be found in [20]

2.2.1.4 Tapered transmission lines

According to general theory of multi section quarter wave transformer different characteristic impedances have been used to match two transmission lines. In other words change in impedance level

obtains in a number of discrete steps. An alternative is to use smooth transition line between load impedance and transmission line which has characteristic impedance that varies continuously from impedance of the line to the load impedance.

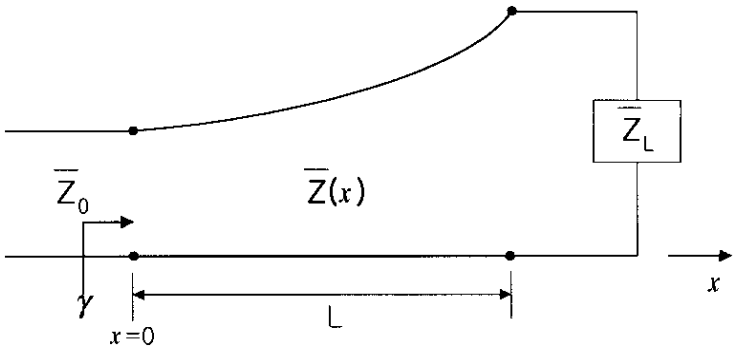

Figure 2.9: A tapered transmission line matching section

Considering the continuously tapered line as being made up of a number of incremental sections of length Δz , with an impedance change $\Delta Z(z)$ from one section to another section will result a following reflection coefficient

$$\Delta\Gamma = \frac{(Z + \Delta Z) - Z}{(Z + \Delta Z) + Z} \qquad (2.17)$$

In the limit as $\Delta Z \to 0$, we have an exact differential

$$d\Gamma = \frac{dz}{2z} = \frac{1}{2}\frac{d(lnZ/Z_0)}{dz}dz \qquad (2.18)$$

Since

$$\frac{d(lnf(z))}{dz} = \frac{1}{f}\frac{df(z)}{dz} \qquad (2.19)$$

Then by using the theory of small reflections , the total reflection coefficient at z=0 can be found by summing all the partial reflection with their appropriate phase shifts:

$$\Gamma(\theta) = \frac{1}{2}\int_{z=0}^{L} e^{-2j\beta z}\frac{d}{dz}\ln\left(\frac{Z}{Z_0}\right)dz \qquad (2.20)$$

Where, $\theta = 2\beta l$. So, if Z (z) is known, $\Gamma(\theta)$ can be found as function of frequency. Further discussion of this topic can be found in [16]. There are some special cases for Z(z) impedance tapers.

- Exponential taper
- Klopfenstein taper

- Triangular taper

Triangular taper will be studied in more details in next section

2.2.1.5 Triangular taper

By considering the impedance function as below

$$Z(z) = f(x) = \begin{cases} Z_0^{\,2(z/L)^2 \ln Z_L/Z_0}, & for\ 0 < z < L/2 \\ Z_0 e^{(\frac{4z}{L} - \frac{2z^2}{L^2} - 1)\ln\frac{Z_l}{Z_0}}, & for\ \frac{L}{2} < z < L \end{cases} \qquad (2.21)$$

Replacing this impedance function in related Γ function, will result in Equation

$$\Gamma(\theta) = \frac{1}{2} e^{-j\beta L} \ln\left(\frac{Z_l}{Z_0}\right) \left[\frac{\sin\left(\frac{\beta L}{2}\right)}{\frac{\beta L}{2}}\right]^2 \qquad (2.22)$$

The magnitude of this result is sketched in fig 2.10.

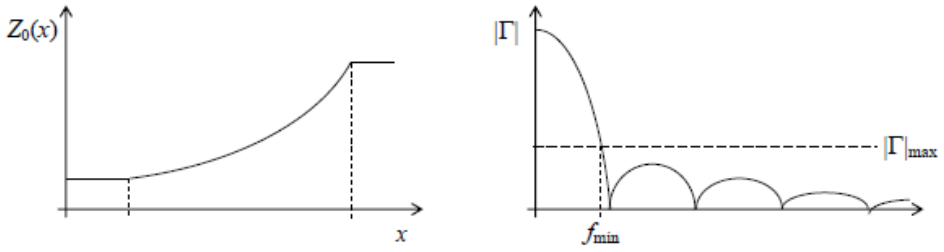

Figure 2.10: The result for Triangular taper

2.2.1.6 Coupled microstrip lines

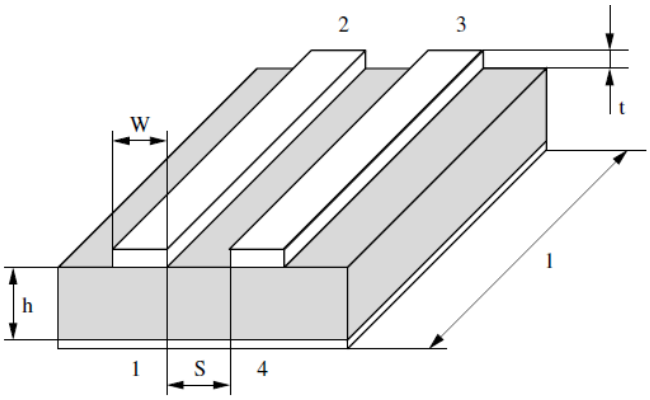

Figure 2.11: Geometry of coupled microstrip

The arrangement that has been shown in figure 2.11 illustrates the basic structure of coupled microstrip lines. Actually a coupled line configuration consists of two transmission lines placed parallel to each other and in close proximity. In such a case there is a continuous coupling between the electromagnetic of two lines. Coupled lines are utilized extensively as basic elements for directional couplers, filters, and a variety of other useful circuits.

General theory for analyzing, coupled mode formulation and even and odd mode methods are described in . Here we will study design equation of the Coupled microstrip line. It should be pointed out that these formulas can be considered as the starting point for the designer, next step will be using the iterative technique or using the commercial codes to improve the accuracy, in this part after explaining design equations for coupled microstrip, the result will be compared with CST microwave studio results.

2.2.1.7 Design equations

Design equations for the Coupled microstrip lines should relate even and odd mode impedance and effective dielectric constant to coupled line geometry; i.e., strip width w, spacing s between the strips, dielectric thickness h and dielectric constant ϵ_r. Static capacitance of the coupled line geometry forms the bases of these equations, see figure 2.12. Here we have basic theory for design equation based on the discussion in [20]

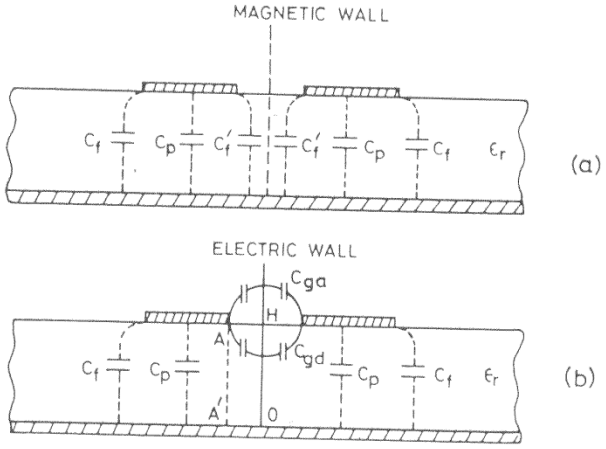

Figure 2.12: separation of capacitance for use in the analyses [21]

The total capacitance for each mode can then be written

$$C_e = C_p + C_f + c'_f \qquad (2.23)$$

$$C_0 = C_p + C_f + C_{ga} + C_{gd} \qquad (2.24)$$

The capacitance C_p simply relates to the parallel plate line value given by

$$C_p = \varepsilon_0 \epsilon_r \frac{w}{h} \qquad (2.25)$$

Also c_f is simply the fringing capacitance due to the due to the each microstrip taken alone, as if for a single strip. This is given by

$$2C_f = \frac{\sqrt{\epsilon_{eff}}}{cZ_0} - C_p \qquad (2.26)$$

Where c is the free space velocity and ε_{eff} and Z_0 are obtained by single strip static TEM methods

An empirical expression for C'_f is given as follows:

$$C'_f = \frac{C_f}{1 + A(h/s)\tanh(8s/h)} \sqrt{\frac{\varepsilon_r}{\epsilon_{eff}}} \qquad (2.27)$$

Where

$$A = \exp\left\{-0.1\, exp\left(2.33 - \frac{2.53w}{h}\right)\right\} \qquad (2.28)$$

As it can be seen in figure 2.12 C_{ga} and C_{gd} represent respectively, odd mode fringing field capacitances for the air and dielectric regions across the coupling gap. C_{ga} was obtained by using an equivalent coplanar strip geometry calculation, yielding

$$C_{ga} = \epsilon_0 \frac{K(k')}{K(k)} \qquad (2.29)$$

Where

$$K = \frac{s/h}{\frac{s}{h} + 2w/h} \qquad (2.30)$$

$$K' = \sqrt{1 - K^2} \qquad (2.31)$$

And the ratio of elliptic function is

For $0 < k^2 < 0.5$

$$\frac{K(k')}{K(k)} = \frac{1}{\pi} \ln\left(2\frac{1+\sqrt{k'}}{1-\sqrt{k'}}\right) \qquad (2.32)$$

For $0.5 < k^2 < 1$

$$\frac{K(k')}{K(k)} = \frac{\pi}{\ln\left\{2(1+\sqrt{k})/(1-\sqrt{k})\right\}} \qquad (2.33)$$

C_{gd} was determined differently

$$C_{gd} = \frac{\epsilon_0 \epsilon_r}{\pi} ln\left\{coth\left(\frac{\pi}{4}\frac{s}{h}\right)\right\} + 0.65\, C_f \left(\frac{0.02}{\frac{s}{h}}\sqrt{\epsilon_r} + 1 - \varepsilon_r{}^{-2}\right) \qquad (2.34)$$

Now the even mode and odd mode characteristic impedances are then:

$$Z_{Oe} = \left(c\sqrt{C_e C_{e1}}\right)^{-1} \qquad (2.35)$$

$$Z_{Oo} = \left(c\sqrt{C_o C_{o1}}\right)^{-1} \qquad (2.36)$$

Where c is the velocity in free space and the second subscript 1 refers to a free space (air line).

More information about effective microstrip permittivity can be found in . Also there are some other synthesis technique using universal graphs are given by Akhtarzad, Rowbotham and Jones and also a family of useful expressions.

2.3 Single-ended 8 port solution with center puck

Block diagram of current descrambler solution has been shown in figure 2.13

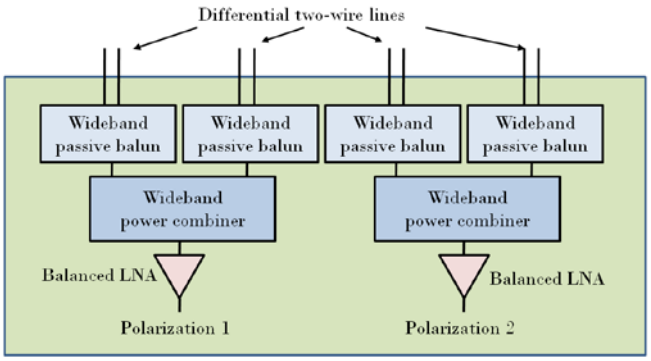

Figure 2.13: descrambling using four passive baluns [9]

Current Descrambling solution consists of eight port descrambling board and eight coaxial ports and separate coaxial 180 hybrids and also wideband power dividers.

The view of descrambler board and center puck has been shown in figure 2.14.

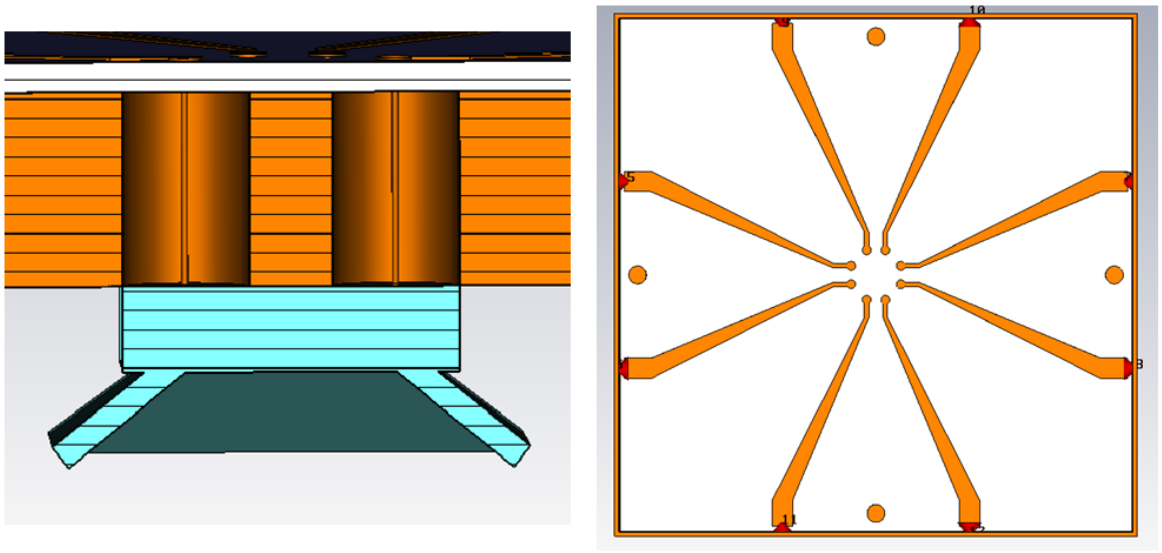

figure 2.14: center puck and current 8 port descrambler board

As we explained before, center puck consists of four vertical two-wire line each one made of two silver plated steel needles. Each needle is soldered at one end to each of the metal strips feeding the log-periodic dipole arrays above the ground plane, and at the other end to a corresponding microstrip line on the descrambling board. The latter forms four pairs of coupled microstrip line with 200 ohm odd mode impedance which is the same as the impedances of the two strip lines feeding the dipoles on the front side of ground plane. The next task is to find a way to match this 200 ohm odd mode impedance to normal 50 ohm impedance of coaxial ports. At the ground plane two wire lines get soldered to the 200 ohm coupled microstrip lines. The width of coupled microstrip can be found according to eq 2.10, then by using the waveguide port impedance can be calculated accurately, see figure 2.15, and optimize to get the best matching. In this case waveguide port gives 196 ohm differential impedance for the coupled microstrip lines that is in good agreement with 200 ohm which

is calculated by the eq 2.11 See figure 2.16. Next step will be using the tapering method, According to what has been explained in section 2.2.1.4. It means that first use the eq 2.21 to find the impedance function for tapering then by using eq 2.14 functions for width of microstrip line can be achieved. So the coupled lines are gradually separated by linear tapering so as to have two out of phase microstrip lines. The computed s parameters complete descrambler board has been shown in figure 2.16.

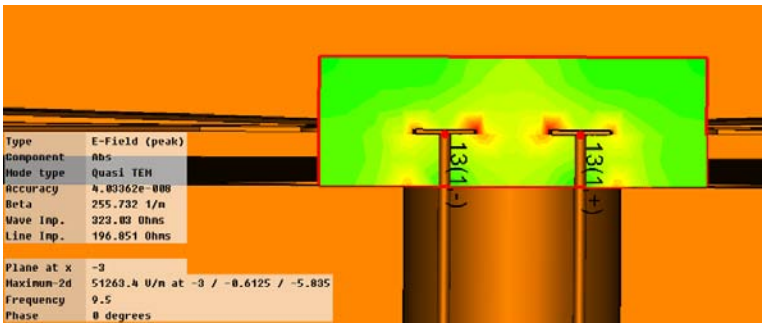

Figure 2.15: field distribution 200 ohm differential line

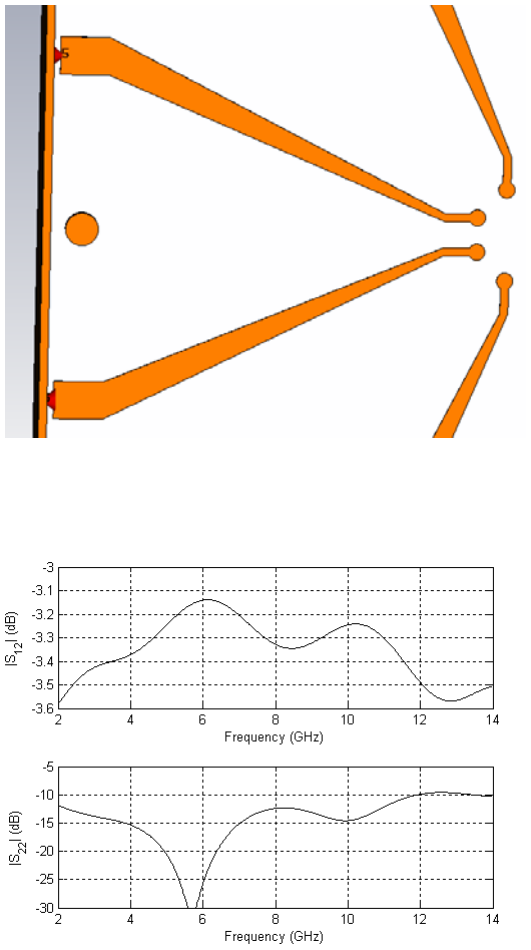

Figure 2.16: matching section in descrambler board and computed S parameters

The next step is to reduce the four out of phase microstrip line to two unbalanced microstrip or coaxial lines, one per polarization. These balanced microstrip lines need a special transition to be connected to unbalanced microstrip or coaxial lines. Such transitions are called baluns, and they are traditionally

integrated as mechanical part of a dipole antenna. In this case the 180 hybrids play the role of the baluns. Two possible diagrams of this kind of transition have been shown in figure 2.17.

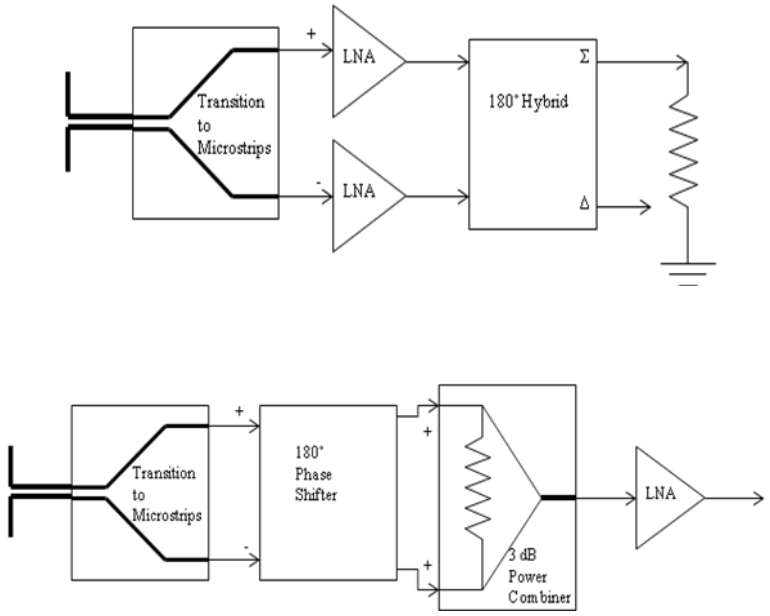

Figure 2.17: passive Balun as 180 phase shifter on one line followed by power combiner [9]

It should be mentioned that the wideband 180 hybrids are lossy and needs to be located behind the LNA not to increase the system noise temperature.

2.4 Advantage and disadvantage of current board

Current descrambling solution with an 8 port descrambling board and eight coaxial ports and separate coaxial 180 hybrids and power dividers is the simplest solution. This scheme is mainly intended for test purposes, and was used in all the Eleven feed that have been manufactured so far.

Studying of figure 2.16, will show that from 2 to 10 GHz degradation will appear mainly due to the mismatch factor, above 10 GHz further degradation will appear due to ohmic and radiation loss. The graph shows that the current version of center puck suffers from losses that increase strongly above 10 GHz. These losses and some recent works for reducing them have been explained in section 2.2.1.

2.5 Room temperature performance and cryogenic performance

Figure 2.18 shows the simulated and measured reflection coefficients of one of the Eleven feed models that has been manufactured for Vertex Antennentechnik GmbH. This model was measured at OSO (Onsala space observatory)

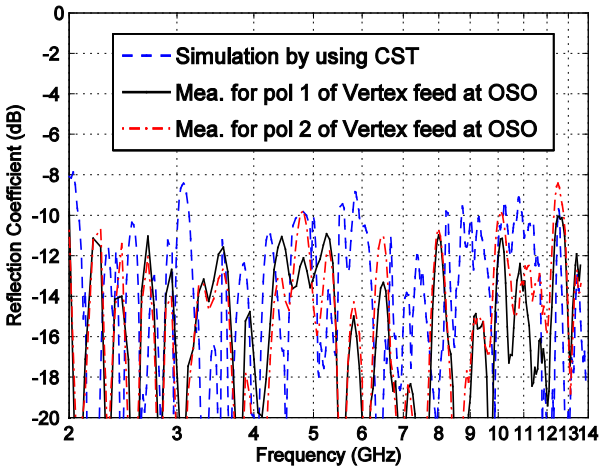

Figure 2.18 : Simulated and measured reflection coefficients of the Vertex model of Eleven feed [9]

It shows that the measured reflection coefficient is below -10 dB over the whole band and agreements between measured and simulated results are quite good. It should be pointed out that mechanical tolerance has effect on the reflection coefficient performance of the feed, which can be seen from the differences between reflection coefficients of two polarizations in above figure.

The Eleven antenna satisfies the condition for constant radiation characteristics of log-periodic array antennas as stated in [9]. Therefore we should expect good performance over the whole 2-14 GHz bandwidth. Before going through the performance of antenna basic theory behind the efficiency of antenna should be explained.

2.6 Efficiencies

This part will explain the different efficiencies for reflector antenna based on the definitions in[22] . In fact there are many factors that reduce the efficiency of the reflector system. Here we will study different subeffciencies according to the discussion in [23] .

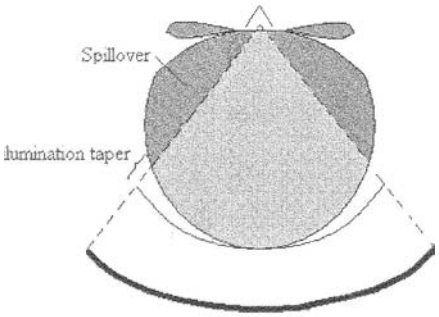

Figure 2.19: illustration of the spillover and illumination efficiency [8]

In order to characterize the performance of the reflector system we use the feed efficiency. The feed efficiency is unity for an ideal case. The feed efficiency is divided into several sub efficiencies. The definition for feed efficiency and all sub efficiencies are given in

$$e_{sp} = e_{BOR1} e_{sp} e_{pol} e_{ill} e_{\varphi} e_{foc} e_{refl} \quad (2.37)$$

BOR_1 Efficiency

The BOR efficiency, e_{BOR} measures how similar is the actual far field of the antenna to BOR type far field. So we should find part of the actual field that is not of the BOR type. Then the ratio between the power in BOR_1 component and the total radiated power will be BOR efficiency.

$$e_{BOR} = \frac{P_{BOR_1}}{P} \quad (2.38)$$

The total radiated power is given in . The numerator should be calculated using the actual far field. It means that we should approximate the far field function with a Fourier expansion, then use the first term of the Fourier series. Radiated power in BOR_1component has been calculated in [22].

$$e_{BOR_1} = \frac{\pi \int_0^{\pi} (|G_E(\theta)|^2 + |G_H(\theta)|^2) \sin\theta d\theta}{\int_0^{\pi} \int_0^{2\pi} \left(\left(|G_{co}(\theta,\varphi)|^2 + \left|G_{xp}(\theta,\varphi)\right|^2 \right) \right) \sin\theta d\theta d\varphi} \quad (2.39)$$

Spillover efficiency

The spillover efficiency e_{sp} is the measure of the fraction of the radiation that misses the reflector as illustrated in figure 2.19.

$$e_{sp} = \frac{P_{rad,BOR,\theta_H}}{P_{rad,BOR}} = \frac{\pi \int_0^{\theta_h} (|G_E(\theta)|^2 + |G_H(\theta)|^2) Sin\theta d\theta}{\pi \int_0^{\pi} (|G_E(\theta)|^2 + |G_H(\theta)|^2) Sin\theta d\theta} \quad (2.40)$$

Polarization efficiency

The power in the crosspolar part of the field will of course be lost. The polarization efficiency, e_{pol}, is thus a measure of how much of the power is contained in the copular and useful part of the far field pattern

$$e_{pol} = \frac{P_{co,BOR,\theta_H}}{P_{,BOR}} = \frac{\pi \int_0^{\theta_H} (|G_{co}(\theta)|^2) Sin\theta d\theta}{\pi \int_0^{\pi} (|G_E(\theta)|^2 + |G_H(\theta)|^2) Sin\theta d\theta} \quad (2.41)$$

Illumination efficiency

The illumination efficiency e_{ill} is a measure of the loss due to the un-uniform illumination of the reflector. The effect is illustrated in figure 2.19.

$$e_{ill} = 2cot^2\left(\frac{\theta_H}{2}\right)\frac{\left(\int_0^{\theta_H} G_{co45}(\theta)\tan\left(\frac{\theta}{2}\right)d\theta\right)^2}{\int_0^{\theta}|G_{co45}(\theta)|\,d\theta} \qquad (2.42)$$

Phase efficiency

The phase efficiency e_{φ} is a measure of the loss due to the phase errors in co polar field. This efficiency is the only efficiency that depends on the location of the feed relative to the focal point of the reflector.

$$e_{\varphi} = \frac{(\int_0^{\theta_H} G_{co45}(\theta)\tan(\frac{\theta}{2})d\theta)^2}{\int_0^{\theta}|G_{co45}(\theta)|\,d\theta} \qquad (2.43)$$

Focal efficiency

A characteristic of log periodic antenna is that they have a frequency dependent phase center location. According to [19] the focal efficiency varies quadratically to the axial displacement of the phase center from the focal point, δ-δ_0. Using this we can approximately express the focal efficiency, e_{foc} as

$$e_{foc} = 1 - 0.151\left(\frac{\delta - \delta_0}{\Delta\delta}\right)^2 \qquad (2.44)$$

Where $\Delta\delta$ defines as displacement of the phase center from the position that maximizes the phase efficiency.

Reflection efficiency

Input impedance of the log periodic antenna is the function of the frequency. This will cause reflections at the feed input and thus reduce the efficiency of the reflector system.

$$\Gamma = \frac{Z_{in} - Z_0}{Z_{in} + Z_0} \qquad (2.45)$$

Where Z_0 is the characteristic impedance of the feed wire. The fraction of the power that is not reflected is of course proportional to the square of the reflection coefficient which means that the reflection or mismatch efficiency is given by

$$e_{refl} = 1 - |\Gamma|^2 \qquad (2.46)$$

Radiation performance of Eleven Feed

The complex far-field functions $G_\theta(\theta, \varphi)$and $G_\varphi(\theta, \varphi)$ of the Eleven feed were measured in the spherical near-field test range at DTU (Technical University of Denmark) . The angular range covered 0^0 to 180^0 for the polar θ value and φ 0^0 to 360^0 for the azimuth φ value, both with intervals of 1^0 with z-axis located vertical to the ground plane.

Figure 2.20 shows the total aperture efficiency and its sub efficiencies as what have been defined in above section, when a feed illuminates a symmetrical paraboloid in which center blockage loss is negligible. The efficiencies are computed both from simulated radiation field functions and measured ones . In both cases the paraboloid has subtended half angle of 60^0, corresponding to F/D= 0.433.

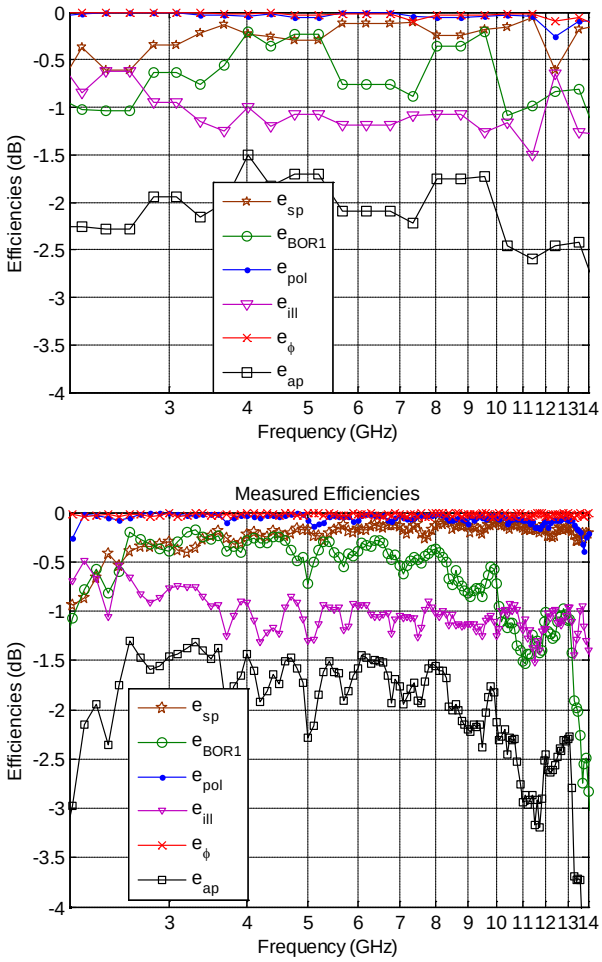

Figure 2.20: 4 Aperture efficiency and its subeffciencies [9]

From above figure it can be observed that BOR_1 efficiency is higher than -1 dB from 2.5 to 10 GHz., higher than -1.5 dB in the range 2-2.5 GHz and 10-13 GHz. The polarization efficiency is high ($e_{pol} > -0.2$ dB) as well as the phase efficiency ($e_\varphi > -0.1\ dB$) which is high due to the constant

phase center. The illumination efficiency e_{ill} is about -1 dB with small variation due to the beamwidth of radiation pattern being almost constant over the whole frequency band 2-13 GHz. This can be seen from figure 2.21 which shows the measured co-and cross-polar radiation pattern of the BOR_1 components in $\varphi = 45^0$ plane.

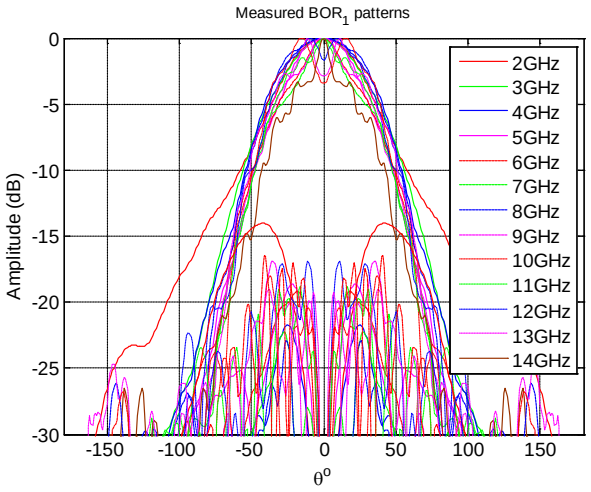

Figure 2.21: measured co-and cross-polar BOR radiation patterns in $\varphi = 45$ plane of the verex model [9]

Chapter III

Investigations of several possible solutions to descrambling board for the Eleven Feed

The main goal for this project is to find a way to reduce the number of ports from eight to four ports and packaging the board with gap-waveguide technology. In this chapter we will explain a summary of theory and simulation results for each possible solution, and then select the best solution in terms of performance and manufacturing issues to integrate as descrambler board and package with gap waveguide.

In order to reduce the number of ports, first step is to combine two in phase 100 Ohm ports. See figure 3.1

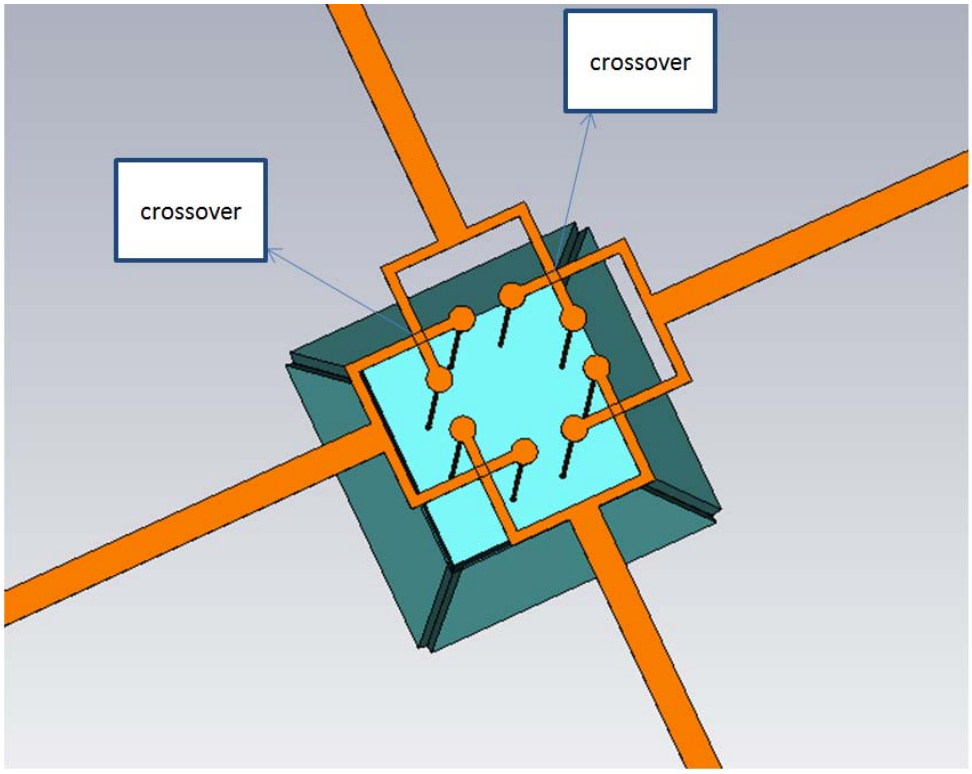

Figure 3.1: basic geometry of cross over in eight port descrambling Board

The main problem with this combining solution is the four crossovers which are seen in figure 3.1. Increased insertion loss, mismatched junctions, additional line cross couplings, poor power handling capability, and difficulty in manufacturing are some of the undesired effects of the crossover. There are some design resembling a Lange coupler is used as crossover. In next section we will study one of these crossovers in more details.

3.1 The Lange Coupler Crossover

To overcome the problems that cause from crossover, different characteristic techniques are available for the crossover design, such as in CPW designs , an expensive laminate is usually needed and there is also an overhead in the fabrication and measurement process. One possible suggestion has been proposed in [24]to use the Lange coupler as the crossover. The advantage of this Crossover is that the space occupied by the Lange coupler is less in compare with other conventional crossovers. The layout of Lange crossover is shown in figure 3.2

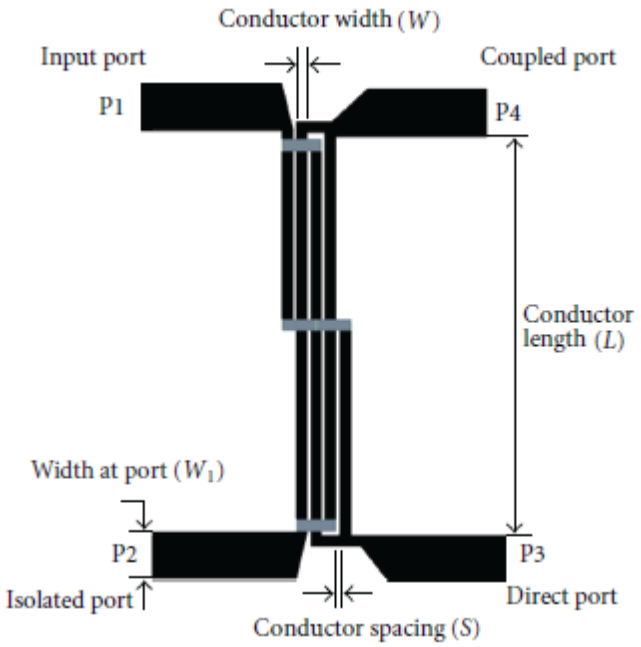

Fig 3.2: layout of the Lange Cross coupler [24]

The measured scattering parameters for this kind of crossover can be found in [24] and it has been shown in figure 3.3.

3.1.1 Problems with Lange Crossover

Theoretically we can use four Lange Crossovers to solve the problem. But the major challenges for this solution are: The Lange coupler Crossover usually uses in the ISM band and UMTS frequency requirements, therefore such a wideband Lange coupler that covers a decade bandwidth is not commercially available, and it cannot be found in literature either.
Furthermore, due to the limited space below the ground plane, it is not possible to use such a large structure as Lange crossover. Size of the crossover is 22.24 × 22.23 mm.

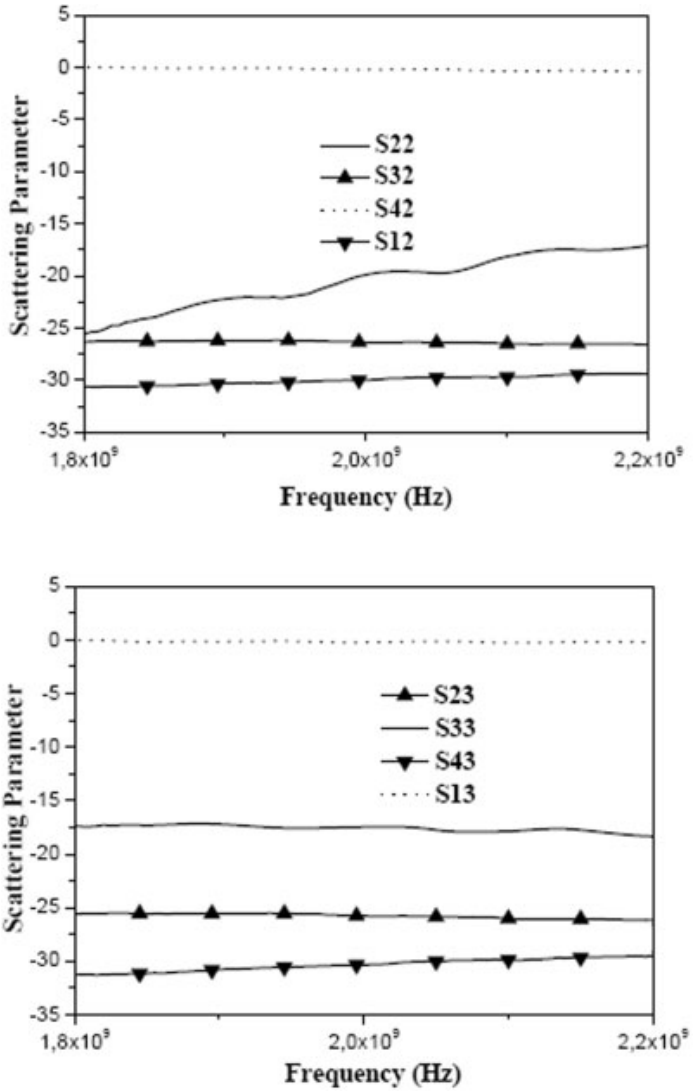

Figure 3.3: computed S parameters for Cross Lange coupler [24]

3.2 Two layer solution

Due to the problems that will cause by crossover, it is more realistic to use two layer solutions which means that combining of in phase ports for each polarization will happen in one layer to avoid crossover microstrips. In other words two 100 ohm branch should combine and make wideband T junction that connects to 50 ohm coaxial port. See figure 3.4

It should be mentioned that in such a wideband structure discontinuities will be problematic, so, it worth to look at the some of the main discontinuity in microstrip before going to the design procedure.

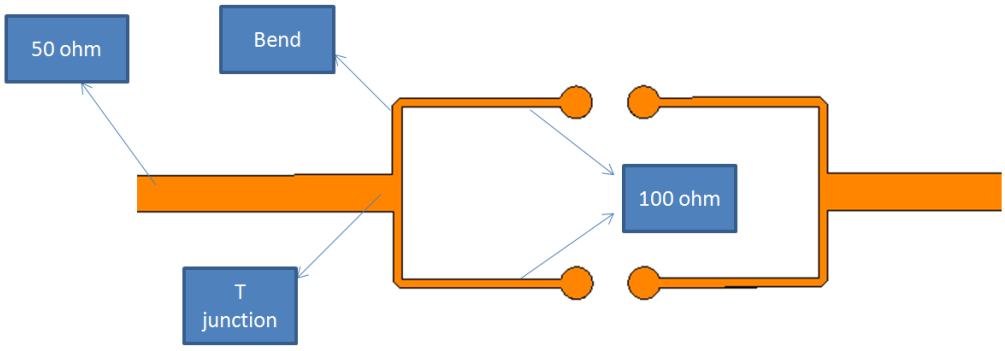

Figure 3.4: different parts of combining section of two ports

3.2.1 Discontinuity in microstrip

An abrupt change in geometry of microstrip conductor will cause to the microstrip discontinuity which is problematic in many applications since electric and magnetic field distributions are modified near the discontinuity. The altered electric field distribution gives rise to a change in capacitance, and the changed magnetic field can be written in terms of an equivalent inductance. Using suitable equivalent circuit including these capacitances and inductances is the main task of analytical study of microstrip discontinuous.

Although these emerging capacitances and inductances have very small values (often <0.1 pF and 0.1 nH) the reactance of these become particularly significant at the higher microwave frequencies, say 10-20 GHz. The performance of amplifiers will be degraded due to the microstrip discontinuities. We can very often neglect these discontinuities when the frequencies involved do not exceed a few GHz. Above approximately 10 GHz they are definitely very significant.

Several forms of discontinuities which are emerging from our circuit requirement will be study in next section:

- Right-angled corners or ‘bends’ (unmetered and mitered)
- T-junction

3.2.2 The right-angled bend or corner

Having quite complex circuits in MMIC field introduced new problems in terms of manufacturing. In order to have more flexibility in layout of the circuit design, microstrip bends is part of every complex circuit. For example it is necessary to feed , between circuits, using lengths of microstrip that include bends. These usually pass through an angle of 90^0. Most often the line does not change width. The bend together with equivalent circuit has been shown in figure 3.5.

The capacitance arises through additional charge accumulation at the corners- particularly around the outer point of the bend where electric field concentrates. The inductors arise because of current flow interruption. This is considerable; especially keep in mind that most of the current flows in outer edges of microstrip.

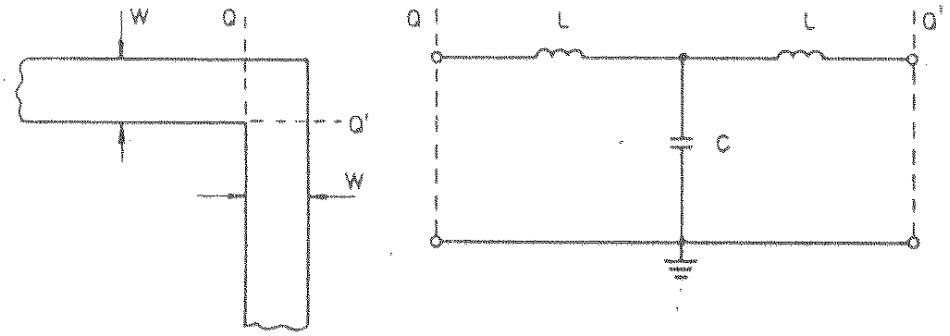

Figure 3.5: Right angled microstrip bend and its equivalent circuit

Edwards in [21]have given closed formulae for the evolution of bend capacitance.

For w/h <1 :

$$\frac{C_{BEND}}{W} = \frac{\frac{(14\varepsilon_r + 12.5)w}{h} - (1.83\epsilon_{r-2.25})}{\sqrt{w/h}} \qquad \frac{pF}{m} \qquad (3.1)$$

For w/h > 1

$$\frac{C_{Bend}}{w} = (9.5\varepsilon_r + 1.25)\frac{w}{h} + 5.2\varepsilon_r + 7.0 \qquad \frac{pF}{m} \qquad (3.2)$$

And inductance:

$$\frac{L}{h} = 100\left\{4\sqrt{\left(\frac{w}{h}\right)} - 4.21\right\} \qquad \frac{nH}{m} \qquad (3.3)$$

The accuracy of eq 3.1 is quoted as within 5 percent . Over the ranges $2.5 < \varepsilon_r < 15$ and $0.1 < \frac{w}{h} < 5$. the accuracy for eq 3.2 is quoted as about 3 per cent. For the range: $0.5 < \frac{w}{h} < 2$

3.2.3 Matched microstrip bends: compensation techniques

Several techniques have been investigated for the compensation of microstrip bends, greatly reducing the effect of capacitance and hence improving the VSWR. In [25] the method of moment has been used to calculate the capacitance and inductance for both curved and mitred bends , the results indicate that a mitred bend produces as good as , or better performance than curved bends at least up to frequency of 10 GHz. Guidance for the design of such a mitred bends are shown in figure 3.6.

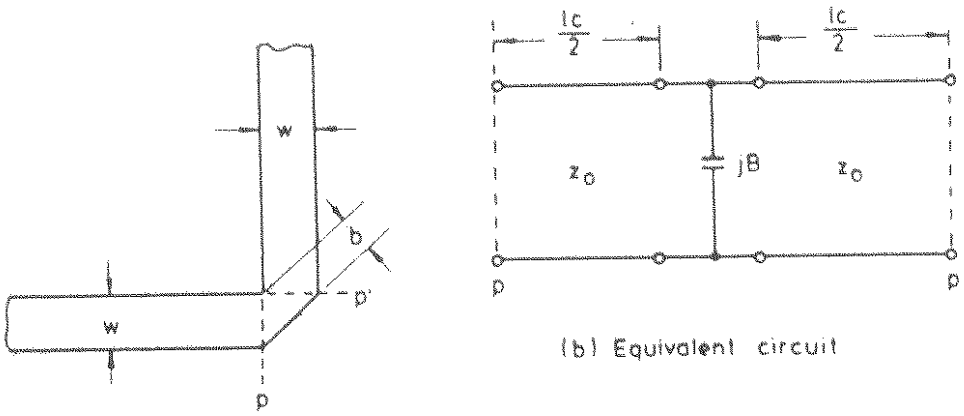

Fig 3.6: chamfered, Right-angled bend together with its equivalent circuit

The equivalent circuit shown in fig 3.6 is for the region between planes P and the p'. The degree of chamfer is generally restricted to around

$$1 - \frac{b}{\sqrt{2}w} = 0.6 \qquad (3.4)$$

So that

$$b = 0.57\, w \qquad (3.5)$$

It is tentatively recommended that approximately this amount of chamfer is applied in the majority of practical cases.

The simulation results for 90 degree bend and 50 % mitring bend has been shown in figure 3.7.

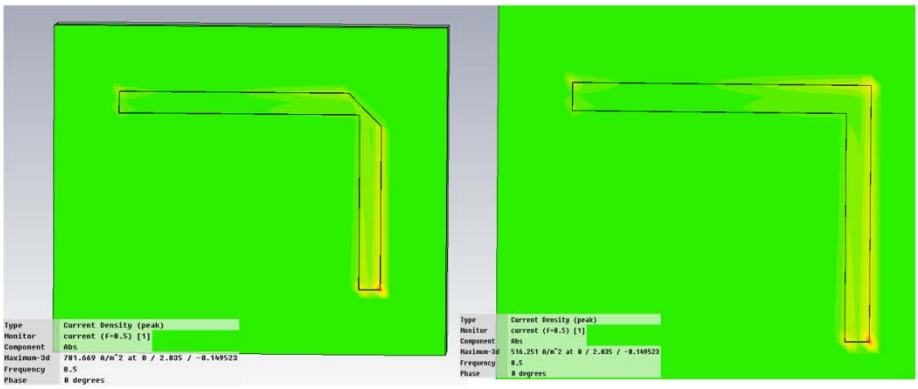

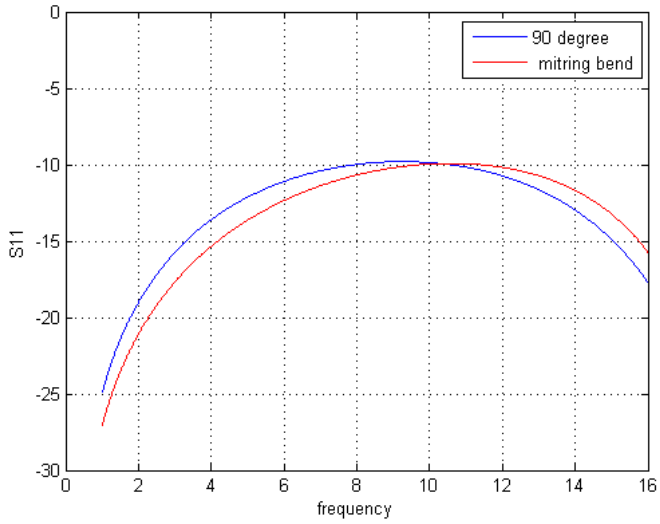

Figure 3.7: field distribution for Right angle bend and mitring bend(down) comparison of the results for two structure

So, using some techniques like mitring it is possible to improve the performance somehow, but the main problem arises from T junction. It means that we should find a wideband T junction that can satisfies the matching requirements from 2 to 14 GHz. In next chapter we will study different combinations of two 100 ohm microstrip lines that connect to the 50 ohm coaxial line see figure 3.8.

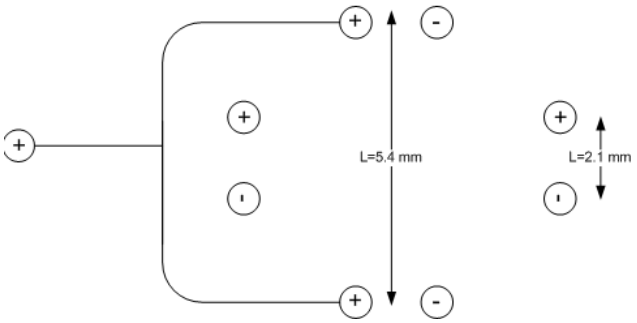

Figure 3.8: Drawing of general combining task

3.3 Fork arc structure

We name the different designs according to the shape of the arcs that they use to combine two 100 ohm lines. So we refer to the first design as fork arc design. See figure 3.9.

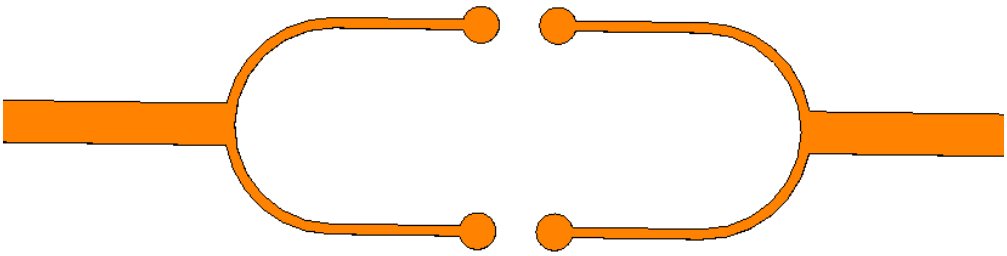

Figure 3.9: Fork arc structure

On e problem for this design and all similar designs is the angle by which 100 ohm lines separate from each other. It seems that, due to the direction of the field in tubes, it is better to two 100 ohm lines separate smoothly. Comparison between two different degrees has been shown in figure 3.10.

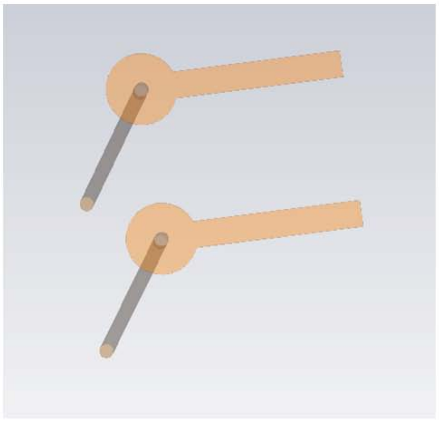

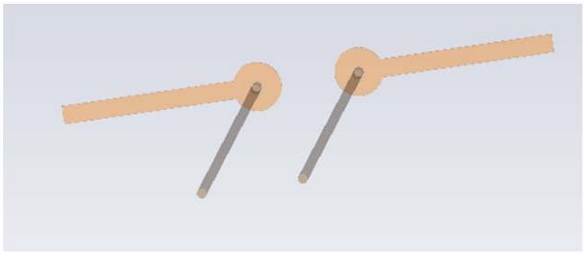

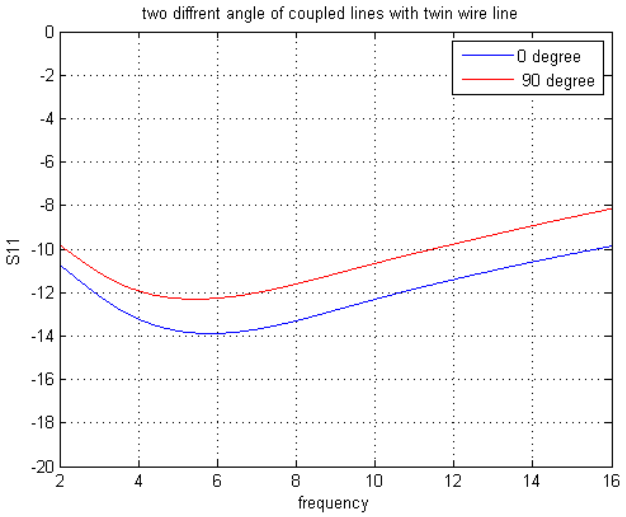

Figure 3.10: two different separation models after holes in the ground plane (left) 0 degree (right) 90 degrees

The return loss for above structure has been shown in figure 3.11.

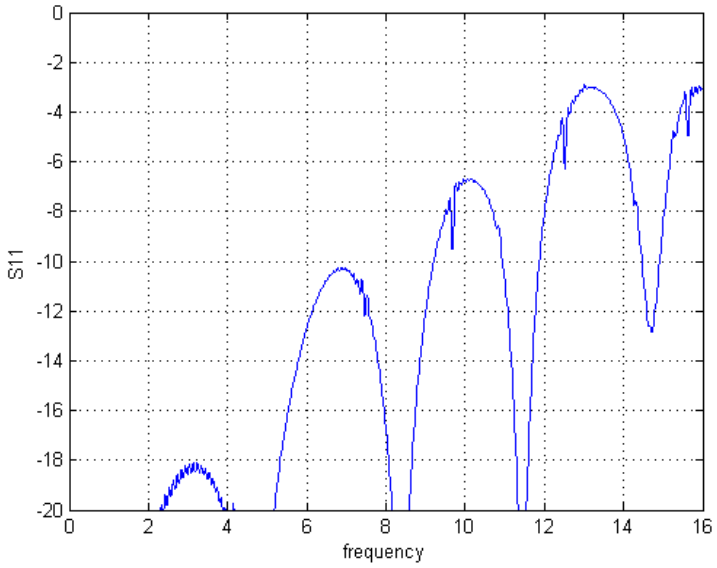

Figure 3.11: results for fork arc structure

It should be pointed out that, changing the length of the fork can affects the results somehow. The optimum result can be achieved by length around 6 mm. but in any case this structure will be problematic in high frequency, especially above 10 GHz.

3.4 Circle arc structure

This structure is more less similar to the pervious one with this difference that now coupled microstrip strip lines smoothly separate from each other.

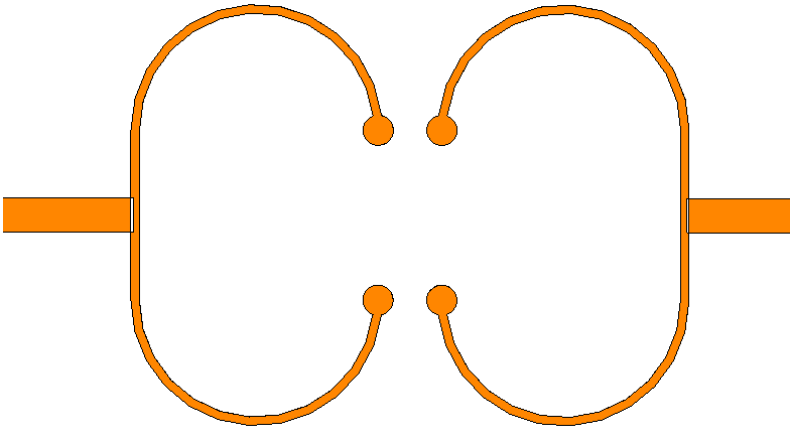

Figure 3.12: CST Model of the circle arc structure

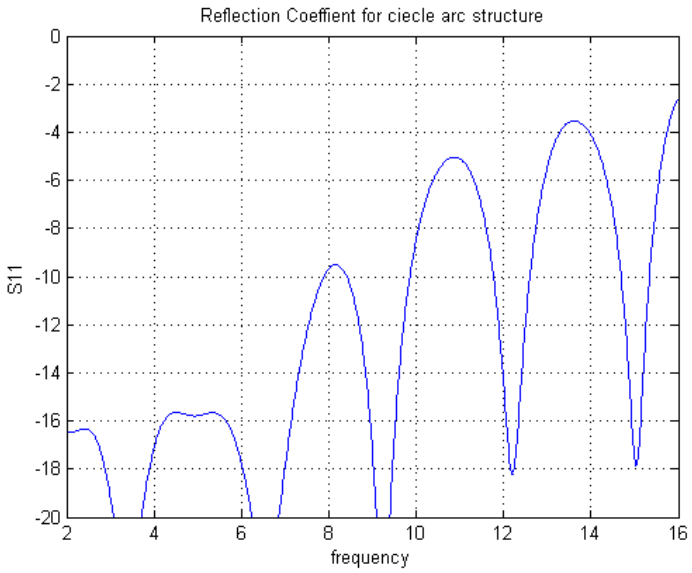

Figure 3.13: results for circle arc structure

It can be observed that still performance will be degraded with increasing frequency.

3.5 Rectangular arc structure

Figure 3.14 shows the same design as before but curve parts have been replaced with mitring bends

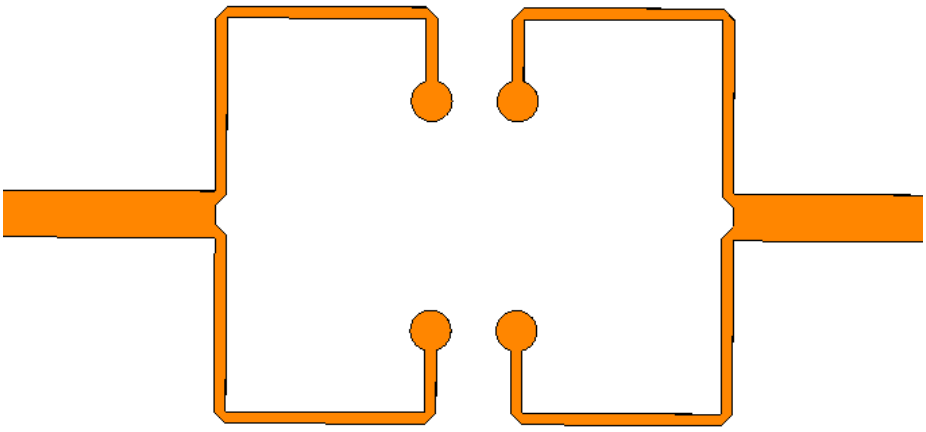

Figure 3.14: CST Model of Rectangular structure

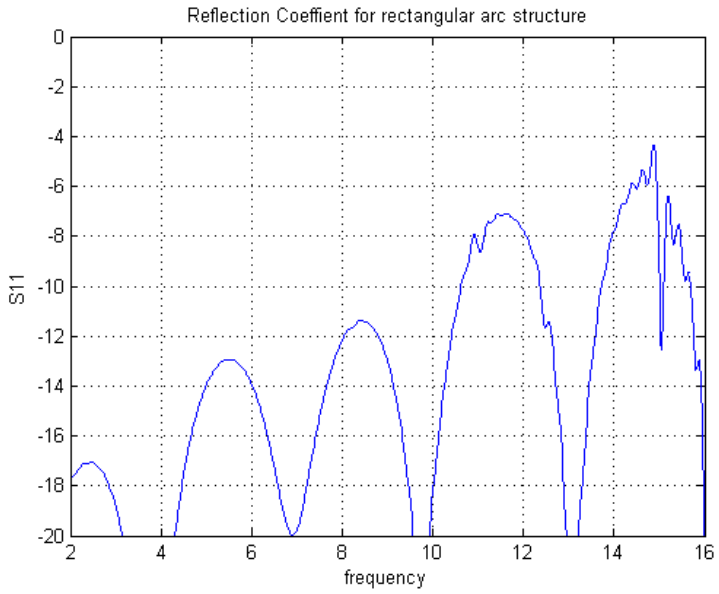

Figure 3.15: Reflection coefficient for rectangular structure

Performance has improved a little, but still far away from what we expect.

3.6 Basic design

This design consists of simple mitring bends and simple T junction, fortunately the result is more promising than the other designs.

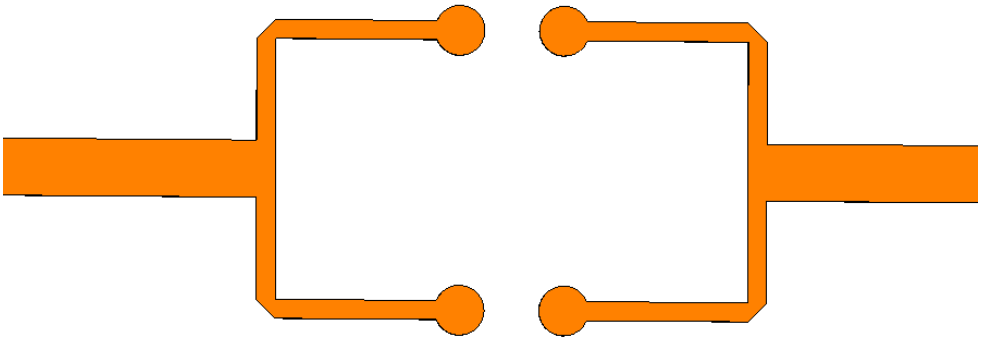

Figure 3.16: CST Model of the Basic Design

Reflection Coefficient for this design has been shown in figure 3.17. To be in the safe side high frequency performance needs further improvement. In order to get better result, we need to somehow design a better wideband T junction. Therefore, further study about T junction discontinuity is required. So, in next section we will study about T junction compensation techniques

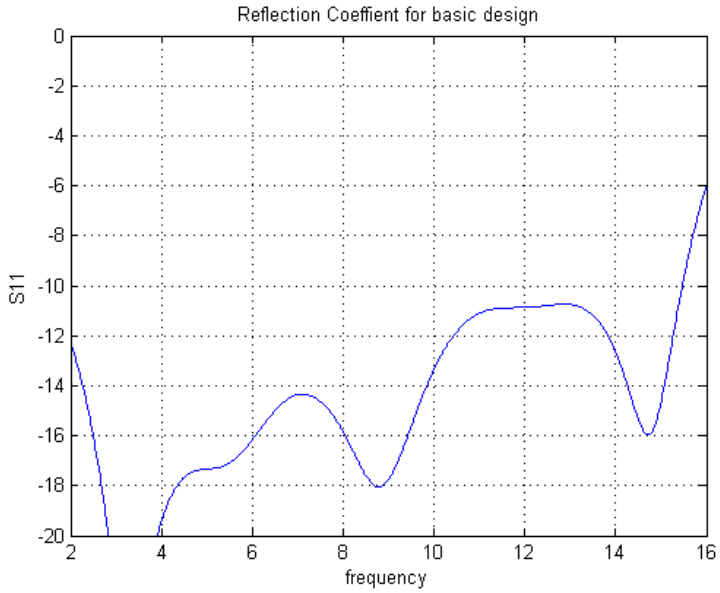

Figure 3.17: Results for Basic Design

3.7 The Microstrip T junction

The T- junction is perhaps the most important discontinuity in microstrip as it is found in most circuits such as impedance networks, stub filters and branch line couplers. A microstrip T junction and its equivalent circuit are shown in figure 3.18. Discontinuity capacitance C_T for this structure has been

calculated in [26]. Their results are shown in figure 3.19. Capacitances shown in this figure are for per unit main-line width. Inductance calculation for T-junctions has been carried out in[27] .their results are shown in figure 3.19. Comparison with the experimental results is also shown. The agreement between the experimental and theoretical results for L_2 is not as good as forL_1.

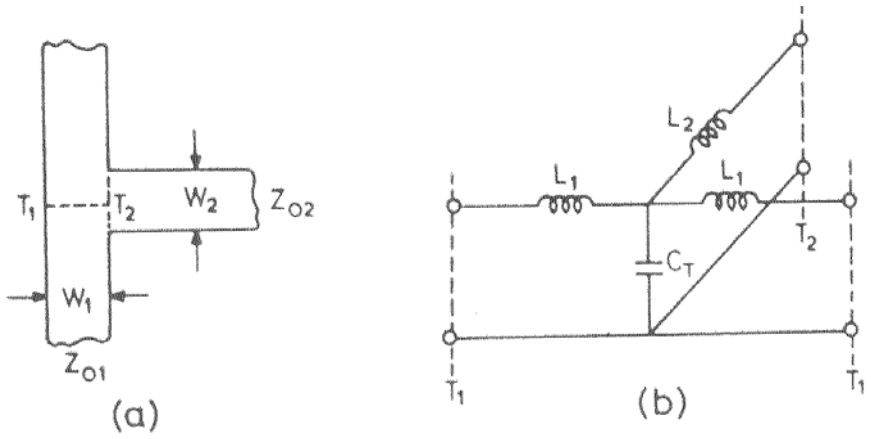

Figure 3.18: Microstrip T junction and its Equivalent circuit [24]

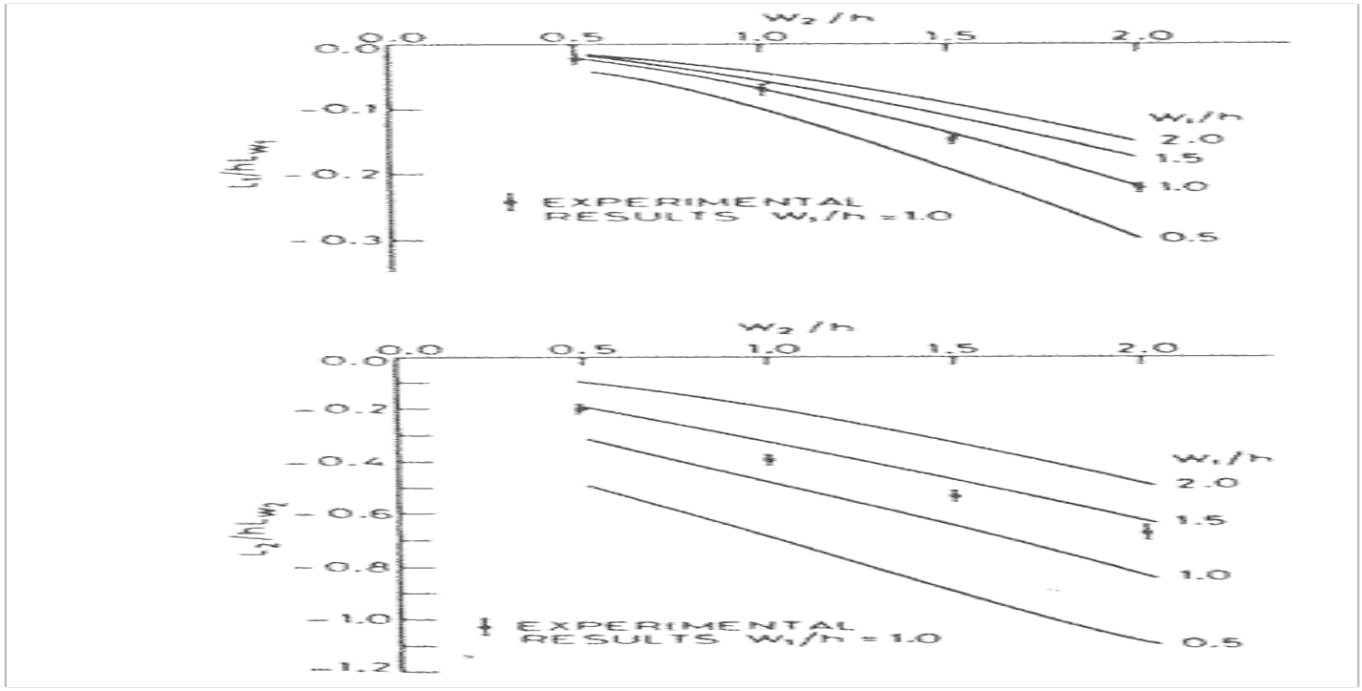

Fig 3.19 : Discountinuty of a microstrip T-junction [24]

The closed form expressions for the discontinuity reactance of the equivalent circuit shown in figure 3.18 with main line impedance of 50 ohm and ε_r=9.9 have also been derived in [28] as follows

$$\frac{C_T}{W_1}\left(\frac{pF}{m}\right) = \frac{100}{\tanh(0.0072Z_0)} + 0.64Z_0 - 261 \quad 25 < Z_0 < 100 \qquad (3.6)$$

Where Z_0 is the characteristic impedance of the stub

$$\frac{L_1}{h}\left(\frac{nH}{m}\right) = -\frac{w_2}{h}\left\{\frac{w_2}{h}\left(-0.016\frac{w_1}{h}+0.064\right)+\frac{0.016}{w_1/h}\right\}L_{w1} \qquad (3.7)$$

$(0.5<(\frac{w_1}{h},\frac{w_2}{h})<2)$

$$\frac{L_2}{h}\left(\frac{nH}{m}\right) = \left\{\left(0.12\frac{w_1}{h}-0.47\right)\frac{w_2}{h}+0.195\frac{w_1}{h}-0.357+0.0283\sin\left(\pi\frac{w_1}{h}-0.75\pi\right)\right\}L_{w_2} \qquad (3.8)$$

$$1<\frac{w_1}{h}<2;\quad 0.5<\frac{w_2}{h}<2$$

Where L_w is the inductance per unit length for a microstrip of length w. the above equations have an error of less than 5 percent .

Here we will compare reflection coefficient result for ordinary T junction and compensated T junction

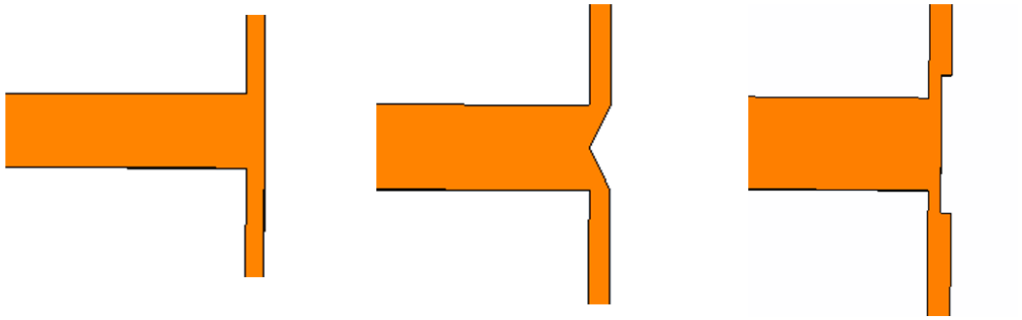

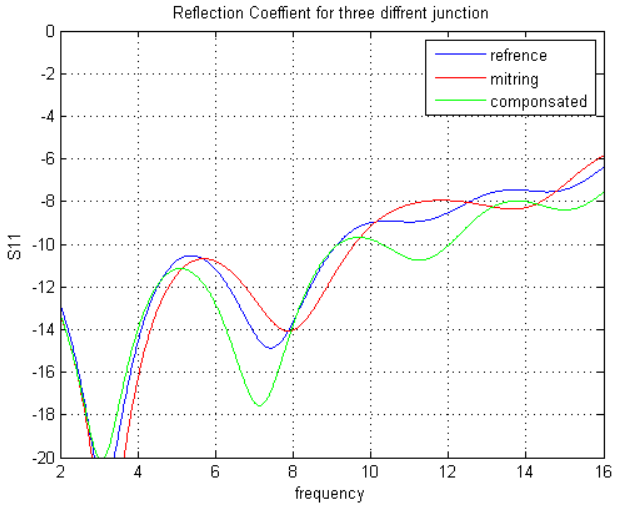

Figure 3.20: Three different Microstrip T junctions and Computed S parameters for them

It can be observed that performance of compensated T junction is better in compare with ordinary and mitring T junction. It can be explained based on this fact that the effect of shunt suseptance in figure 3.18 can be compensated by changing microstrip width near the junction as shown in figure 3.21. The length θ_1, θ_2 and characteristic impedances (Z_{m1},Z_{m2}) of the modified portions near the junction can be derived from the values of discontinuity reactances.

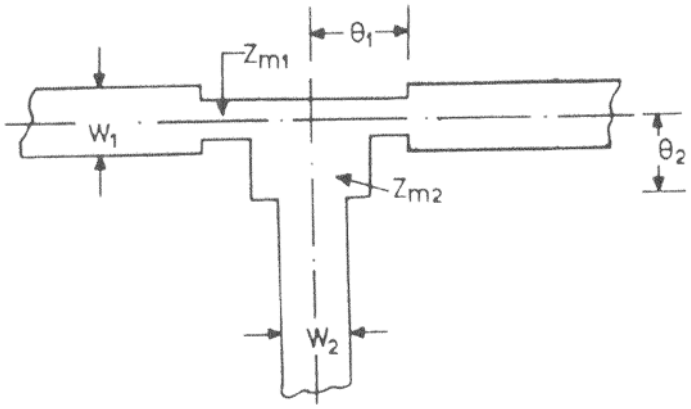

Figure 3.21: Drawing of the Compensated T junction [24]

3.8 Compensated T junction

As we can see in figure the result for compensated T junction is encouraging in compare with normal T junction. Therefore, in this section we will study more about the compensated T junction.

Cohn in [29] proposed slot line as new type of transmission line to be used with or instead of microstrip lines which makes it possible to design a new class of microstrip components. According to the[30] for microstrip technology a narrow slot can be made in ground plane and will act as separate and accessible transmission line and if both lines, the strip and the slot line intersect, coupling take

place, which is symmetrical if the lines are perpendicular to each other. Due to this fact several designs for wide band directional couplers and magic T have been proposed by Cohn, Siegl and Garcia[31] . Aboosh in [32] proposed a novel planar ultra wideband in phase power divider which use the a slot in shape of narrow rectangle in the middle of the ground plane, also to efficiently couple the signal between the slot line and two output ports the end of the slot line has been compensated with an inductive element in the form of circular slot. Configuration of proposed power divider has been shown in figure 3.22.

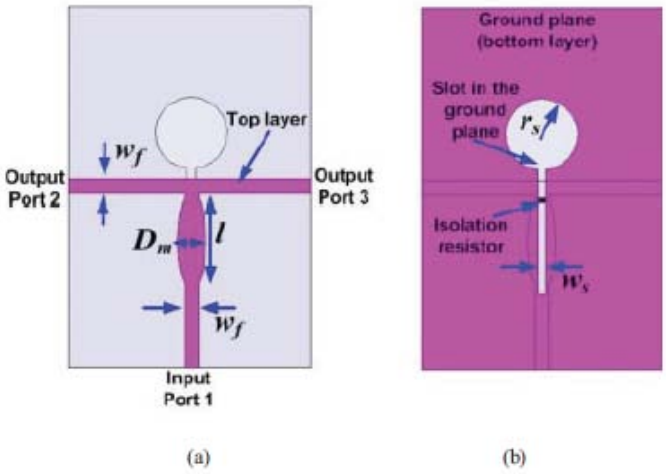

Figure 3.22: A new Wideband power divider using Elliptical section [32]

Another useful technique is to use the elliptical microstrip patch above the slot line. Shape of the coupled microstrip patch was chosen to be elliptical because it represents a tapered shape which enables a broadband performance based on this fact that small reflections will cancel each other in such a structure.

Using above background, in this section we will design a wideband T junction. First we start with adding the slot lines on the ground plane below the strip.

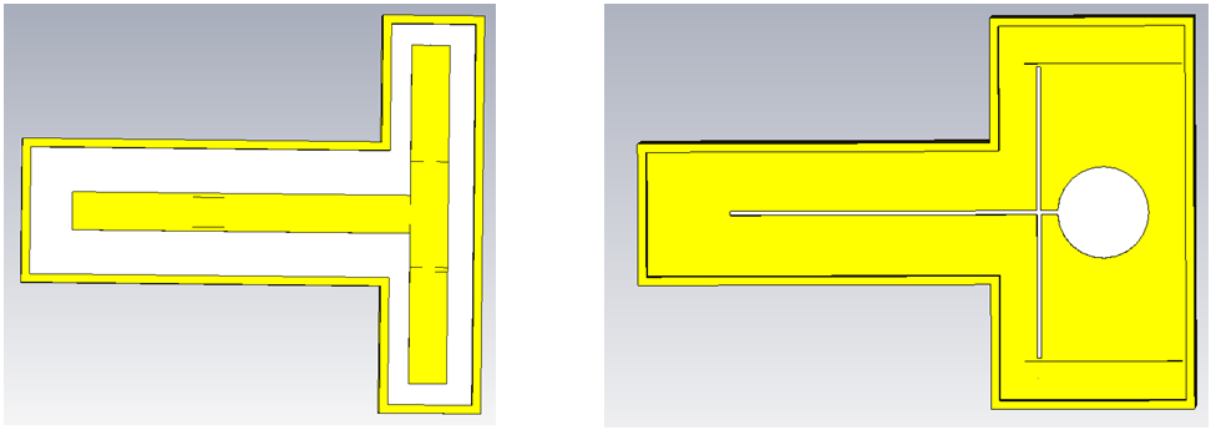

Figure 3.23: view of the microstrip power divider and slots in the ground

It can be observed in figure 3.24 that using slots in the ground plane improve the performance, but, it still needs more modification to achieve wideband performance.

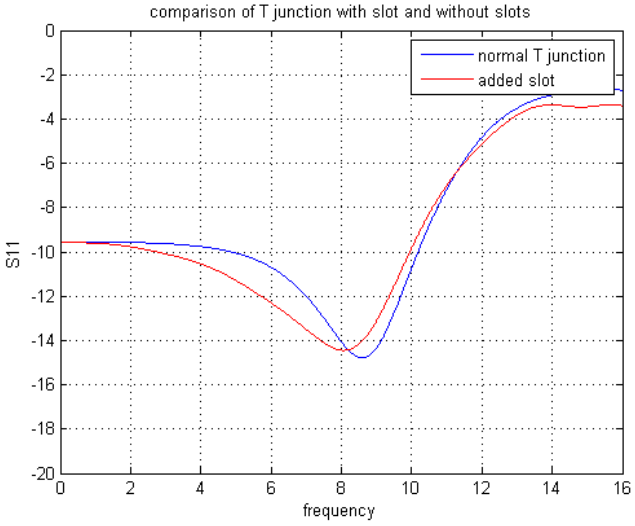

Figure 3.24: Comparison between results of Normal T junction and T junction with slots in the ground

Then, with keeping the slots we add the tapered patch microstrip above the slots on the ground plane, as we expect, according to the theory of small reflections return loss will be improved, since small reflection from different sections of structure will cancel each other.

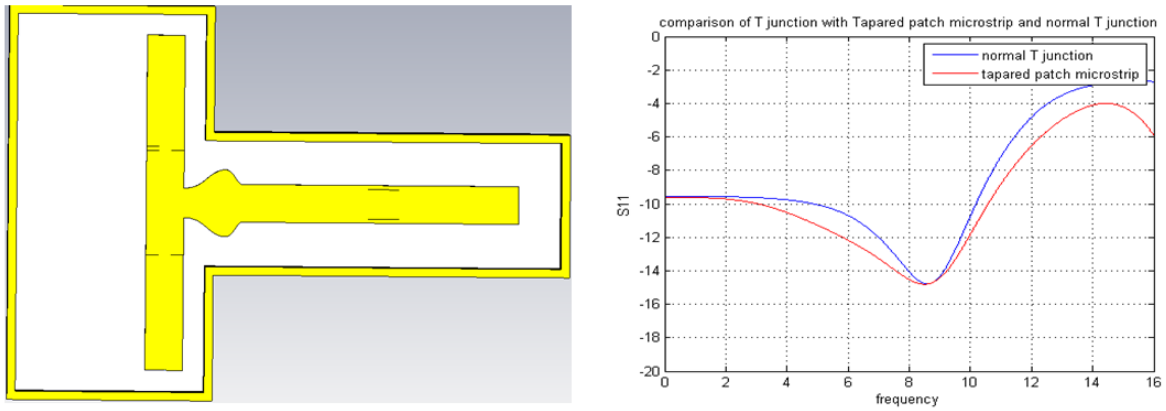

Figure 3.25: CST Model of microstrip T junction with Elliptical section and computed S parameters

In next step, according to the we will study effect of changing microstrip width near the junction.

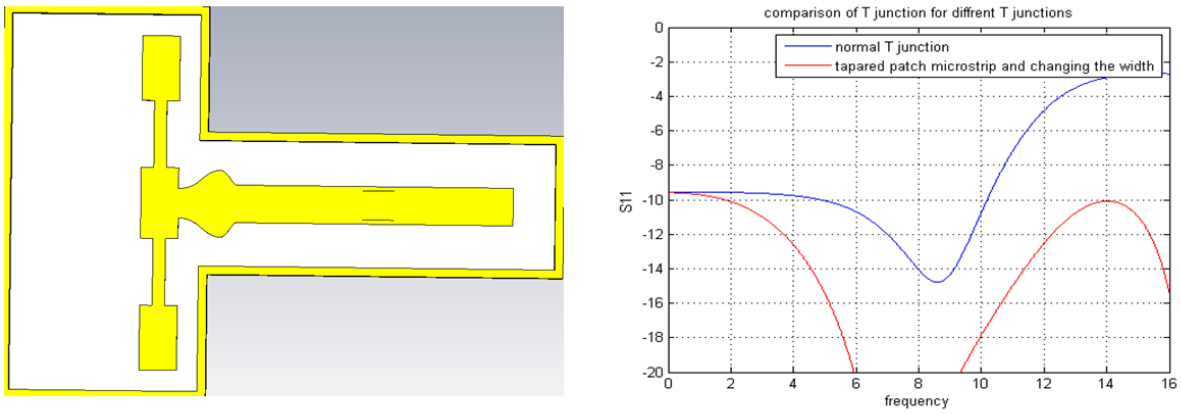

Figure 3.26 : CST Model of Compensated microstrip T junction with Elliptical section and computed S parameters

It can be observed that the result for new structure is much better than the normal T junction. It can be explained based on this fact that the effect of shunt susceptance in equivalent circuit can be compensated by changing microstrip width near the junction, therefore adjusting length of discontinuities near the T junction can be a helpful tool for optimization of whole structure.

Next part will be comparison between the best results that can be achieved by new designed power divider and available commercial power divider.

3.9 Measured results : comparison between commercial power divider and new wideband power divider

The results presented here, are measured using vector network analyzer. Datasheet for used power divider can be found in index B. It is to be noted that due to the symmetry, results only presented for port 2.

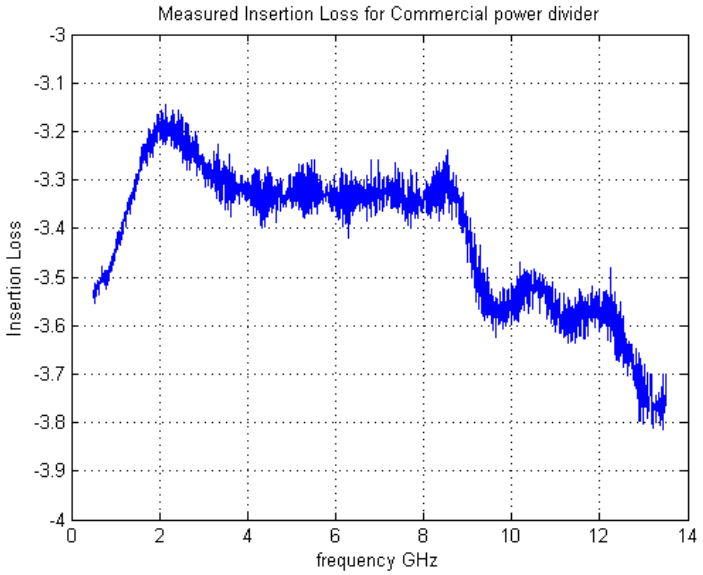

Fig 3.27: Measured results for commercial power divider

Figure 3.27 shows the insertion loss for commercial power divider, it can be seen that until 9 GHz insertion loss is less than -0.4 dB and for the whole band width is less than -0.8 dB.

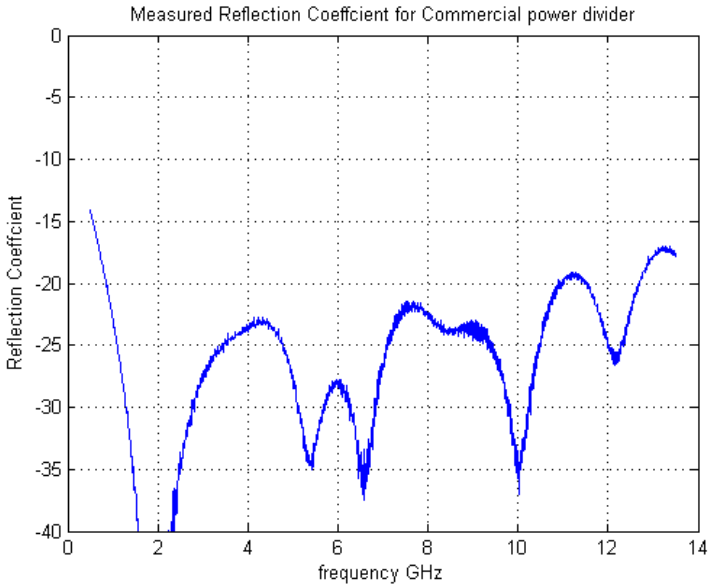

Figure 3.28: Measured results for commercial power divider

Figure 3.28 shows reflection coefficients for 1:2 commercial power dividers. The return loss for the input port is better than -20 dB until 12 GHz.

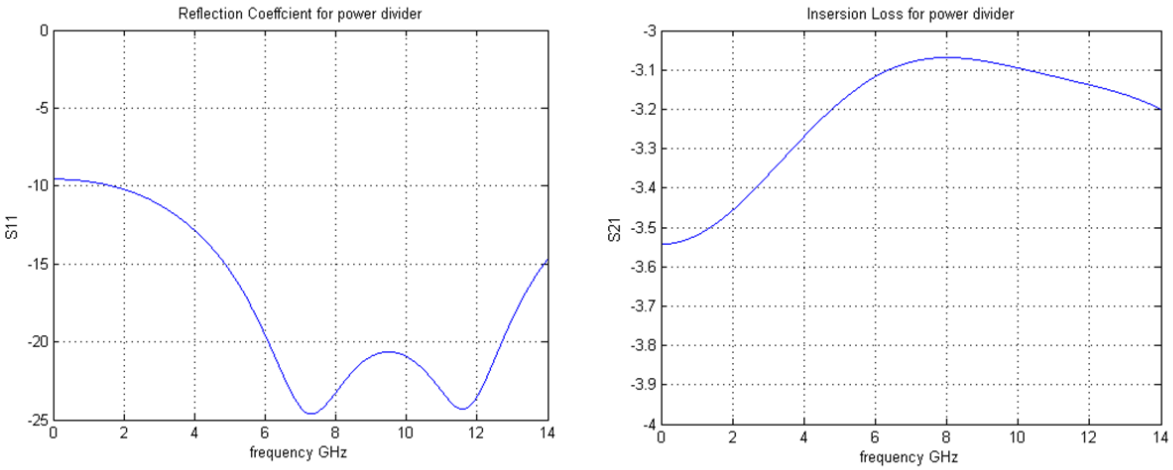

Figure 3.29: Simulated results for New designed power divider

Comparison of results of new designed power divider and commercial power divider shows that new power divider have a better insertion loss especially in high frequency. Another advantage is the compact size which is much smaller in compare with commercial power divider. The dimension is 10*11 mm.

3.10 Application for Wideband power divider

Two different applications can be considered for wideband power divider. First, it could be consider as power divider that feed two co-polar ports of each polarization. It will be same as pervious tries to combine co-polar ports. See figure 3.30

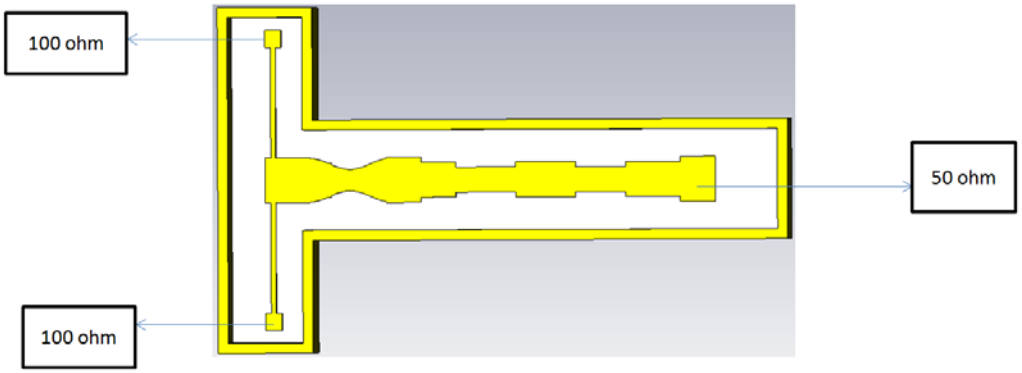

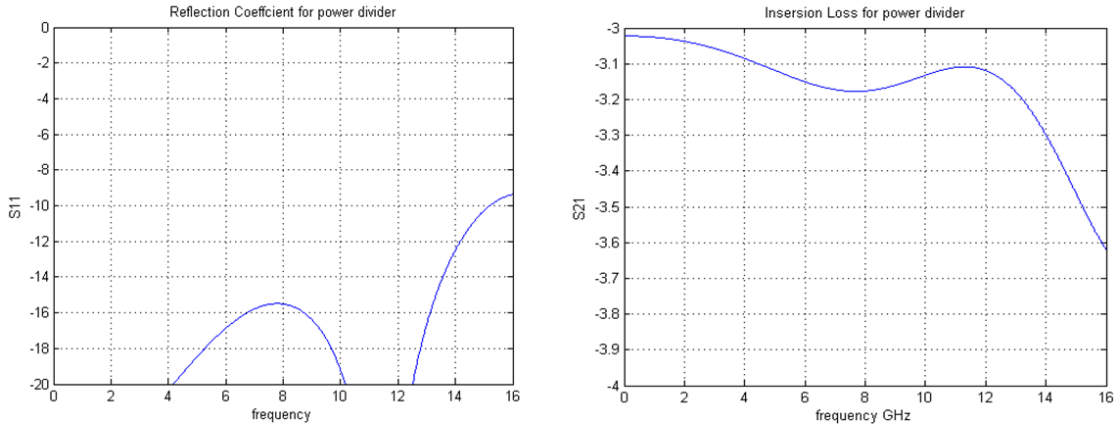

Figure 3.30: CST Model and simulated result for new designed power combiner

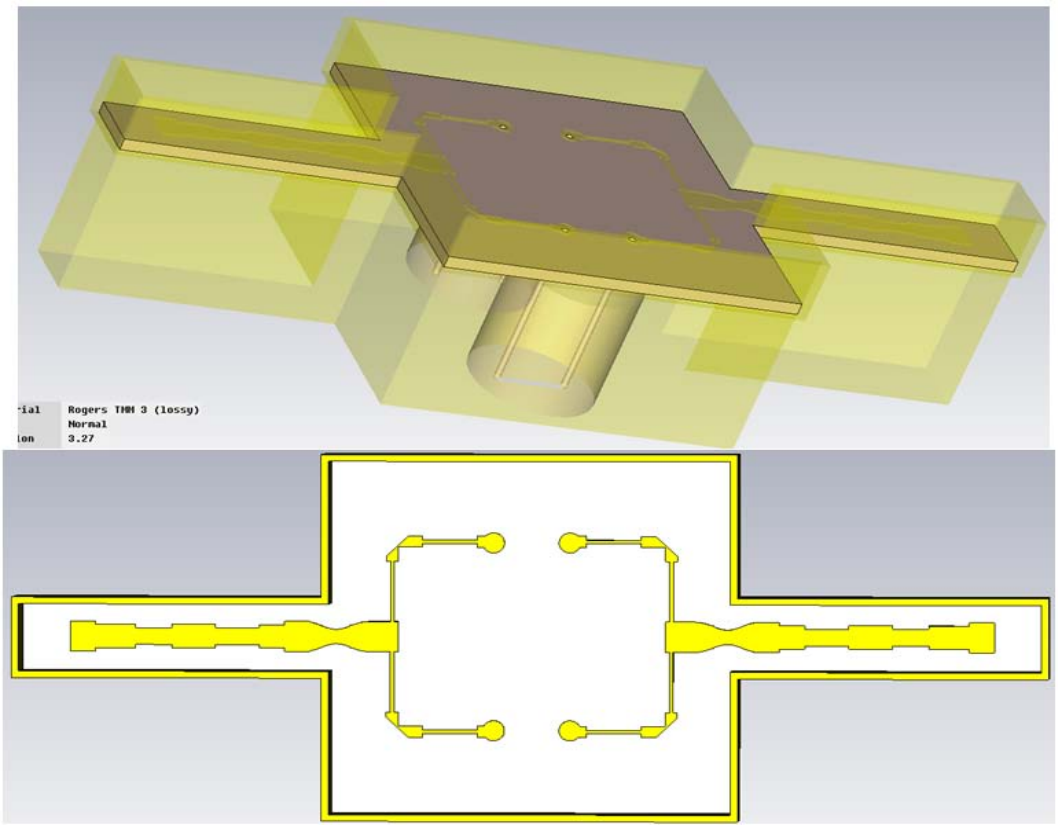

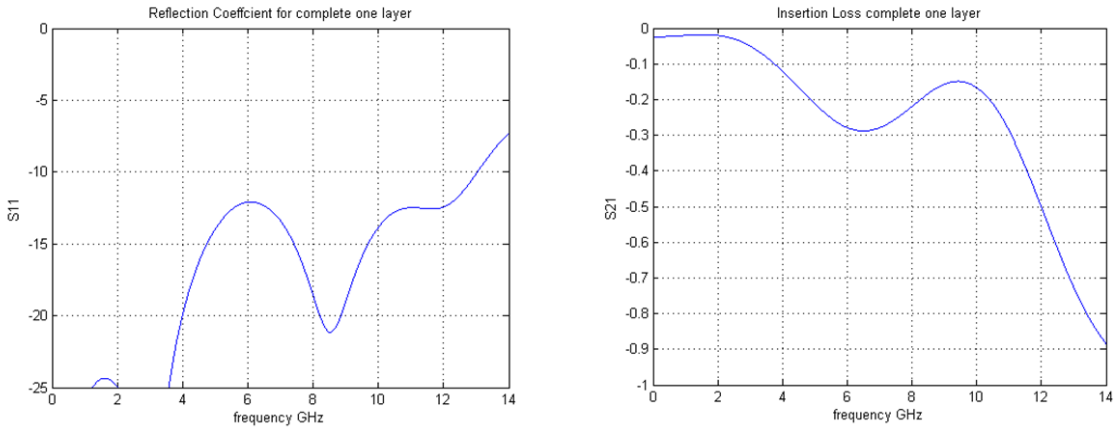

Figure 3.31 : final results for ultra wideband power divider in application in Descrambler Board

Another possible scenario has been shown in figure 3.32. The idea is to use a matched wideband power divider after180 hybrid. It should be mentioned that regardless of what solution will be used for feeding network, wideband power divider is required. It will be explained more in next chapter, when we introduce new wideband passive Balun solution as new circuitry board. Therefore, in any cases wideband matched power divider will be part of solution.

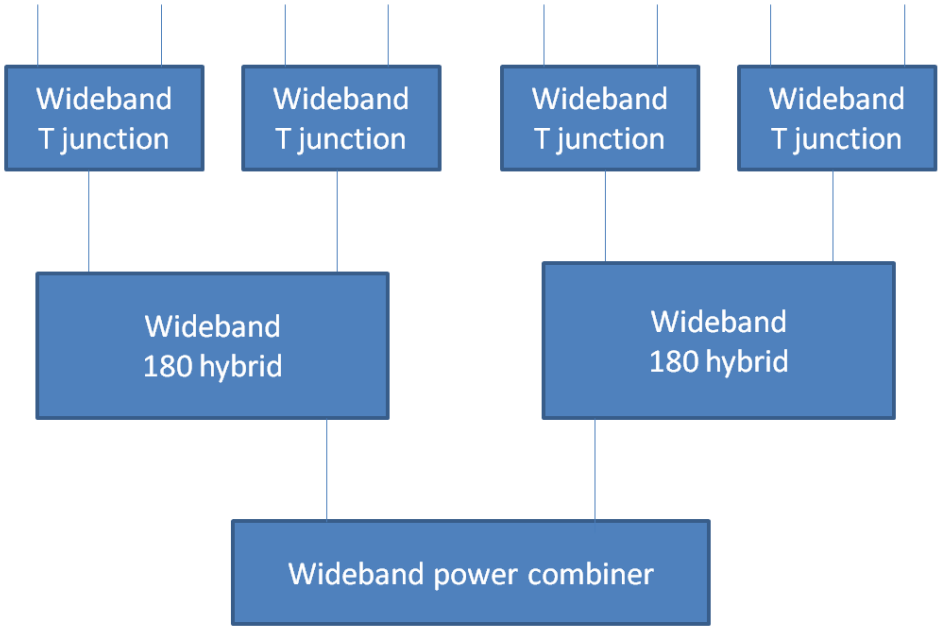

Figure 3.32: configuration of descrambler board using wideband power combiner

Figure 3.33 shows views of complete wideband T junction in two layers. It should be mentioned here that all of the simulated results have been done considering the Perfect Magnetic Conductor (PMC) in

top of the each layer. The complete theory and realization technique will be explained in next chapter during packaging section.

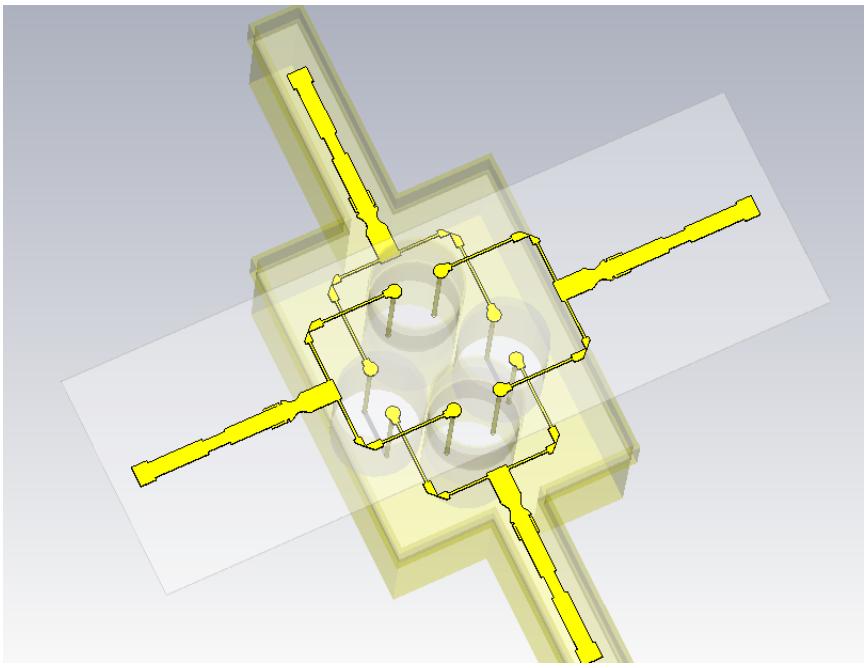

Figure 3.33: CST Model of the two layer structure of four

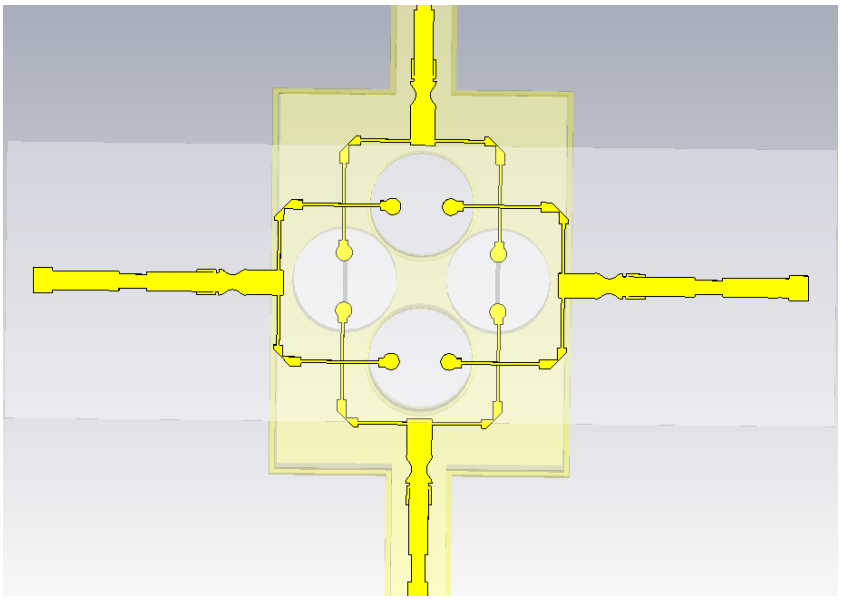

Figure 3.34: top view of two layer structure

Chapter IV

New Passive Balun solution

4.1 Introduction

One of the main drawbacks of two layer descrambler board that has been studied in pervious chapter is difficulties that are related to the manufacturing. In addition of constraints those are imposed by electrical design, mechanical restriction also should be considered by designer. Another important factor is that cost which is increased by using two layer solutions.

The idea is to use the wideband passive Balun for feeding each dipole petal to decrease the number of ports to 4 and then using the wideband power combiner for each polarization. Block diagram of descrambler board using four passive Baluns has been shown in figure 4.1.

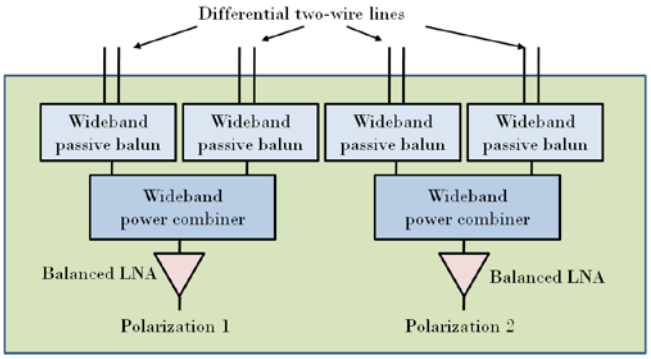

Figure 4.1: configuration of the eleven feed using four passive balun [9]

Baluns with 2-14 GHz bandwidth or similar are not commercially available, and they cannot be found in the literature either. The purpose of this chapter is to design a wideband Balun which can cover 2-14 GHz bandwidth.

The basic idea for starting the design is based on the Vivaldi antenna which is a categorized under the frequency independent antennas. Basically we start with study of Vivaldi antenna, and then continue design, in such a way that instead of radiating field from the end section, guide the balanced wave to the dipole petals.

Using this kind of wideband Baluns, makes it possible to realize scenario that has been shown in figure 4.1. It should be mentioned that, current state of art Wideband cryogenic LNAs which are developed at Caltech have frequency band from 4 to 12 GHz at the moment with the typical gain around 37 dB in 11 K and typical average noise temperature below 4k at 11k cryogenic temperature

4.2 Vivaldi antenna

The Vivaldi antenna is member of the class continuously scaled, gradually curved, end-fire travelling wave antennas [34]. At different frequency different parts of the antenna will radiate, while the size of the radiating part is constant in wavelength. Although, Vivaldi antenna has theoretically unlimited operated frequency, with constant beam width over this range, But, practically the operating bandwidth is limited by the transition from the feeding transmission line to the slot line of the antenna and by the finite dimension of the antenna. Geometry of Vivaldi antenna has been shown in figure 4.2

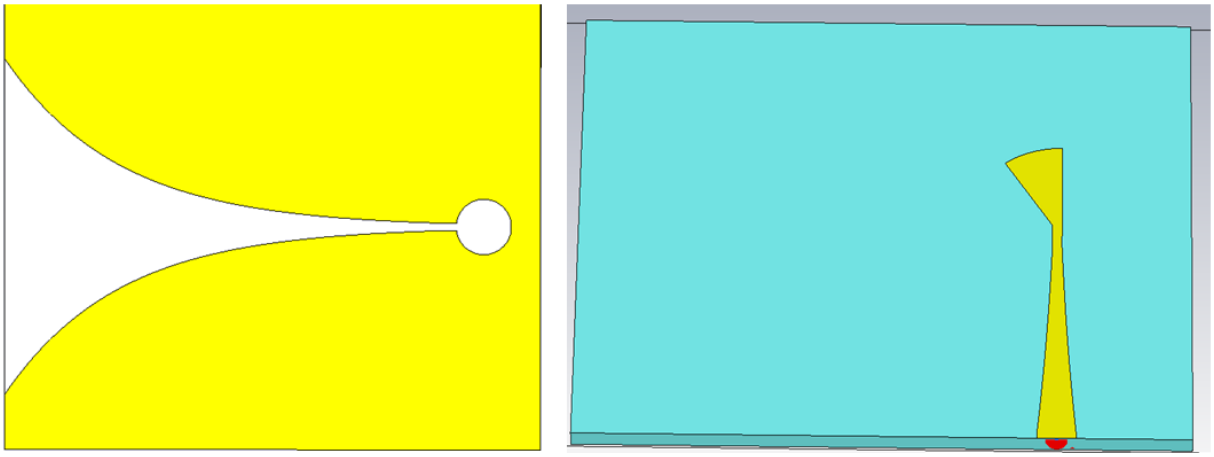

Figure 4.2: Vivaldi antenna top and bottom view

Many different designs have been purposed for Vivaldi antenna. But in any design two major subject should be considered:

- The transition from the main transition line (microstrip line in figure 4.2) to a slot line, for feeding the antenna; this should have a very wide operating frequency range and low reflection coefficient, to match the 50 ohm commercial coaxial cable. different shapes for capacitive part of the line can be found in the different references.
- The dimensions and the shape of the antenna, to obtain the required bandwidth, side lobes and back lobes, over the operating frequency range.

The idea can be explained by this fact that the energy in the travelling wave is tightly bound to the conductors when the separation is very small compared to the free space wavelength and becomes progressively weaker and more coupled to the radiation field as the separation increases

There are many applications for such a wideband antenna. The first application reported for videos receiver module. Due to the compact size and lightweight, they are good choice for see through wall application (STW). But the main point that we are interested in, is the impressive bandwidth that Vivaldi antenna can exhibit. There are two kind of Vivaldi antenna, one is the tapered slot antenna which can be seen in figure 4.2 and another one is the antipodal Vivaldi element which exhibits a very wide operating frequency range[35].

4.3 Wideband Balun

The idea for wideband balun is based on this fact that we should design balun similar to the Vivaldi antenna which is guide the wave in the unbalanced form instead of radiation from end of the structure. The starting point for simulation can be considered as below.

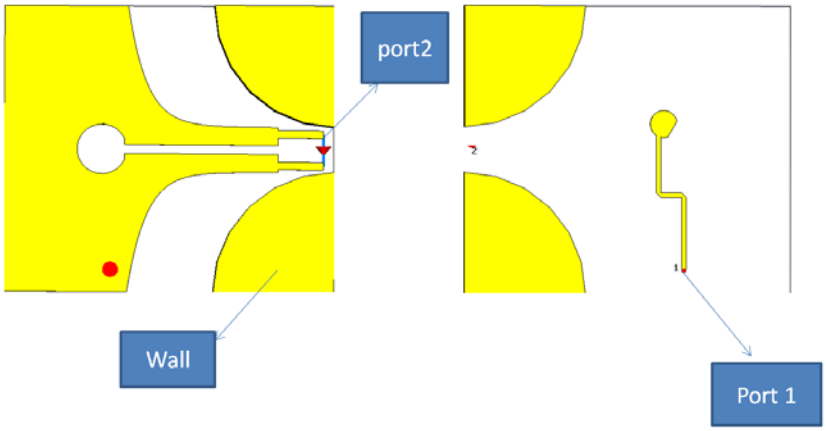

Figure 4.3: top and bottom view of the wide band Passive Balun

As it can be observed in figure 4.3, the main difference between Antenna and Balun comes from up layer which is designed to guide the wave to the coupled microstrip line (port 2) with removing metal parts from two sides of the substrate.

The preliminary result has been shown in figure 4.4

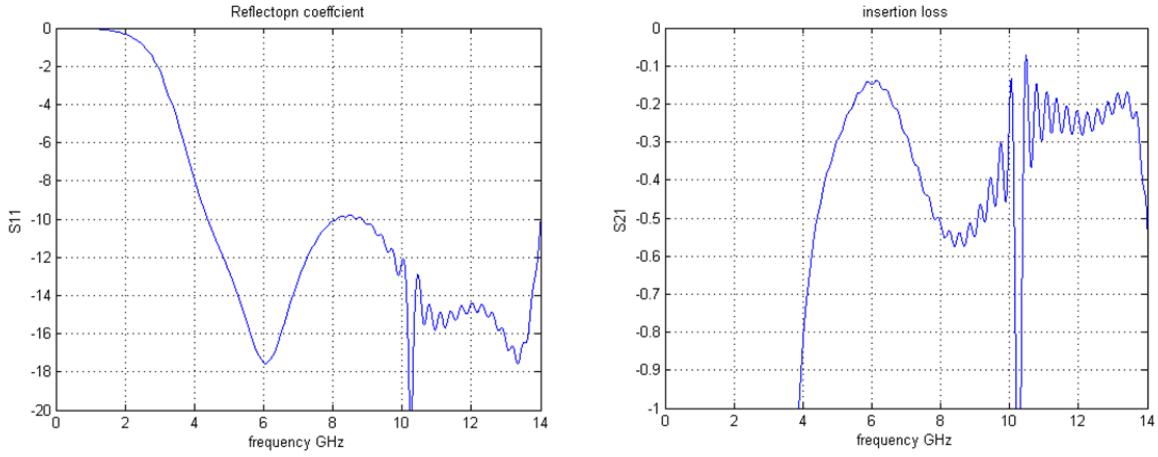

Figure 4.4: Computed S parameters for Prelimiray Model of the Passive Balun

The results are both encouraging and a bit of disappointment. It exhibit wide band performance. On the other hand performance it suffers from resonance and also bad performance in low frequency.

The fact is that, first we should find the parameters that affect the performance of the Balun and then using optimization to achieve the best performance. Here we will study in detail about all the effective parameters in performance of the balun.

It is common to use the elliptical profile in the Vivaldi antenna. Here also it can be used for the outer side of each branch. One useful formula for designing has been purposed in [36].

$$y = c_1 e^{Rx} + C_2 \qquad (4.1\ \ a)$$

$$C_1 = \frac{y_2 - y_1}{e^{Rx2} - e^{Rx1}} \qquad (4.1\ \ b)$$

$$C_2 = \frac{y1e^{Rx2} - y2e^{Rx1}}{e^{Rx2} - e^{Rx1}} \qquad (4.1\ \ c)$$

Where R is defined as the opening rate and $P_1(x_1.y_1)$ and $P_2(x_2,y_2)$ is first and last point of the exponential taper. So in this case opening rate can be consider as the parameter.

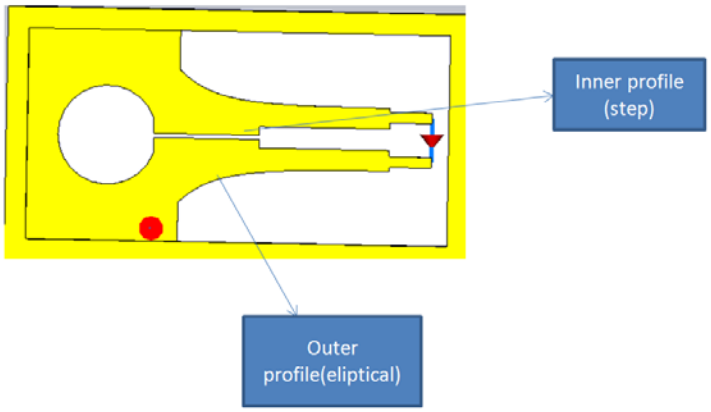

Figure 4.5: Top view of the passive Balun

Diameter of circle slot and microstrip feeding is also effective parameter. Some guidelines for the antenna counterpart have been purposed in [37]. Some results for parameter study have been shown in figure 4.6

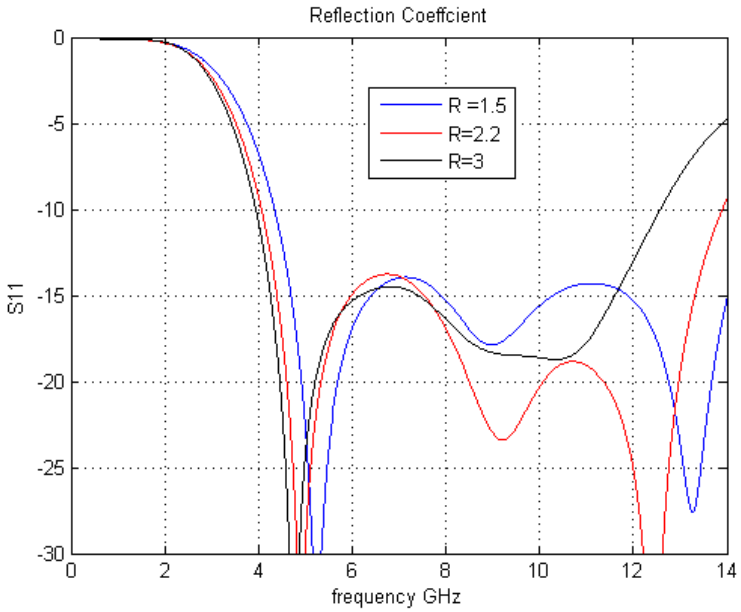

Figure 4.6: Comparison of three different profiles for Passive Balun

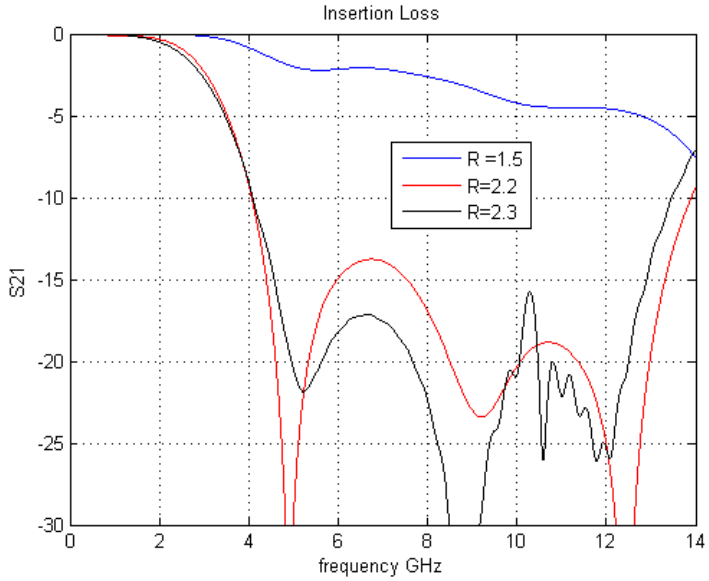

Figure 4.7: Comparison of three different profiles for Passive Balun

Figure 4.7 shows that best performance can be achieved with circle stub with radius 2 and circle slot with radius 2.2. It should be mentioned that although circle slot with radius equal 2.3 mm gives a better reflection coefficient but performance suffers from resonance at 9 GHz. See figure 4.8. Generally it means that the dimensions of cavity are also an important factor for performance of the Balun. Here we try to get the most possible compact size for the Balun.

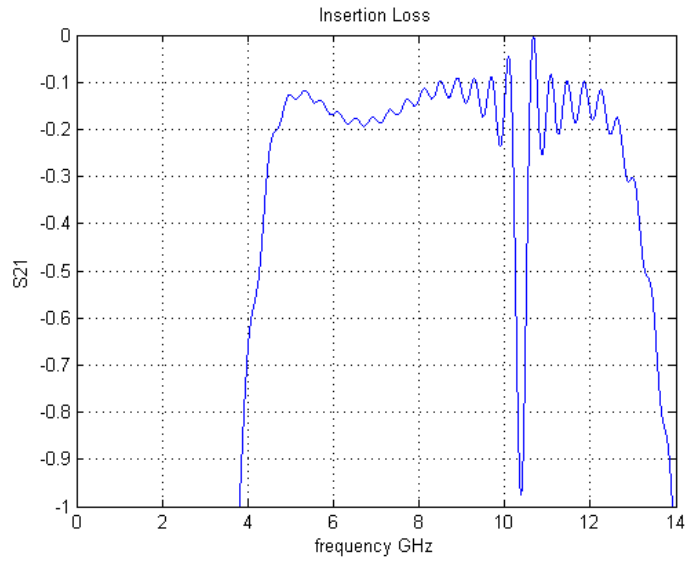

Figure 4.8: Resonance Due to the large dimension of the cavity

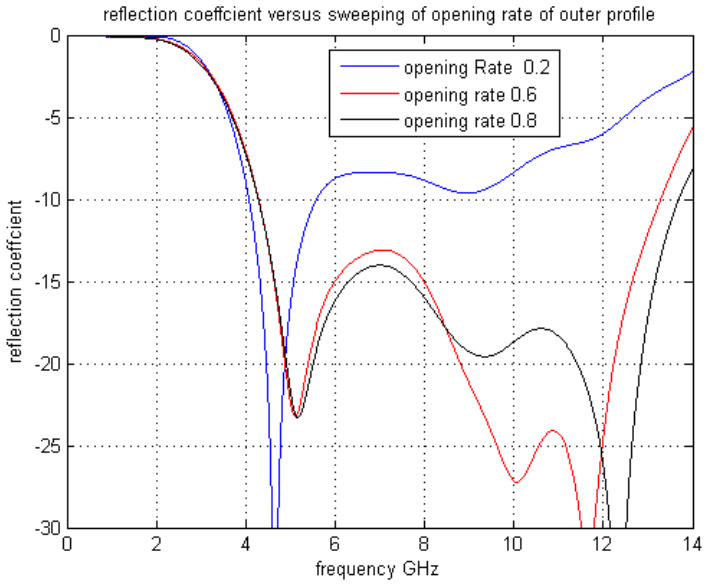

Figure 4.9: Comparison of three different profiles for Passive Balun

The most important factor for wideband performance is the coupling between microstrip line and slot line in up layer which is controlled by location of microstrip line and shape of the inner part of the structure. There are two different choices for inner part. It can be designed as step structure (figure 4.9) or elliptical profile (figure 4.10).

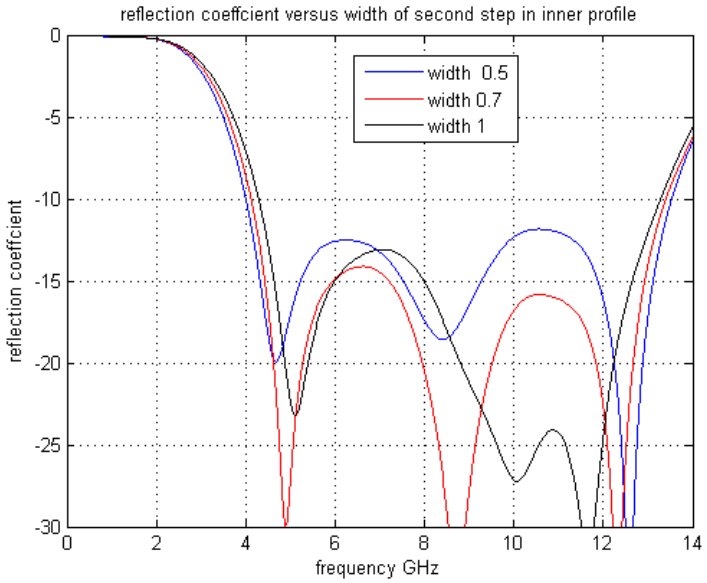

Figure 4.10: Comarison of three diffrenet profile for Passive Balun

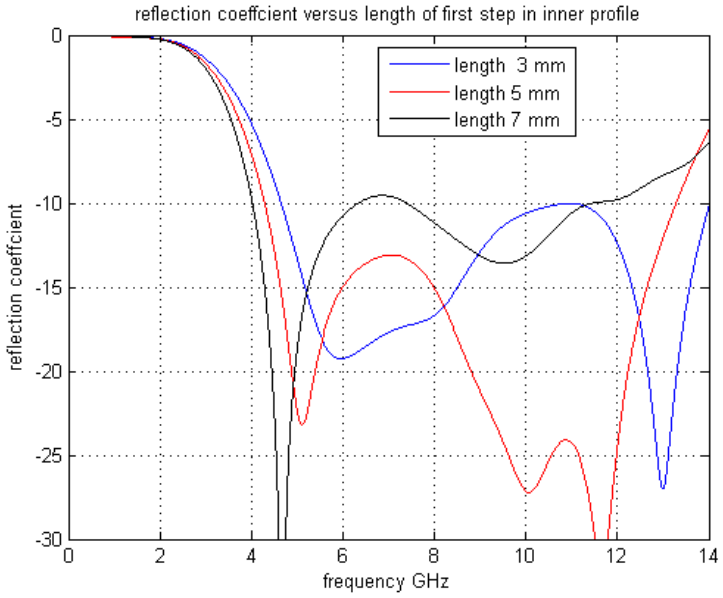

Figure 4.11: Comparison of three different profiles for Passive Balun

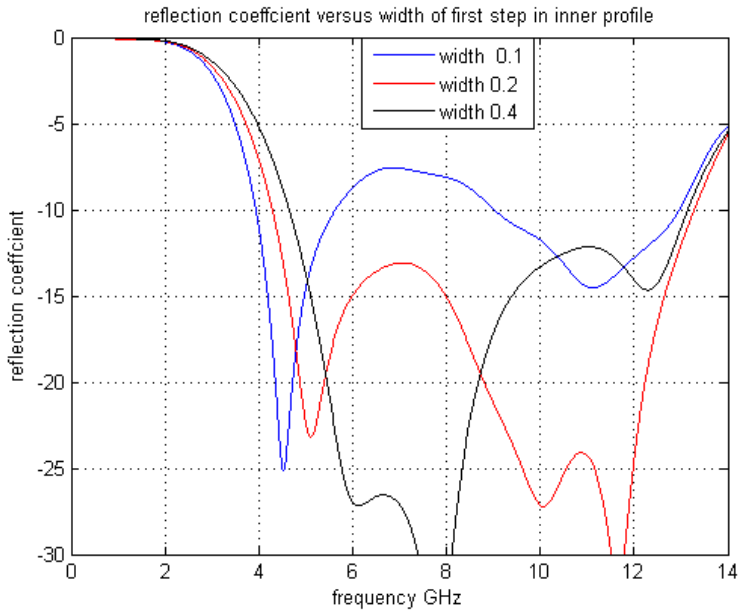

Figure 4.12: Comparison of three different profiles for Passive Balun

4.4 Microwave resonator

The new descrambler board has potential to excite cavity modes in operated frequency bandwidth. It is therefore very important to find these resonance frequencies to remove or shift them to higher frequencies. We therefore need to study more about the cavity modes and microwave resonators. Here we will explain the theory of microwave resonator based on the chapter 6 in [20] .

4.4.1 Theory

A cavity can be considered as a volume enclosed by a conducting surface and whiten which an electromagnetic field can be excited. The electric and magnetic energies are stored in the volume of the cavity can be dissipated in the metallic walls or dielectric which fills the cavity. The fields in the cavity maybe excited, or coupled to an external circuit, by means of small coaxial line probes or loops. Alternatively, the cavity maybe coupled to the waveguide by means of the small aperture in a common wall. The aim of this chapter is to find relation between resonant frequency and size of the cavity. Below we will study about two different kinds of cavities based on the discussion in [20] .

4.4.2 Rectangular waveguide cavities

The geometry of rectangular cavity is shown in figure 4.13. It consists of a length d of the rectangular waveguide shorted at both ends (z=0, z=d). First, considering a lossless cavity we can determine the resonant frequency, and then we determine the Q according to the perturbation method . For finding the Q, we treat the cavity like rectangular waveguide which is terminated on both ends with metal walls(x=0,a and y=0,b). Then it is only necessary to enforce the boundary conditions that $E_x = E_y = 0$ on the end walls at z=0, d.

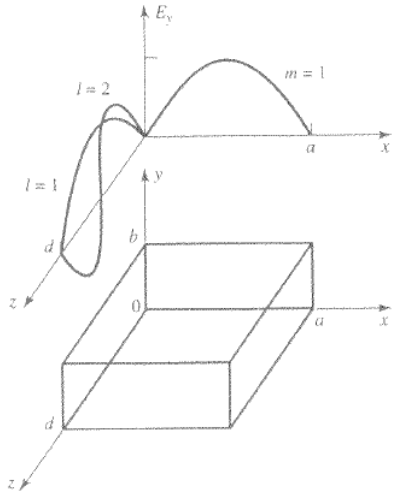

Figure 4.13: a rectangular cavity and the electric field distributions [20]

We know that the TE_{mn} or TM_{mn} for the rectangular waveguide mode can be written as

$$E_t(x,y,z) = e(x,y)\left[A^+e^{-j\beta_{mn}z} + A^-e^{-j\beta_{mn}z}\right], \qquad (4.2)$$

Where $e(x,y)$ is the transverse variation of the mode, and A^+, A^- are arbitrary amplitudes of the forward and the backward traveling waves. The propagation constant of the m, nth TE or TM mode is

$$\beta_{mn} = \sqrt{k^2 - (\frac{m\pi}{a})^2 - (\frac{n\pi}{b})^2} \qquad (4.3)$$

Where k=$\omega\sqrt{\mu\epsilon}$, and μ, ε are the permeability of the material filling the cavity. Applying the condition that $E_t = 0\ at\ z = 0$ to implies that $A^+ = -A^-$ (as we should expect for reflection from a perfectly conducting wall). Then the condition that $E_t = 0$ at z=d leads to the equation

$$E_t(x,y,d) = -e(x,y)A^+2jsin\beta_{mn}d = 0 \qquad (4.4)$$

The only nontrivial ($A^+ = 0$) solution thus occurs for

$$\beta_{mn} d = l\pi \quad l = 1,2,3, \ldots \ldots \qquad (4.5)$$

Which implies that the cavity must be an integer multiple of half guide wave-length long at the resonant frequency. No nontrivial solutions are possible for other lengths or for frequencies other than resonant frequencies. The rectangular cavity is thus a waveguide version of the short circuited $\frac{\lambda}{2}$ Transmission line resonator.

A resonant wave number for the rectangular cavity can be defined as

$$K_{mnl} = \sqrt{(\frac{m\pi}{a})^2 + (\frac{n\pi}{b})^2 + (\frac{l\pi}{d})^2} \qquad (4.6)$$

Then we can refer to the TE_{mn} or TM_{mn} resonant mode of the cavity, where the indices the indices m, n, l refer to the number of variations in the standing wave pattern in the x,y,z directions, respectively. The resonant frequency of the TE_{mn} or TM_{mn} mode is then given by

$$f_{mnl} = \frac{ck_{mnl}}{2\pi\sqrt{\mu_r \epsilon_r}} = \frac{c}{2\pi\sqrt{\mu_r \epsilon_r}} \sqrt{(\frac{m\pi}{a})^2 + (\frac{n\pi}{b})^2 + (\frac{l\pi}{d})^2} \qquad (4.7)$$

If $b < a < d$, the dominant resonant mode will be the TE_{101} mode corresponding to the TE10 dominant waveguide mode in a shorted guide of length $\frac{\lambda_g}{2}$. The dominant TM mode is the TM_{110} mode.

4.4.3 Circular waveguide cavities

Here we have the theory for circular cavity which is similar to rectangular cavity. So, we can solve the problem for circular waveguide which is terminated in both ends with metal walls. Since the dominant circular waveguide mode is the TE_{11} mode, the dominant cylindrical cavity mode isTE_{111}.

Circular cavities are often used for microwave frequency meters. The cavity is constructed with a moveable top wall to allow mechanical tuning of the resonant frequency, and the cavity is loosely coupled to a waveguide with small aperture. In operation, power will be absorbed by the cavity as it tuned to the operating frequency of the system.

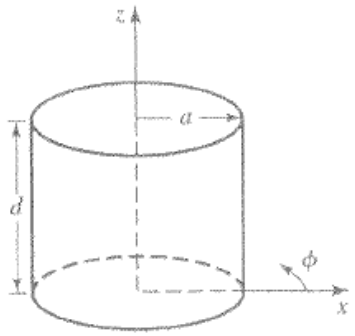

Figure 4.14: A cylindrical resonant cavity [20]

The geometry of a cylindrical cavity is shown in figure 4.14. As in the case of the rectangular cavity, the solution is simplified by beginning with the circular waveguide modes, which already satisfy the necessary boundary condition on the circular waveguide wall. We have eq 4.8 for transverse electric field of circular waveguide mode.

$$E_t(x,y,z) = e(\rho,\varphi)\left[A^+e^{-j\beta_{mn}z} + A^-e^{-j\beta_{mn}z}\right], \qquad (4.8)$$

Where $e(\rho,\varphi)$ represents the transverse variation of mode, and $A^+$and $A^-$are arbitrary amplitudes of the forward and backward traveling waves. The propagation constant of the TE_{nm} mode is

$$\beta_{nm} = \sqrt{k^2 - (\frac{p'_{nm}}{a})^2} \qquad (4.9)$$

While the propagation constant of the TM_{nm}, mode is,

$$\beta_{nm} = \sqrt{k^2 - (\frac{P_{nm}}{a})^2} \qquad (4.10)$$

Where k=$\omega\sqrt{\mu\varepsilon}$

Now in order to have E=0 at z=0, d, we must have$A^+ = -A^-$, and, and

$$A^+ \sin\beta_{nm}d = 0, \qquad (4.11)$$

$\beta_{nm}d = l\pi$, for $l = 0,1,2,3,\ldots$.

Which implies that the waveguide must be an integer number of half-guide wavelengths long. Thus , the resonant frequency of the TE_{nml} mode is

$$f_{nml} = \frac{c}{2\pi\sqrt{\mu_r \epsilon_r}}\sqrt{(\frac{P'_{nm}}{a})^2 + (\frac{l\pi}{d})^2} \qquad (4.12)$$

And the resonant frequency of the TM_{nml} mode is

$$f_{nml} = \frac{c}{2\pi\sqrt{\mu_r \epsilon_r}}\sqrt{(\frac{P_{nm}}{a})^2 + (\frac{l\pi}{d})^2} \qquad (4.13)$$

Then the dominant TE mode is the TE_{111} mode, while the dominant tm mode is the TM_{110} mode.

4.4.4 Cavity modes in Passive Balun

As it has been shown in figure 4.15 our passive Balun is the two layer structure and includes cavity in feeding part, so it is possible to have resonance in operated bandwidth. Actually it is very crucial for the performance of the Balun to remove these resonances or shift them to higher frequencies. In this part first we look at the possible resonances that will happen in the desired band width and then try to remove or shift them to higher frequencies due to this fact that according to the formula 4.6 & 4.13 the resonances will shift to higher frequencies if we reduce the dimensions of the cavity.

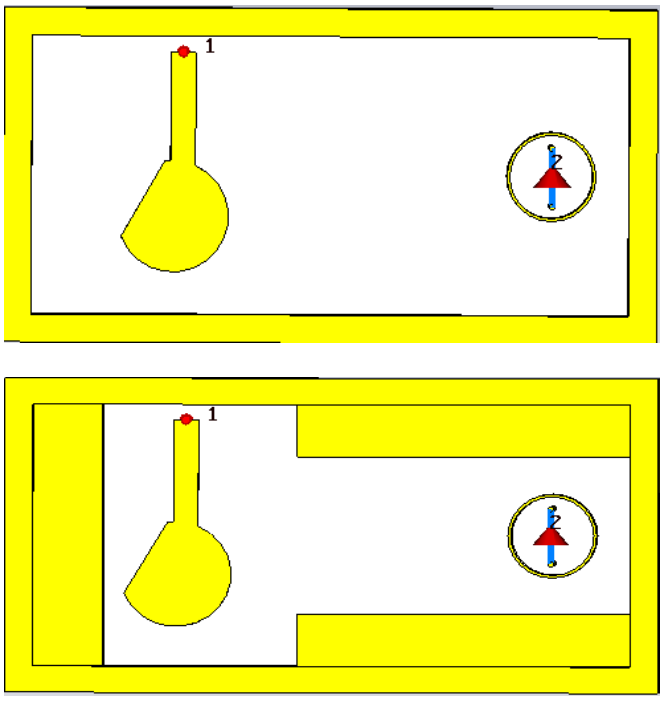

Figure 4.15: Bottom view of the passive Balun with and without cavity

It should be mentioned that we cannot have the metal below the upper metal parts, since it destroy the field in high frequency. So this can be considered as the restriction for having the smaller cavity. On the other hand height of the cavity is the degree of the freedom, but unfortunately affects the bandwidths and low frequency performance of the Balun. Figure 4.16 shows return loss of the passive Balun for different values of Air Gap in feeding port. Figure 4.17 shows return loss of passive Balun for reduced dimensions of cavity and simple cavity.

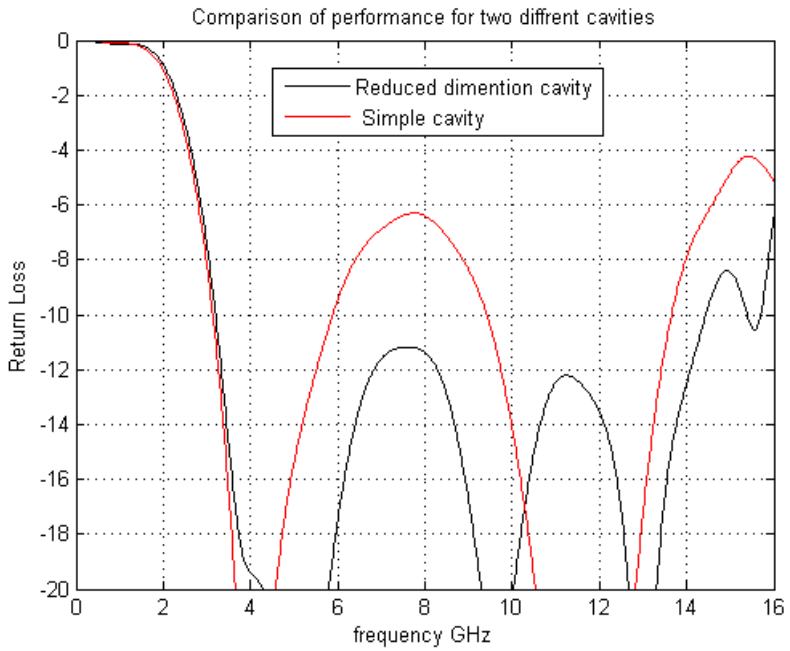

Figure 4.16: Comparison of the performance for simple cavity and reduced dimension cavity

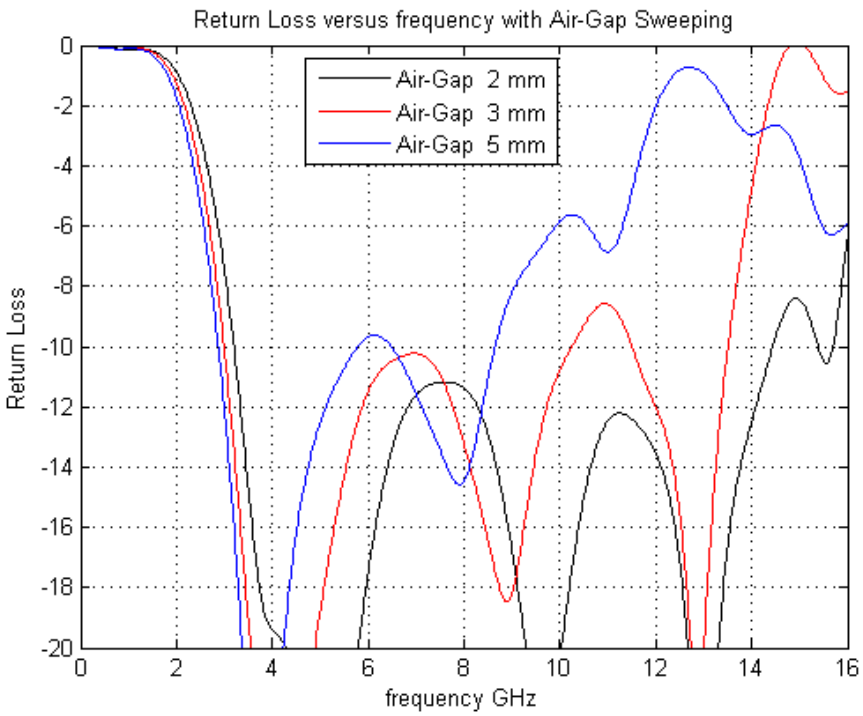

Figure 4.17: Comarison of three diffrenet Air gap for Passive Balun

It can be observed from the figure 4.18 that air gap around 2 mm gives the better performance and also reduced dimensions cavity is much better in terms of matching efficiency.

So according to the above discussion we should find the optimum dimensions for the cavity height that gives the best performance and also avoid the resonance in the operated bandwidth.

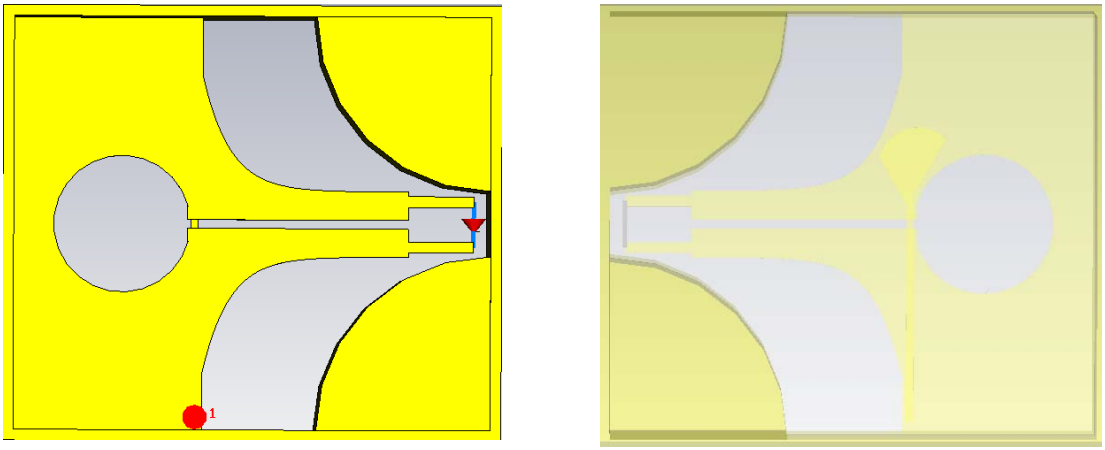

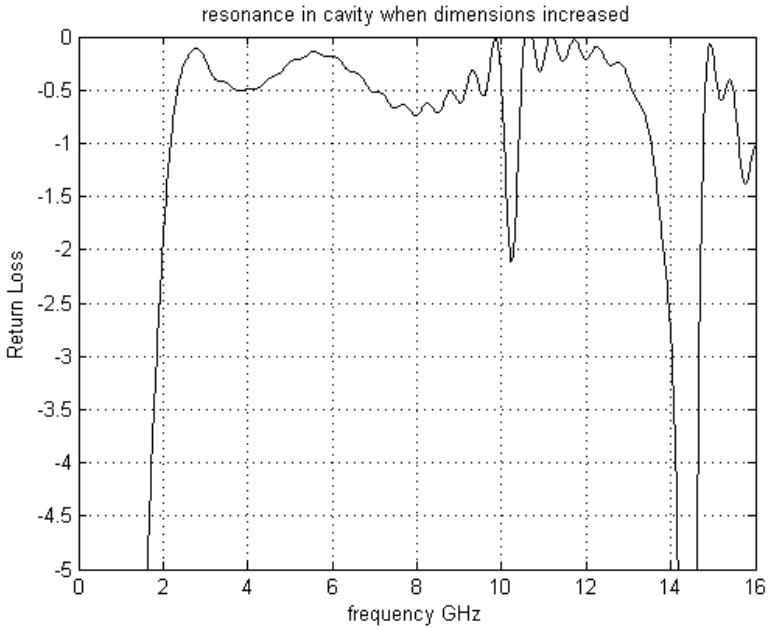

Figure 4.18: CST Model Top and Bottom view of passive Balun (Bottom) Computed Return Loss

We can see in figure 4.18 that increasing dimensions of the cavity introduced resonance to the result in 10 and 14 GHz.

4.5 Center Puck

Figure 4.19 shows the configuration of current center Puck. It supports four vertical two wire lines, each one made of two silver plated steel needles. Each needle is soldered at one end to each of the

metal strips feeding the log periodic dipole arrays above the ground plane, and at the other end to a corresponding microstrip line on the descrambling board

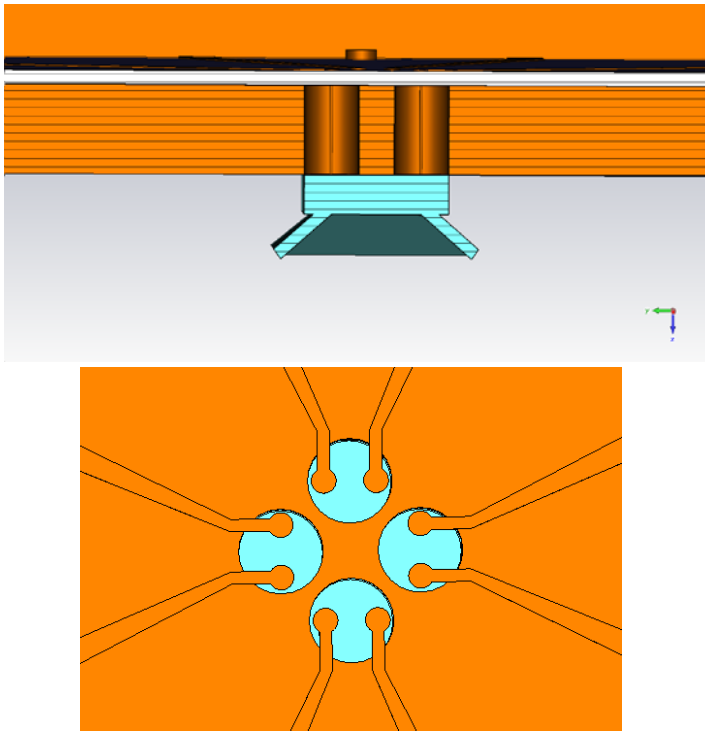

Figure 4.19: Cross section and top view of the center puck

Center puck has been consists of two parts. First, four hole in ground plane which is filled with air to provide 200 ohm diffrential impedance same as the Antenna impedance . diameter of the hole is calculated from formula 2.10

$$Z = \frac{1}{\pi}\left(\frac{\mu_0}{\varepsilon'}\right)^{\frac{1}{2}}\left[ln\left(2p\frac{1-q^2}{1+q^2}\right) - \frac{1+4p^2}{16p^4}(1-4q^2)\right] \qquad (4.14)$$

Where the dimensions of the parralel steel needle lines (seperation, needle diameter) are matched such that parralel wires get soldered at the center of the strips, and simultanously give 200 ohm characterstic impedance.

$$Z = \frac{1}{\pi}\left(\frac{\mu_0}{\varepsilon'}\right)^{1/2} cosh^{-1}\frac{D}{d} \qquad (4.15)$$

Second, two millimeter thickness of TMM3 substerate which provide the mechanical support for soldering above the ground plane. As we will show later untill 10 GHz most of the degradation will appear due to the mismatch factor, and further degradation below this will indicates ohmic and raditaion losses wich is appeared above 10 GHz.

Below we compare two diffrenet center pucks, current design and new design based on this fact that by extending tubes 1 millimeter we can reduce thickness of substerate which is important factor for improving insertion loss for high frequency applications.

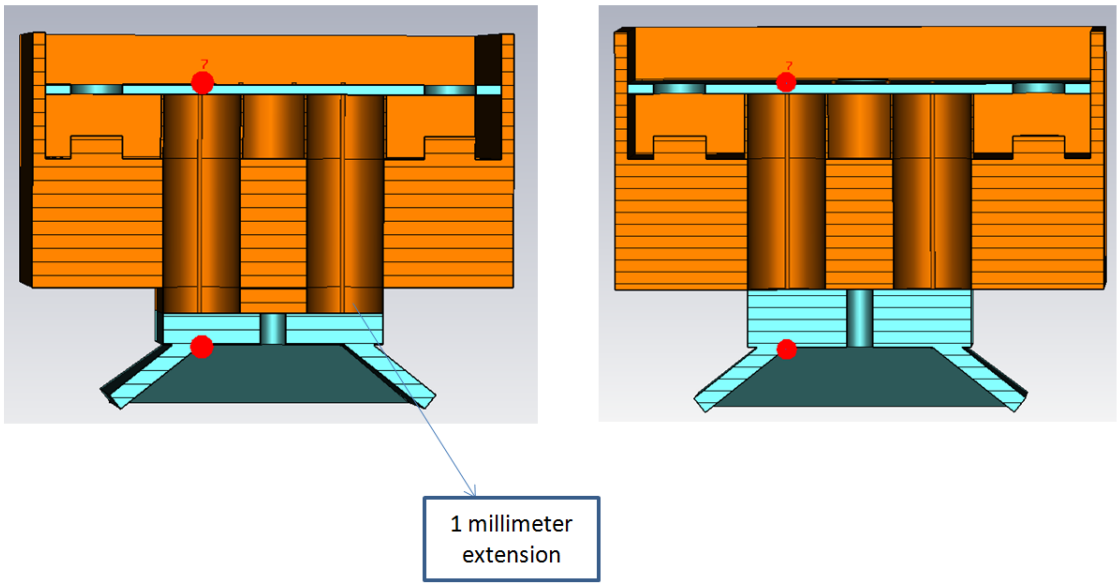

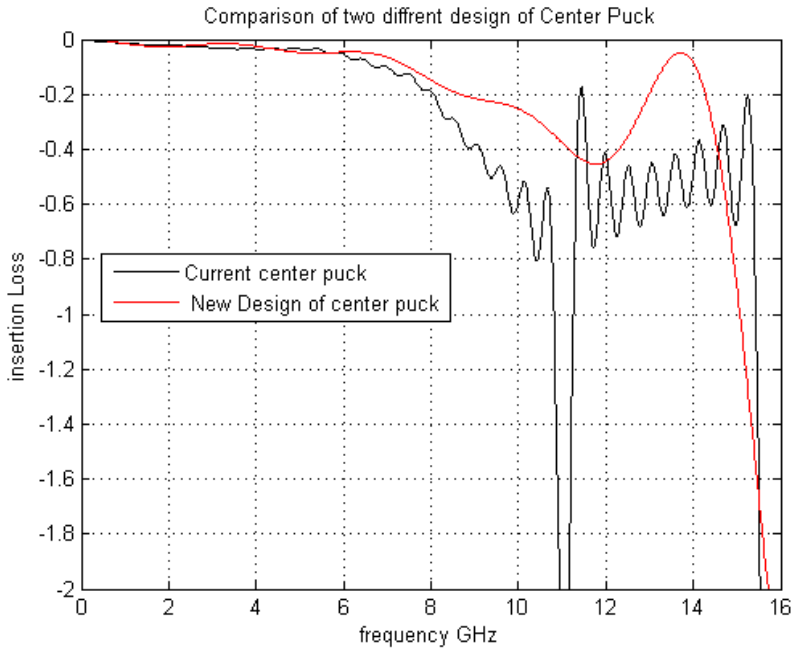

Figure 4.20: Comparison between Performance of current and new center puck

It can be observed from figure 4.20 that extension of tubes or reducing tickness of the substerate will cause to significant improvement in insertion loss. In section 6.1 we have more studies about this design and manifacturing problems due to this change.

Another possibility for changing in center puck is the material inside the tubes. We can substitute air filled tubes with teflon filled tubes. Here we will show performance of the teflon filled tubes in compare with air filled tubes.

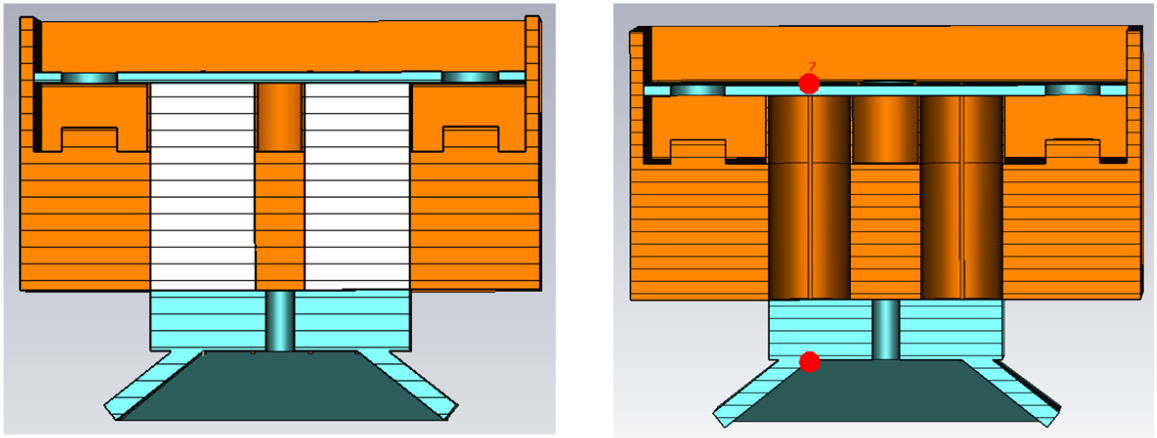

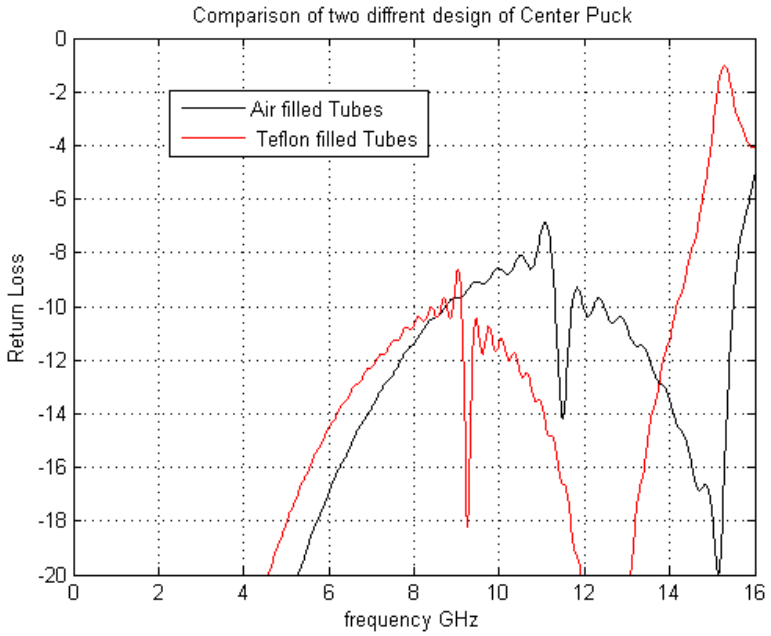

Figure 4.21: comparison of performance of two different design of center puck

It seems that teflon filled tubes has better performance above 10 GHz application. Diameter of the teflon filled can be calculted from equation 2.9 and it is around 3.8 mm.

It should be mentiond that although according to the simulation reducing the tickness of the substerate gives much better performance in terms of the insertion loss, but at peresent we can not manufacture such a center puck because the petal should be mounted in the specefic angle with its phase center in the center of the ground plane and also with only 1 mm tickness of TMM3 we can not provide sufficient mechanical support for petals.see figure 4.22.

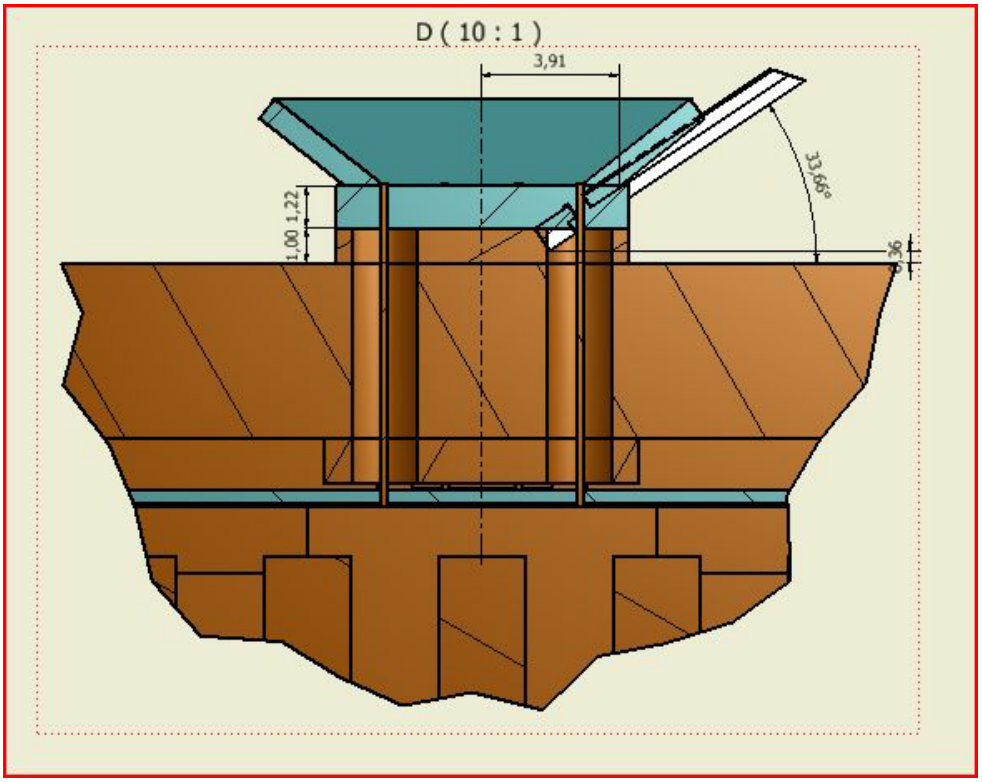

Figure 4.22: drawing of petals with new center puck

The new center puck (the part in copper) is 1mm thick + 1.22mm of isolator. So it cannot provide mechanical support for petals and the only alternative is to keep the current design of the center puck.

4.6 Surface waves in substrate

We use the lossy TMM3 as substrate ($\varepsilon = 3.27$) with thickness t=0.5 mm. Until now we have assumed that we can have the same shape of the substrate as the cavity shape. The main idea behind this fact is to avoid wave to leak to other parts of substrate, figure 4.23 shows field distribution when we have the rectangular substrate.

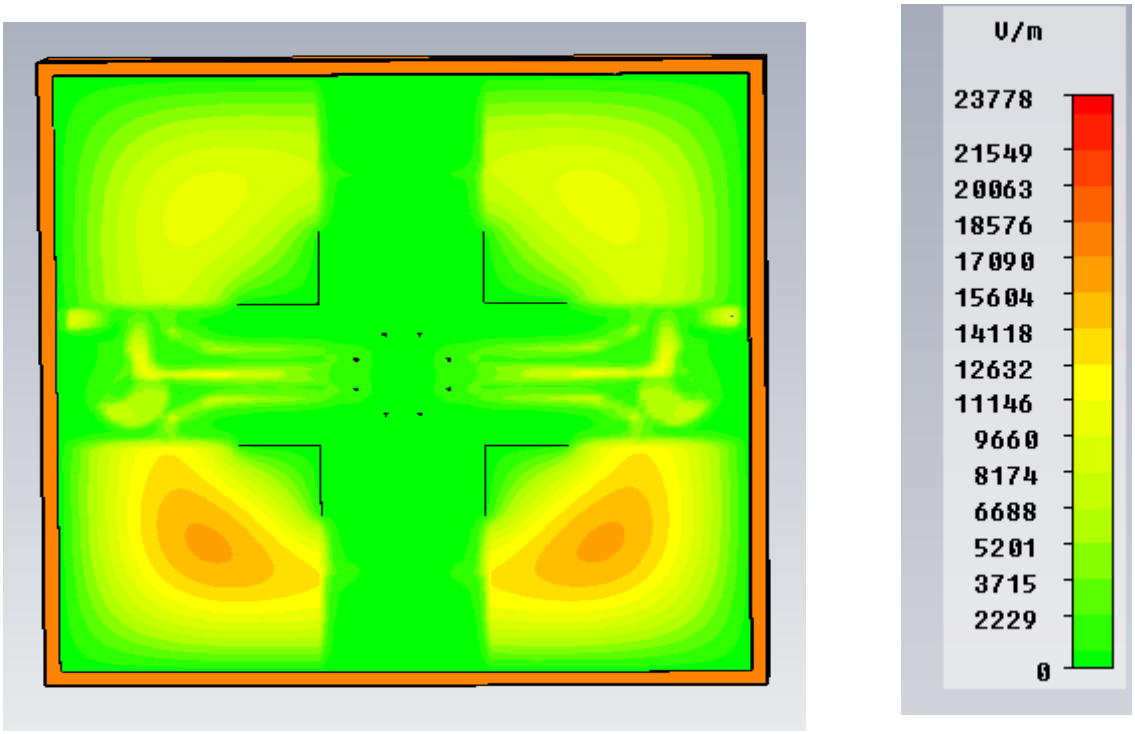

Fig 4.23: field distribution for rectangular waveguide

4.7 Basic theory of surface waves

Depend on the frequency band there are different illustration for surface waves. In optics, they are called surface plasmons, but in radio frequencies, they are simply called surface currents. Considering electromagnetic waves, that decay exponentially away from the dielectric interface gives insight for analytical investigation of surface waves and then as interesting result we find that this kind of waves can only exist in materials with a non-positive dielectric constant [38]. The same result can be achieved by starting from different point of view. Due to this fact the effective surface impedance can be assigned for each material, for metals it can be determined by the skin depth. We find that the skin depth is equivalent to the surface wave penetration depth, and thus surface waves are not nothing more than ordinary surface currents, which are well understood at radio frequencies. Here we will explain the basic theory behind surface waves based on the [38] .

4.8 Dielectric interface

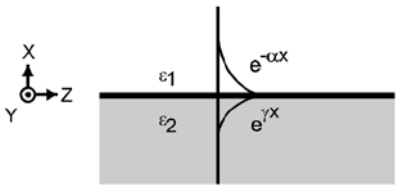

Figure 4.24: A surface Wave between two dissimilar media

Surface waves can occur on the interface between two dissimilar materials, such as metal and free space. To derive the properties of surface waves on general interface, begin with two materials having two different dielectric constants, ϵ_1 and ε_2. The surface is in the YZ plane, with material 1 extending in the +X direction and material 2 in the –X direction as shown in figure 4.24.

For waves to be bound to the surface , assume it decays in the +X direction with decay constant α, and in the –X direction with decay constant γ . consider first a TM surface wave, for which $E_y = 0$. The electric field in material 1 has the following form, in which the factor $e^{j\omega t}$ is implicit.

$$E_X = A.e^{-jkZ-\alpha X} \qquad (4.16\ a)$$

$$E_y = 0 \qquad (4.16\ b)$$

$$E_Z = B.e^{-jkZ-\alpha X} \qquad (4.16\ c)$$

In material 2, the electric field has the same form, given below.

$$E_X = A.e^{-jkZ+\gamma X} \qquad (4.17)$$

$$E_y = 0 \qquad (4.18)$$

$$E_Z = B.e^{-jkZ+\gamma X} \qquad (4.19)$$

Here A, B, C, and D are constants. Recall the following Maxwell's equations.

$$\nabla \times B = \frac{\varepsilon_r}{c^2}\frac{\partial E}{\partial t} \qquad (4.20)$$

$$\nabla \times E = -\frac{\partial B}{\partial t} \qquad (4.21)$$

These can be combined to yield the equation below.

$$\nabla \times \nabla \times E = -\varepsilon_r \frac{\omega^2}{c^2}\frac{\partial^2 E}{\partial t^2} \qquad (4.22)$$

This can be expended explicitly, bearing in mind that the Y derivative of the electric field on both side is zero.

$$X\left(-\frac{\partial^2 E_x}{\partial z^2}+\frac{\partial^2 E_Z}{\partial x \partial z}\right)+Z\left(\frac{\partial^2 E_x}{\partial x \partial z}-\frac{\partial^2 E_Z}{\partial x^2}\right)=\varepsilon\frac{\omega^2}{c^2}(xE_x+zE_z) \qquad (4.23)$$

By inserting equation 4.16 into equation 4.23, we obtain equations for the fields above the surface.

$$K^2A + jk\alpha B = \varepsilon_1\frac{\omega^2}{c^2}A \qquad (4.24)$$

$$jk\alpha A - \alpha^2 B = \varepsilon_1 \frac{\omega^2}{c^2} B \qquad (4.25)$$

Similarly, by inserting equation 4.24 into equation 4.26, we obtain equations for the fields below the surface.

$$K^2 C - jkYD = \varepsilon_2 \frac{\omega^2}{c^2} C \qquad (4.26)$$

$$-jkYC - Y^2 D = \varepsilon_2 \frac{\omega^2}{c^2} D \qquad (4.27)$$

Finally, the tangential electric field and the normal electric displacement must be continuous across the interface, as specified by the following boundary conditions.

$$A = C \qquad (4.28\ a)$$

$$\varepsilon_1 B = \varepsilon_2 D \qquad (4.28\ b)$$

We can combine equation 4.26 and equation 4.25 to solve for the wave vector, k, and the decay constants, α and Y.

$$K = \sqrt{\frac{\varepsilon_1 \varepsilon_2}{\varepsilon_1 + \varepsilon_2}} \frac{\omega}{c} \qquad (4.29\ a)$$

$$\alpha = \sqrt{\frac{-\varepsilon_1{}^2}{\varepsilon_1 + \varepsilon_2}} \frac{\omega}{c} \qquad (4.29\ b)$$

$$Y = \sqrt{\frac{-\varepsilon_2{}^2}{\varepsilon_1 + \varepsilon_2}} \frac{\omega}{c} \qquad (4.29\ c)$$

These equations describe surface waves on a general interface between two dissimilar dielectric materials. For simplicity, assume that one of the materials is free space, $\varepsilon_1 = 1$.

Dropping the subscript from ε_2 , we obtain the following results.

$$K = \sqrt{\frac{\varepsilon}{1 + \varepsilon}} \frac{\omega}{c} \qquad (4.30\ a)$$

$$\alpha = \sqrt{\frac{1}{1+\varepsilon}}\frac{\omega}{c} \qquad (4.30 \quad b)$$

$$\Upsilon = \sqrt{\frac{-\varepsilon^2}{1+\varepsilon}}\frac{\omega}{c} \qquad (4.30 \quad c)$$

Discussion about surface waves, continue by considering two different conditions for ε. If ε is positive, then α and Υ are imaginary and the waves do not decay with distance from the surface; which explains propagation of plane waves through the dielectric interface. On the other hand if ε is less than -1, or if it is imaginary, the solution describes a wave that is bound to the surface and decay exponentially with distance. These TM surface waves can occur on metals or other materials with non-positive dielectric constants.

The solution for TE surface waves can be obtained from the foregoing analyses by the principle of duality. If the electric fields are exchanged, and μ is substituted for ε, the solution above can be applied to the TE cases.

4.9 Possible solutions for avoiding surface waves in substrate

To avoid wave to leak to the other parts of substrate we should cut the substrate in extra parts. Figure 4.25 shows the required shape of the substrate to avoid surface waves in substrate.

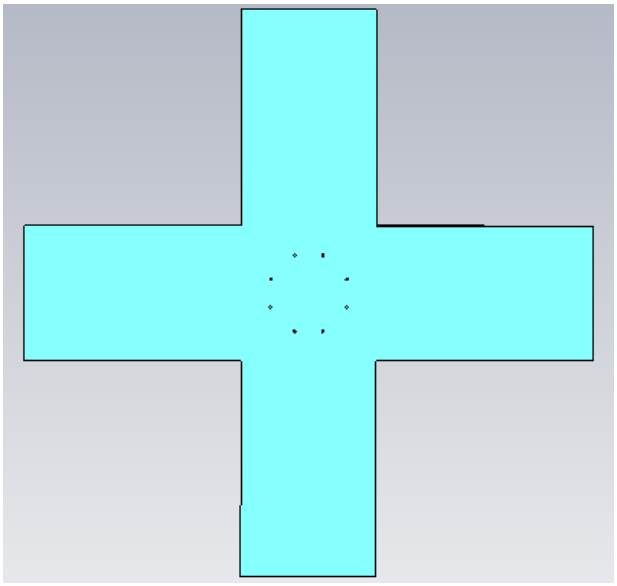

Figure 4.25: plus shape microstrip

Although with such a shape of substrate problem with surface waves will be solved, but the fact is this shape of substrate will be problematic in terms of manufacturing and soldering. It should mentioned that thickness of substrate is around 0.5 mm and due to some design consideration (see section 6.1) it

does not have mechanical support in center, so by removing the side parts of substrate it will be tricky to provide mechanical support for the board.

There are some alternative solutions for providing mechanical support. First solution is based on the increasing the thickness of the substrate to another available commercial thickness. See Appendix B (t=0.79 mm). The point is, increasing thickness of substrate has an extreme effect in coupling part and degrade the performance significantly. So, it is required to optimize the whole structure which is very time consuming. Figure 4.26 shows the best obtained performance after increasing thickness of substrate.

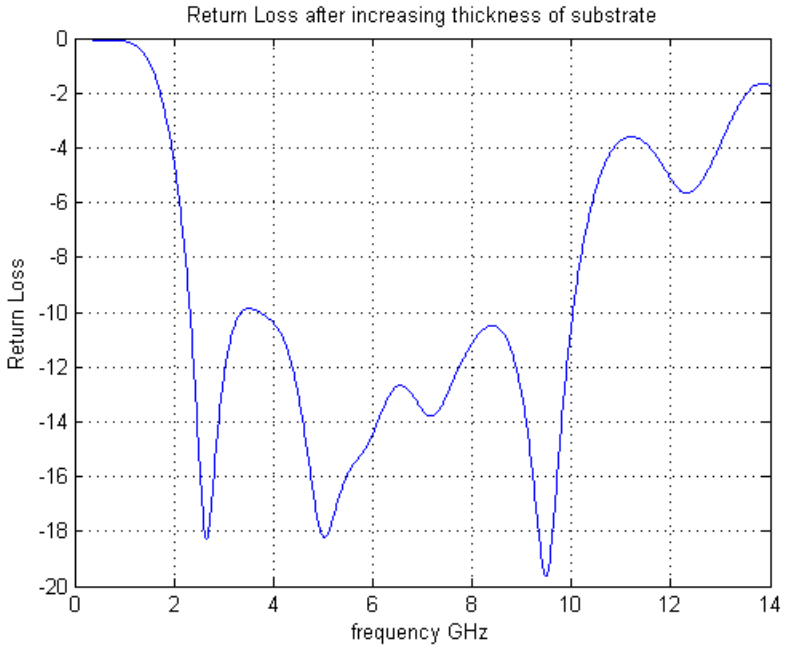

Figure 4.26: Simulation result after increasing 87thickness

It can be observed that not only the performance degrade with increasing thickness, also the bandwidth will reduce to 2-10 GHz.

4.9.1 Photonic crystals

Photonic band gap materials are a new type of artificial materials, which are the photonic analogs of semiconductors, since The behavior of electromagnetic waves in photonic crystals is similar to behavior of electron in semiconductor. These artificially engineered periodic materials which control the propagation of electromagnetic waves may play a role that is as important in the field of photonics as the laser plays today in the optoelectronic systems.

Since the discovery of photonic crystals (PC), they are of interest for applications like efficient microwave device or optical lasers. Another exciting application for Pc's which is more interested for us is using as a substrate for antenna configurations.

Microstrip antenna is the popular type of the antenna which is received lots of attention in last two decades. The major problem with microstrip antenna is the low efficiency which is mainly due to the

high percentage of loss in the substrate. So, for many years, finding a creative solution to have the high efficiency and compact size together was a challenging problem in this field.

PC's can offer a real solution to this problem. Utilized in patch antenna configurations as substrate, PC's suppress both substrate modes and surface waves which are excited by the radiating element. Suppression or reduction of surface waves not only improves antenna efficiency, but also reduces side lobe level that is caused by diffraction of the surface waves at the edges of the antenna substrate.It should be mentioned that, using tick substrate with high dielectric value may cause 60% loss.

Physical theory behind the suppression of surface waves by photonic crystals can be found in [39]. Also gives a comprehensive description of suppression of surface waves by high impedance surfaces and band gaps. Here we present a theory for surface wave in substrate and using via holes to suppress them.

Surface waves properties are summarized in the dispersion diagram shown in figure 4.27. Unlike the conventional high impedance surfaces, grounded dielectric slab can support the TM waves in all frequencies and TE waves in frequencies above the cut off has been given expression below

$$f = \frac{c}{4t\sqrt{\varepsilon - 1}} \qquad (4.31)$$

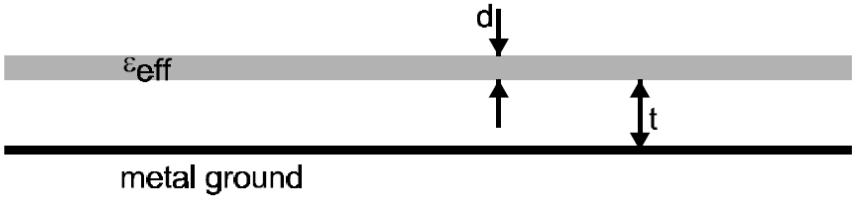

Figure 4.27: effective medium model for capacitive sheet above the ground plane [38]

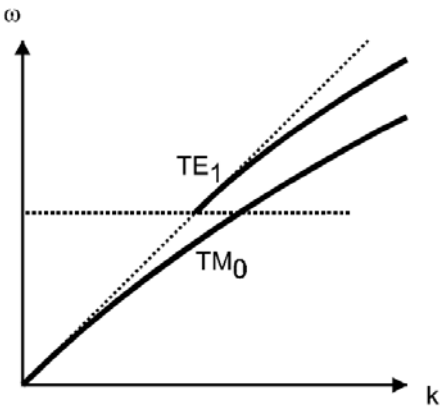

Figure 4.28: Dispersion curves for surface waves on a grounded dielectric slab [38]

4.9.2 The Role of the Conducting Vias

The importance of the conducting vias can be understood by adding metallic corrugation to the grounded dielectric slab. By increasing the frequency, the wave penetrates into the corrugations to finally fit inside the one of them and cease to propagate (see figure 4.29). This condition, illustrated in figure 4.29 occurs when the structure is one quarter wavelength tick.

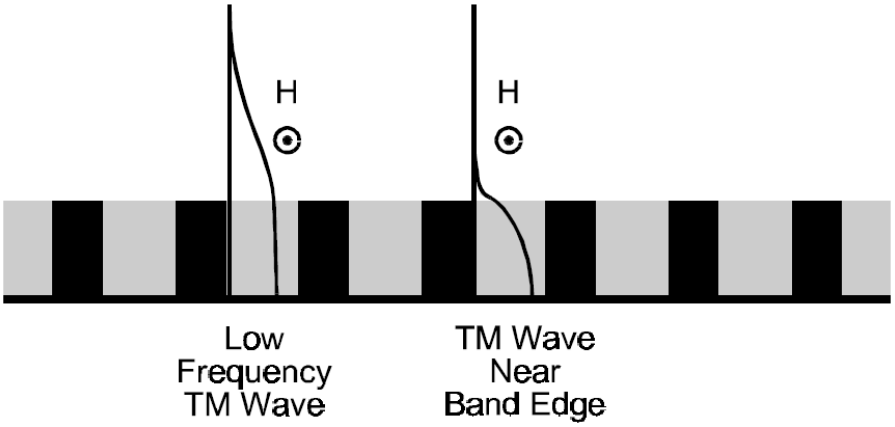

Figure4.29: Metal corrugations preventing high frequency TM surface waves [38]According to the

discussion in adding via holes to the grounded dielecteric acts like a high impedance surface. figure 4.30 shows an equavalent circuit for the structure before adding the via holes.. Although the capacitive layer does not support propogating TM surface waves, the inductive metal surface below it does. So, this structure without connecting via holes is like the suspended dielecteric layer above the metal plate.

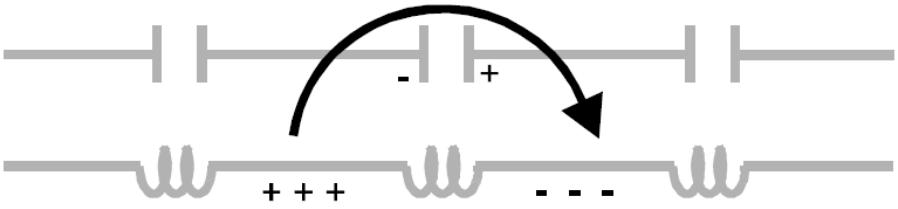

Figure 4.30: Effective circuit in the absence of conducting vias

Adding via holes will change the nature of structure.The vertical electeric field of the TM surface wave causes currents to follow through the vias, as shown in figure 4.31. now we have connected network of capacitors and inductors which acts similar to the network of the paralel resonators near bandgap. Above the the resonace frequency, the circuit is capacitive , and the structure does not support TM surface waves.

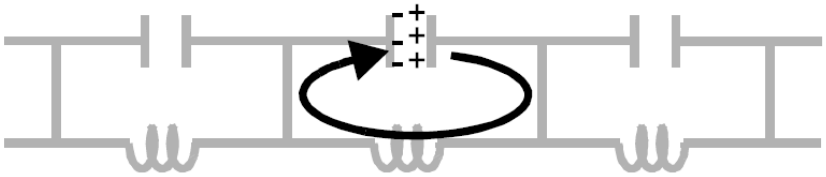

Figue 4.31: Vertical conducting vias linking the two surfaces together[38]

4.9.3 Simulation results for via holes in substrate

As the starting point we try the substitute cross shape substrate with rectangular substrate. Figure 4.32 and 4.33 show results for rectangular substrate when PMC (perfect magnetic conductor) and open boundary condition have been applied to the structure.

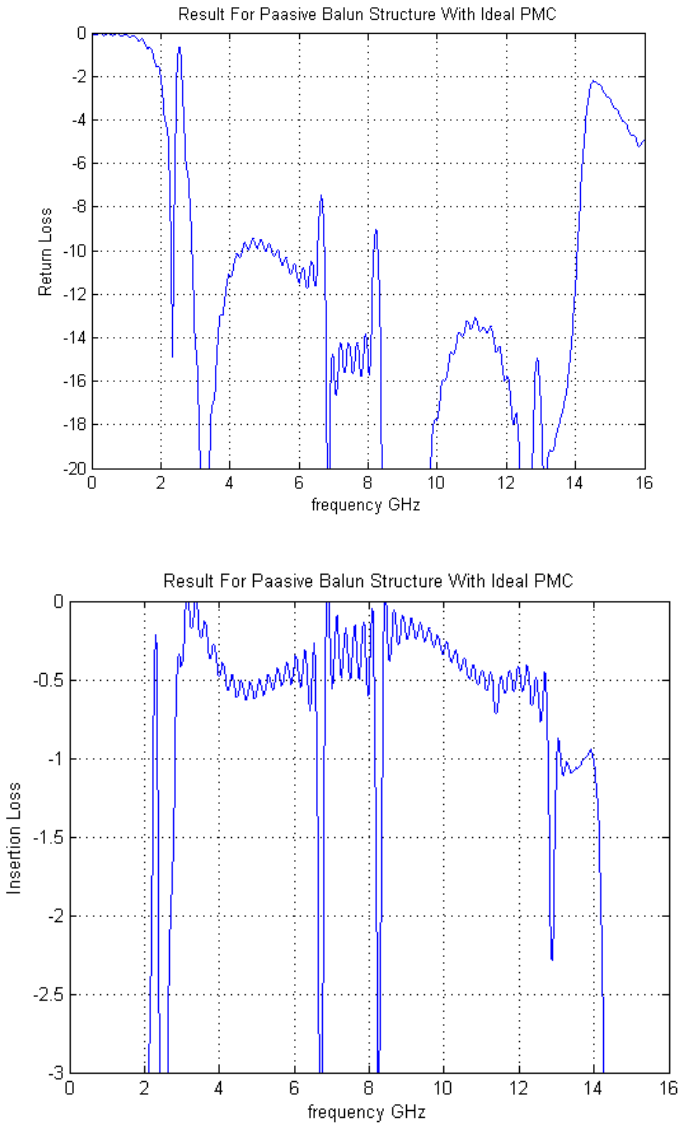

Figure 4.32: computed S parameters for structure with PMC top layer

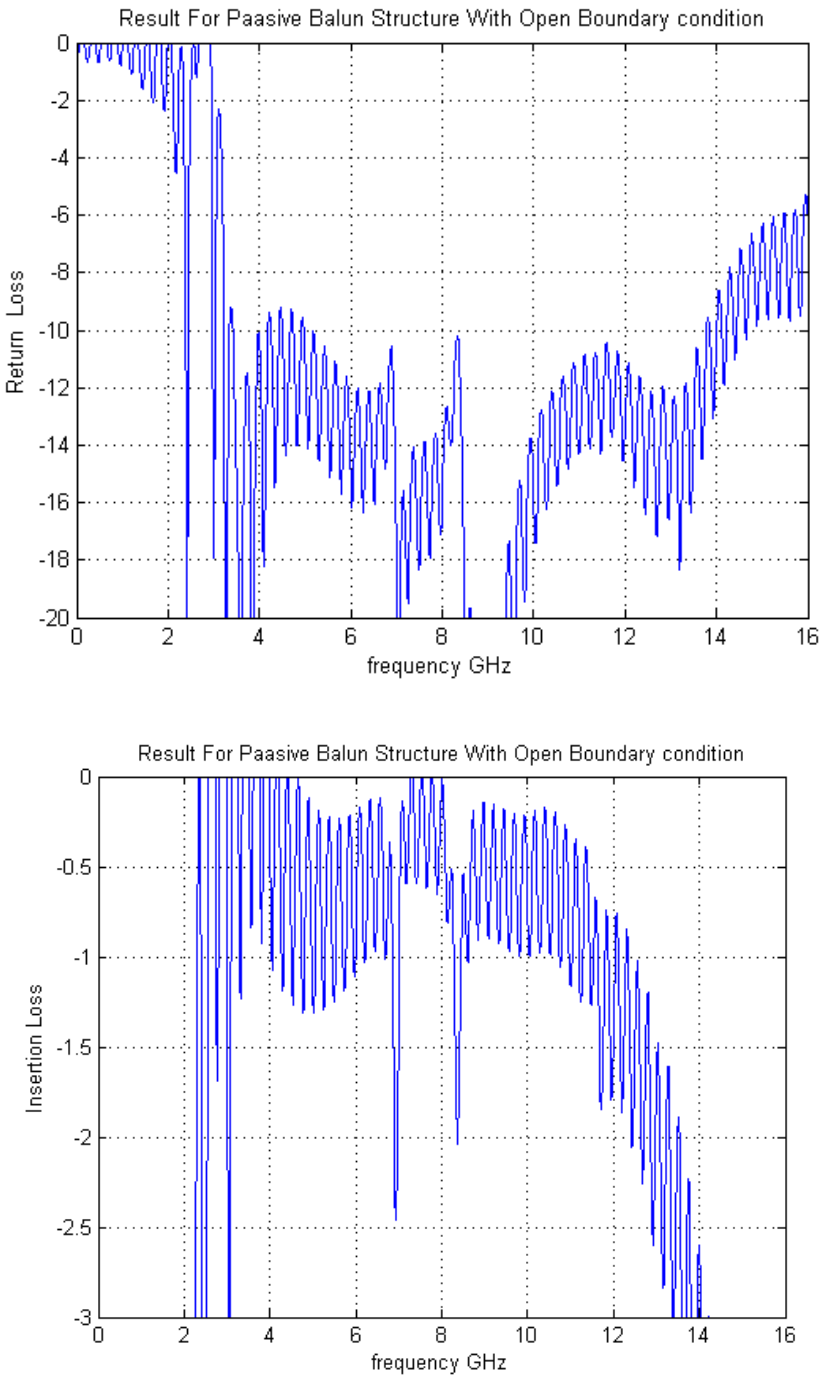

Figure 4.33: computed S parameters for structure with open boundary coundition

Then , we try to design a rectangular wave guide, and substitute side walls with metal via holes in the subsrate. We expect to have the similar results in compare withrectangular waveguide. We can actually say that , this new structure is SIW (Substrate Integrated Waveguide)Waveguide. Complete theory and explanation for this kind of structure has been given in [40] .

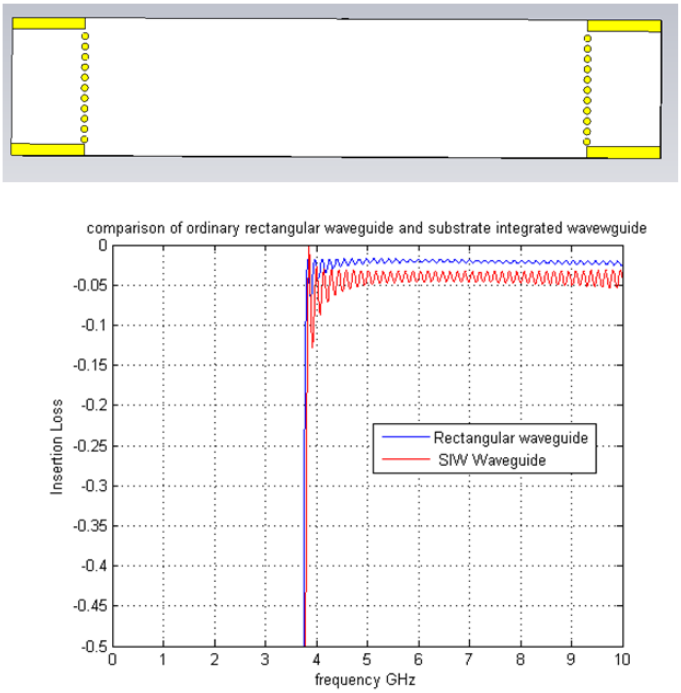

Figure 4.34: comparisin between rectangular waveguide and SIW waveguide

Figures 4.34 shows promising result for substititing side walls of rectangular waveguide with metal via holes. Therefore, we can use the same concept in our structure. The idea is to use the rectangular substrate but to avoid propogating surface waves due to the resonance which is caused by large dimentions of the side walls drill via holes in substrate below the sidewalls of Passive Balun can be utilized. Top view of the new substrate passive Balun structure for one polarization has been shown in figure 4.35

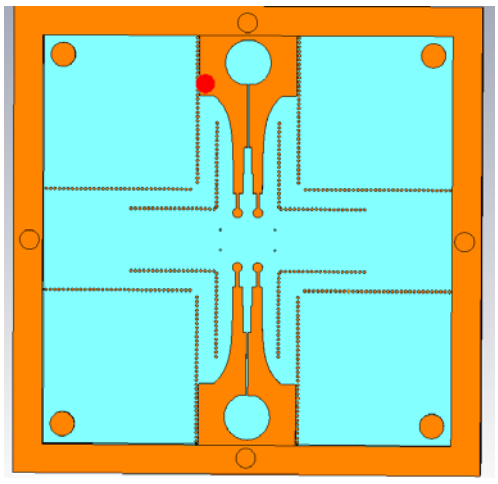

Figure 4.35: top view of new designed substrate

Figure 4.36 show results for one polariziation of passive Balun Board. The results are promising in terms of avoiding surface waves in operated bandwidth which is very similar to the cross shape substrate.

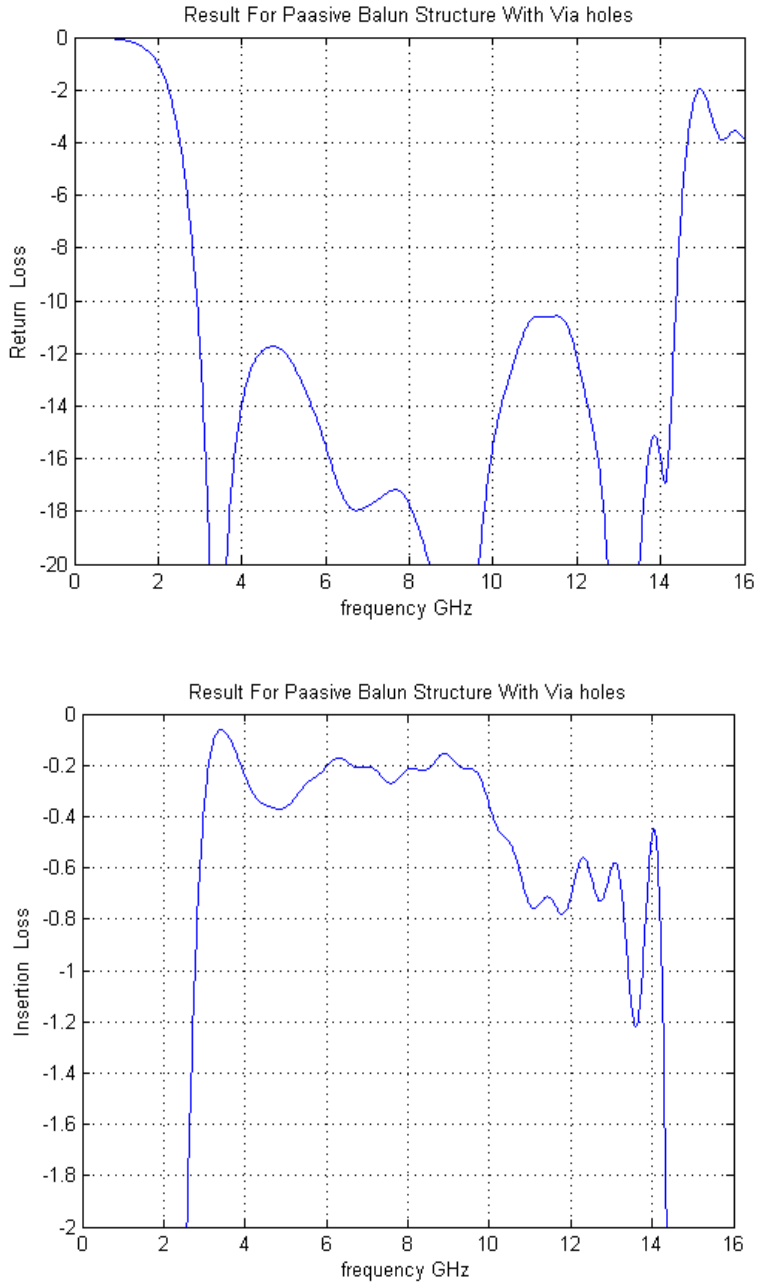

Figure 4.36: computed S parameters for passive Balun with via holes

4.10 Integration of four wideband Baluns

The next step for designing the board is to integrate four wide band Baluns to feed four log-periodic antennas below the ground plane. Here we will have important parameters for wideband passive Balun which are obtained after optimization.

Parameter	Value
Opening Rate	0.6
Radius of radial stub	2 mm
Radius of circle slot	2.2 mm
Air gap in Ground Plane	3 mm
Width of the slot in first step	0.16 mm
Width of the slot in second step	0.8 mm
Width of the slot in third step	1 mm

Table 4.1: characteristics of wide band passive Balun

Figure 4.37 shows the top and bottom view of the board for two polarizations. Side view has been shown in figure 4.38.

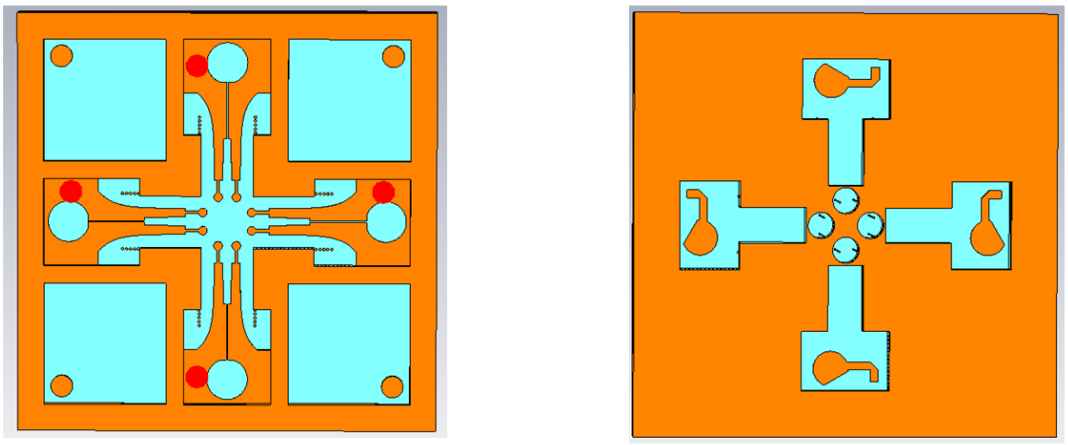

Figure 4.37: top and bottom view of integration of four wide band Baluns

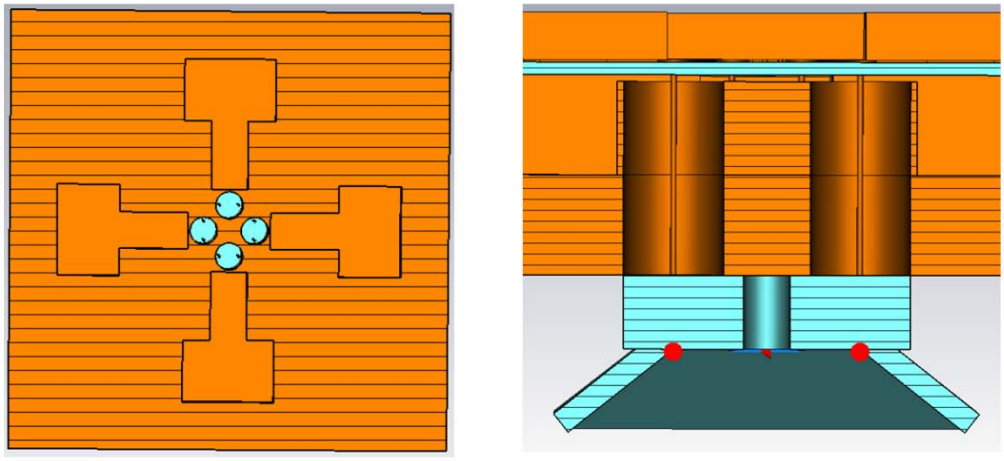

Figure 4.38: cross section and top view of center puck in new design

The design of the Balun was carried out by parameter study and dimension tuning for the following parameters: diameter of the slot-line cavity, size of the microstrip line stub, taper profile at the outer side of the transform, size and number of steps of the slot line transformer. The parameter study and dimension tuning was done by simulations using CST MS. Some design guidelines can be concluded as follows. The diameter of the slot-line cavity and the size of the microstrip line stub affect mainly the performance at the lower end of the frequency band. The taper profile of the slot line affects the performance at the higher end of the band, and the dimensions of the steps of the slot line transformer affect the bandwidth. The challenging problem is the diameter of the feeding stub and circle slot which affects lower end of frequency band and also changes the coupling part in passive Balun. Finding the optimum values for these circle slot and circle stub is the difficult job which affects the performance significantly.

The final result after optimization has been shown in figure 4.39

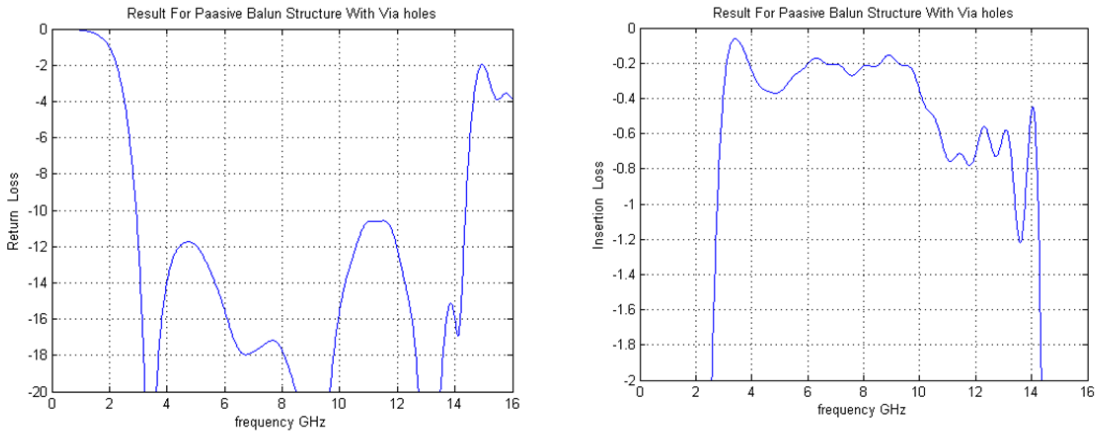

Figure 4.39: computed s parameters for integration of four passive Baluns

Chapter V

Packaging with Gap Waveguide technology

An important issue in the design of the descrambling circuits with or without integrated LNAs is the packaging. Due to the nearly decade bandwidth of the operating frequency, cavity modes will be created in normal metal box packages, which will destroy performance. The pervious solution for cavity resonances was putting absorbing materials in the top of the box. The disadvantage with this technique is the huge loss that will be added to the board by absorbing material. A new packaging technology has been developed at Chalmers [41]which has been used in the current 8 port design [18]. The cavity mode suppression is based on using a lid of nails. The suppression technique is based on the concept of gap waveguides. In this section, first, we will present a little background about bandgaps between parallel metal plates then use this technology to suppress the parallel plate cavity modes.

5.1 Theory

In the last 8-10 years, researchers have tried to design an artificial electromagnetic material that exhibits especial characteristics as the realization of the perfect magnetic conductor which does not exist naturally. Such materials are often referred to as meta-material. The first attempt for PMC realization was the so called soft and hard surfaces [42]. The idea partly comes from the transversely corrugated horns which are popular designs for feeding large reflector antennas [43]. The PMC strips can be realized as the metal grooves with effectively quarter wavelengths depth. The characteristics of the PEC/PMC strip grids are that the anisotropic boundary conditions allow waves of arbitrary polarization propagate along the strips (hard surface case), whereas they stop wave propagation other directions along the surface and, in particular, orthogonally to the strips (soft surface case). So it is comparable with EBG surface [38] that stops wave propagations along it in all direction but only for TM waves. (Soft surfaces support both TM and TE waves but only in one direction)

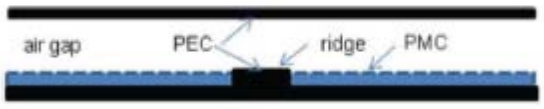

Figure 5.1: cross section of canonical ridge waveguide [47]

Using the result from a new way of using hard surface in transverse electromagnetic (TEM) parallel plate waveguide in order to kill higher order modes [44], local surface waves along each groove of a hard surface were detected. [45] Introduced a new waveguide based on the improved and simplified version of the geometry in [46], which is located in the gap between parallel plates.

The new waveguide is located in the gap between metal surfaces. Smooth parallel metal surfaces will guide vertically polarized TEM waves in the gap between them, in any direction without any low

frequency cutoff. These TEM waves are global parallel-plate modes whereas the quasi TEM waves of the ridge gap waveguide are local waves following one ridge. It is crucial for the performance of the gap waveguide that all kinds of global parallel plate modes are prohibited from propagating. This is achieved by texturing the metal surface on both sides of the ridge in such a way that it gets high impedance surface and provides cutoff for the global parallel plate modes.

The principle of operation of the gap waveguide is based on the following theoretical facts that can be derived from the Maxwell equations :

- NO waves can propagate in any direction in the gap between a PEC and a PMC if the gap height $h < \frac{\lambda}{4}$.
- No waves can propagate in any direction between PEC and an EBG surface if the gap height is smaller than a specific height that depends on geometry of the bandgap surface.

The idea is to use the same concept as [39] and employ the pin surface as a lid to suppress parallel plate modes and cavity modes when descrambler board are packaged and shielded.

Figure 5.2: sketch of the proposed mode suppression technique [47]

An example of application of lid of nails for suppression of cavity modes in microstrip circuit has been shown in figure 5.2. According to the [47]the main parameters for optimizing in such a structure are the distance from the end of the nails to the substrate which is main parameter determining the bandwidth of the structure, and also the radius and period of the pins. An extensive parameter study about EBG structure and soft surfaces has been done in [47]. Figure 5.3 shows dispersion diagram for the infinite lid of the nails above grounded substrate of thickness t=0.5 mm.

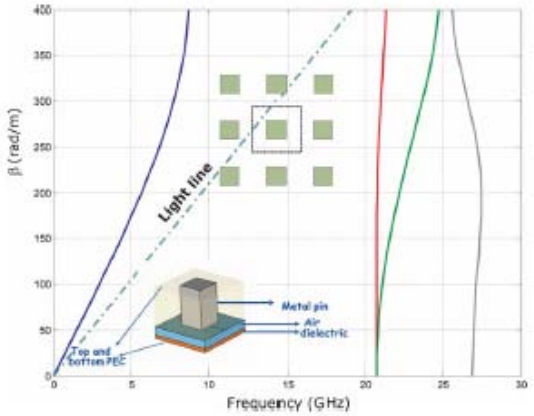

Figure 5.3: dispersion diagram of the infinite lid of the nails above grounded [47]

5.2 Simulated results for bed of nails

As the starting point we start with designing bed of the nails with calculating height of the pins. We start with estimation of $\frac{\lambda_{max}}{4}$ for the height of the pins

$$f = 14\,GHz \quad \Rightarrow \lambda \simeq 2\,cm \implies \frac{\lambda}{4} = 5\,mm \qquad (5.1)$$

Then choose the d=7 mm for period and w=3 mm for width of the pins. Optimum values can be achieved using optimization tool in CST MS. The best values are given in Table 5.1.

Parameter	Value
Height of the Pins	5.38 mm
Width of The Pins	5 mm
Air Gap	1.5 mm
Period of the Pins	5 mm

Table 5.1: characteristics of the lid of nails

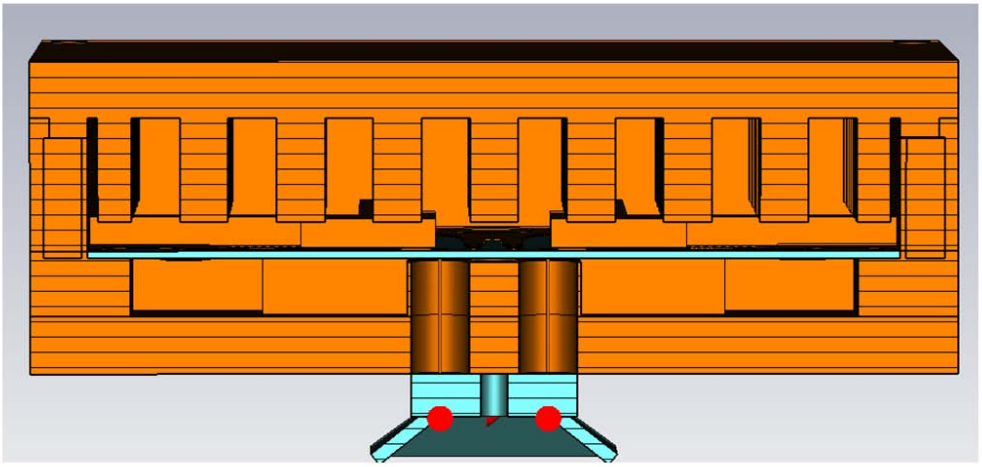

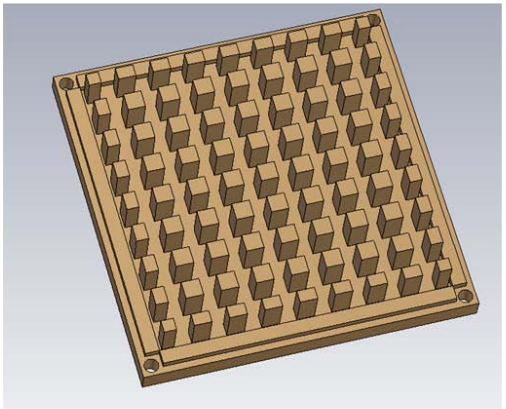

Figure 5.4: (up) cross section of the final board including lid of nails (down) lid of nails

Figure 5.4 shows the geometry of the bed of the nails. It should be mentioned that according to [47] air gap is the most critical factor in bandwidth of the band gap, and also according to our study the smaller gap height results the larger bandwidth. We choose h=1.5 mm.

5.3 Integration with Antenna

Until now we have used the 200 ohm discreet port as the output port of the descrambler board, now we can replace this 200 ohm discreet port with the real impedance of the antenna to increase the accuracy of the simulations. There are two possible solutions for integration with antenna, first we can replace 200 ohm impedance with real impedance of the antenna and then calculate the reflection coefficient for the integrated structure or connect the board directly to the antenna and simulate the whole structure. We will investigate both solutions in this section.

5.3.1 Real impedance of the antenna

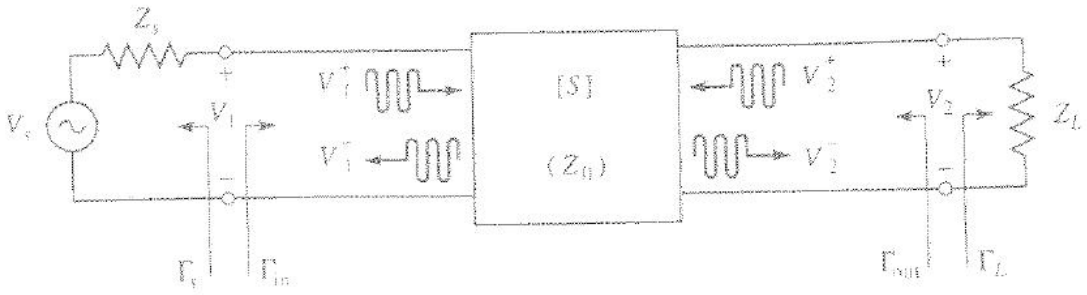

Figure 5.5: two port network

Consider an arbitrary two port network connected to the source and load impedance Z_s and Z_L, respectively, as shown in figure 5.5. The reflection coefficient seen looking toward the source is

$$\Gamma_s = \frac{Z_s - Z_0}{Z_s + Z_0} \qquad (5.2)$$

Where Z_0 is the characteristic impedance reference for the S parameters of the two-port network. In general, the input impedance of the terminated two-port network will be mismatched with the reflection coefficient given by Γ_{in}, which can be determined by the following analyses.

From the definition of the S parameters that $V_2^+ = \Gamma_L V_2^-$, we have

$$V_1^- = S_{11}V_1^+ + S_{12}V_2^+ = S_{11}V_1^+ + S_{12}\Gamma_L V_2^- \qquad (5.3)$$

$$V_2^- = S_{21}V_1^+ + S_{22}V_2^+ = S_{21}V_1^+ + S_{22}\Gamma_L V_2^- \qquad (5.4)$$

Eliminating V_2^- from eq 5.3 and solving for $\frac{V_1^-}{V_1^+}$ gives

$$\Gamma_{in} = \frac{V_1^-}{V_1^+} = S_{11} + \frac{S_{12}S_{21}\Gamma_L}{1 - S_{22}\Gamma_L} = \frac{Z_{in} - Z_0}{Z_{in} + Z_0} \qquad (5.5)$$

So we found a useful formula that can give the reflection coefficient of the whole structure if we know S parameters of the two port network and also reflection coefficient of the load impedance.

We can easily get the required S parameters from the CST MS and also we have the value for the real impedance of the antenna in required bandwidth. Figure 5.6 shows the result for the board after connecting to the board.

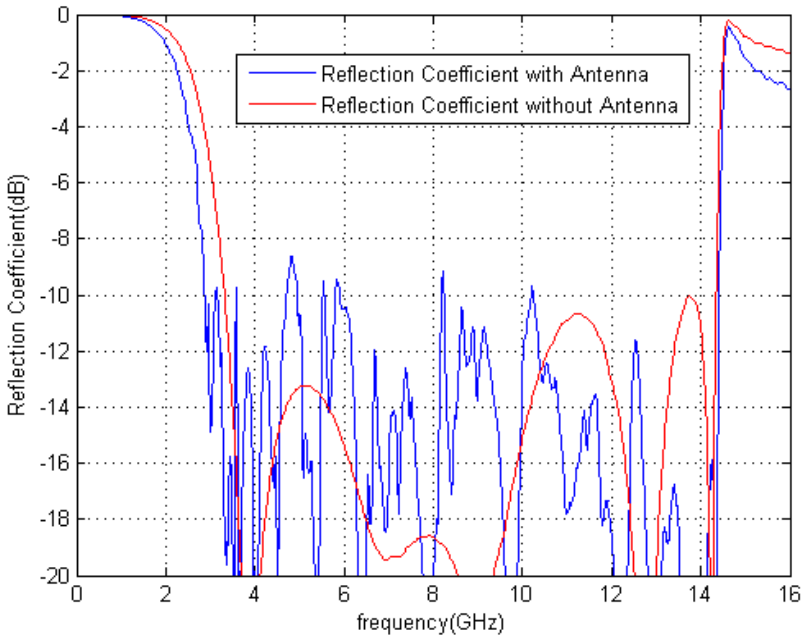

Figure 5.6: result after integration with antenna

Figure 5.6 shows the good result for integration with antenna from 3 to 14 GHz.

5.3.2 Connection to the antenna

Here, the idea is to connect the antenna to the board and simulate the structure to get the final reflection coefficient from the structure. Figure shows the geometry of Eleven feed antenna and figure 5.7 shows the Reflection coefficient for eleven feed. The fact is connecting board to antenna is not realizable in terms of simulation because of unreasonable number of mesh that we get from the CST. The trick is to simulate only part of the structure. It means that simulate antenna plus tubes with 200 differential impedance. Geometry has been shown in figure 5.8.

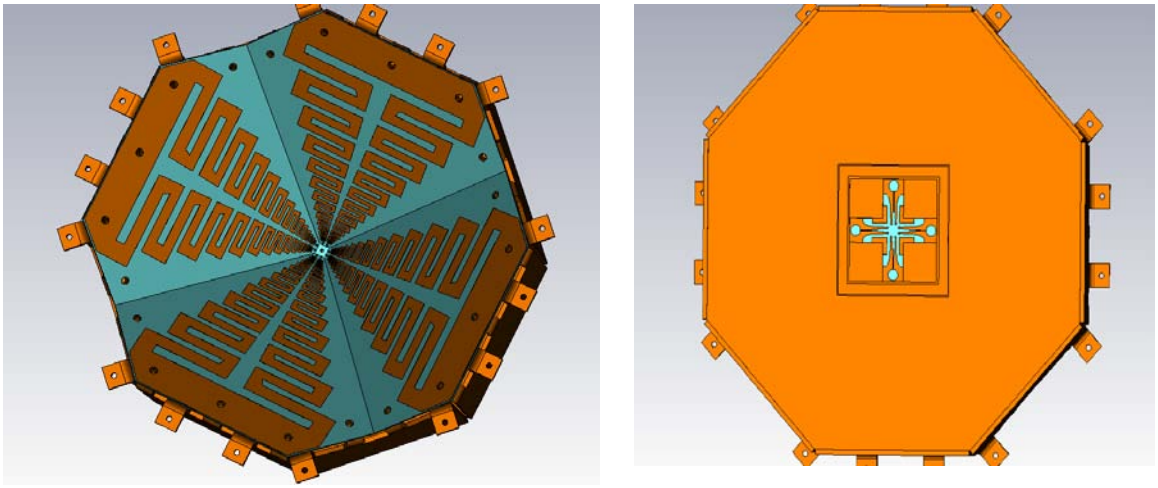

Figure5.7: Eleven antenna

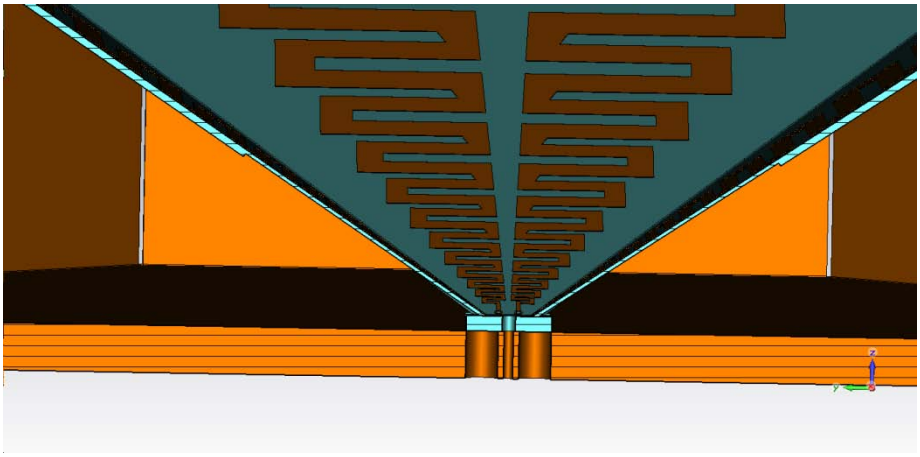

Figure 5.8: cross section of antenna and tubes

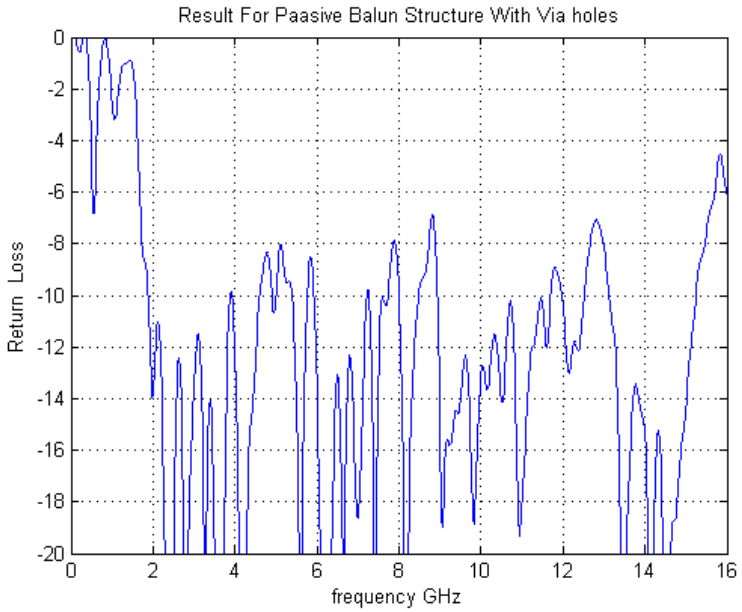

Figure 5.9: simulation result tubes and antenna

5.4 Complete solution

Figure 5.9 shows the block diagram of a passive Balun descrambling solution. Four wideband baluns are connected directly to the four two-wire lines. One wideband power combiner and a wideband cryogenic single-ended LNA are used to generate the single output port for each polarization.

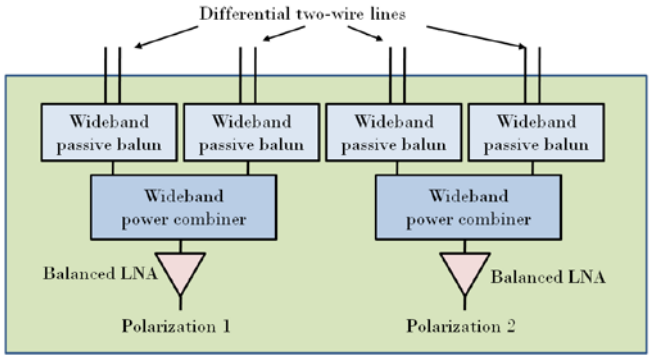

Figure 5.10: Passive Balun solution for LNA-integration circuit [9]

This solution has several advantages: first, only two single ended LNAs are needed, and it is not required that they are identical. Second, the above mentioned wideband passive Balun has a very good common mode suppression of more than 20 dB due to its geometry se figure 5.10.

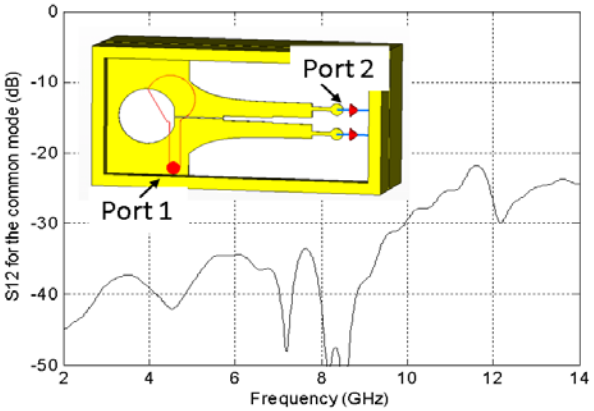

Figure 5.11: Insertion loss from port2 to port 1 for common mode of the new wideband balun

Third, the LNAs can be disconnected from the descrambling board without changing the convenient 50 ohm port impedance. Thereby, the antenna itself can be tested without the LNAs even without replacing the descrambling board.

On the other hand , compared to the active Balun descrambling, the ohmic losses and mismatch factor of the passive Baluns and the power combiners will increase the noise temperature the system. Under the cryogenic temperature, the mismatch loss will be the noise temperature contributor of the two.

Chapter VI

Validation

6.1 Validation

In order to validate the results that has been obtained by simulations, we should manufacture the board and measure the reflection coefficient of the board with antenna. Regarding manufacturing limitations, some modifications should be done in the final design. The summery of most important modifications have been given below:

- According to discussion in section 6.1 it would be easier for manufacturing to have a rectangular substrate instead of plus shape see figure

6.1.

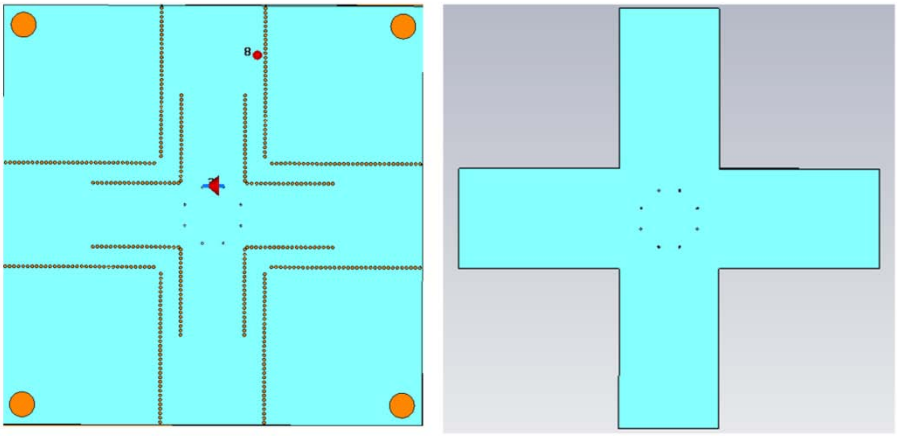

Figure 6.1: two possible alternative for shape of the substrate

- In manufacturing point of view the, placement of the stripline connector is not desired since there is a too little space for connector, see figure 6.2. So one possible solution is to bend the microstrip line 90 degree

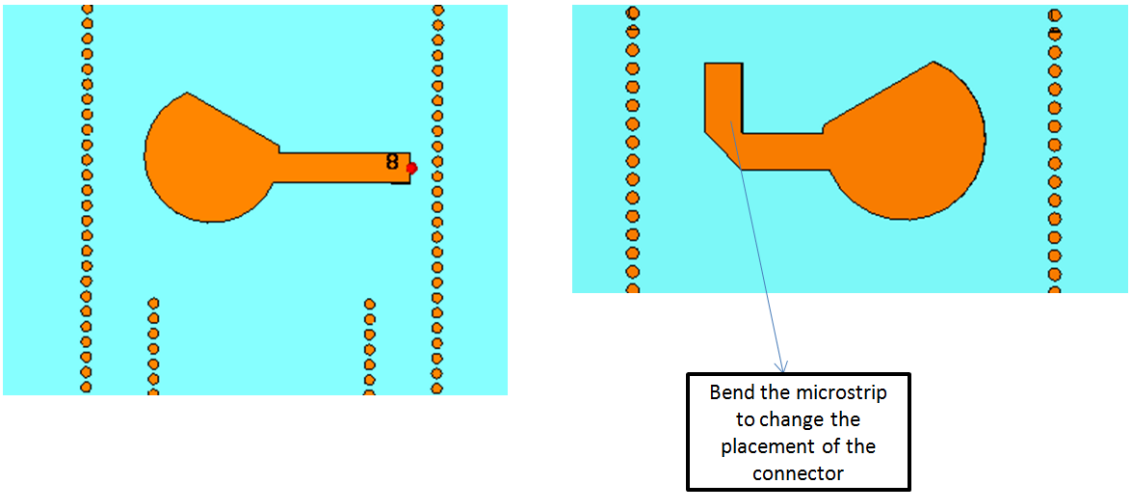

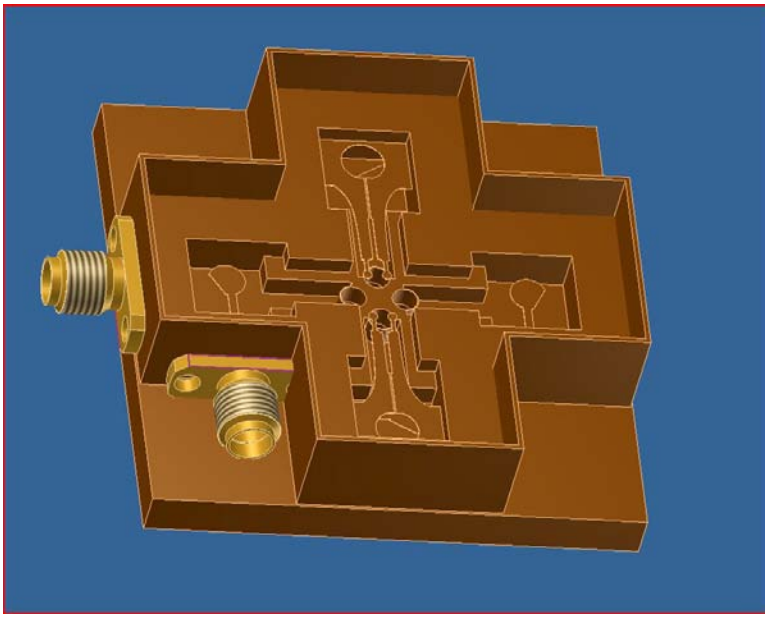

Figure 6.2: the placement of SMA connector should change 90 degree

1- Another constraints refers to the wall of the cavity which is thin for manufacturing and also we should consider this fact that the distance between edge of the board edge and the connector should be same as the substrate in the dielectric for example 3.2 mm see figure 6.3

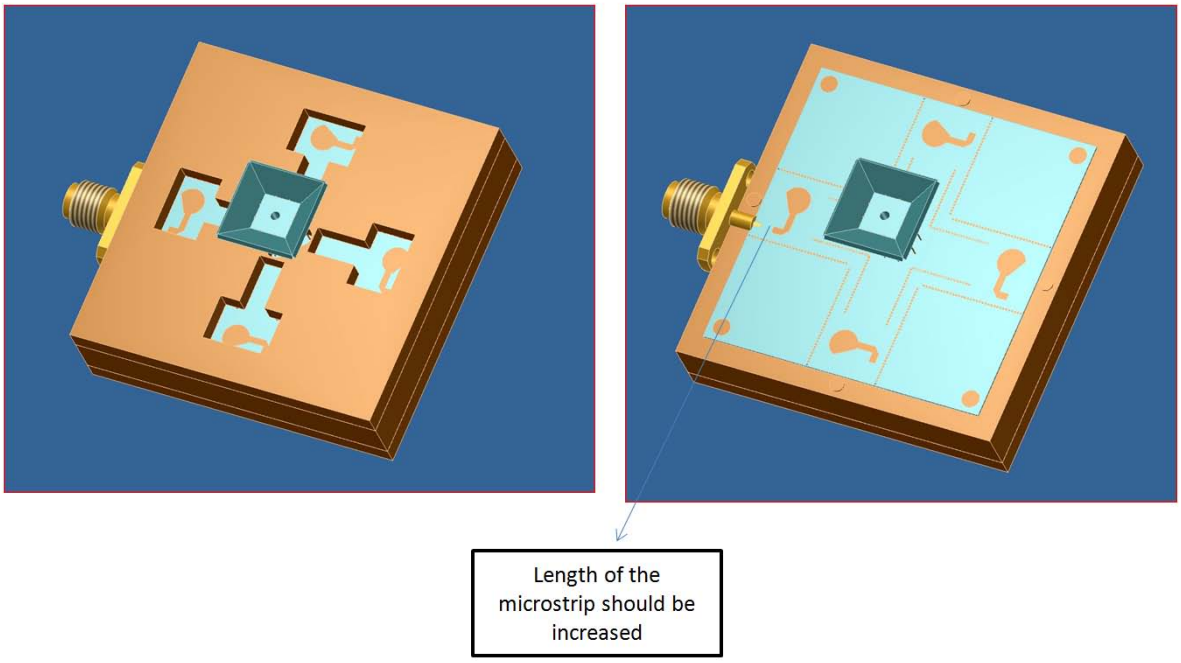

Figure 6.3: thickness of surrounding metal around the board should be equal to the dielectric in the standard SMA connector

In the designs that we had until now, we used the four tubes out of the ground plane had only 0.1 mm metal surrounding it. This cannot mill out of copper, therefore we should replace it with another realizable structure. Figure 6.4 shows the one possible solution, the trick is to use the metal box including four holes instead of four extended tubes out of ground plane. Also to avoid the metal below the Balun, we can have the 0.2 mm air gap between substrate and holes in the metal.

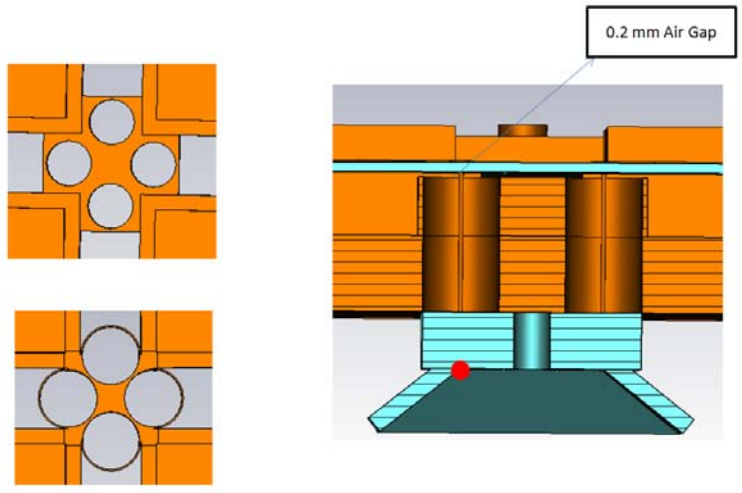

Figure 6.4: comparison between simulated model and modified version for manafacturing

Measurement Result

In order to validate the results obtained by CST microwave studio, the structure has been manufactured and measured using two port network analyzer. Figure below shows photo of manufactured board.

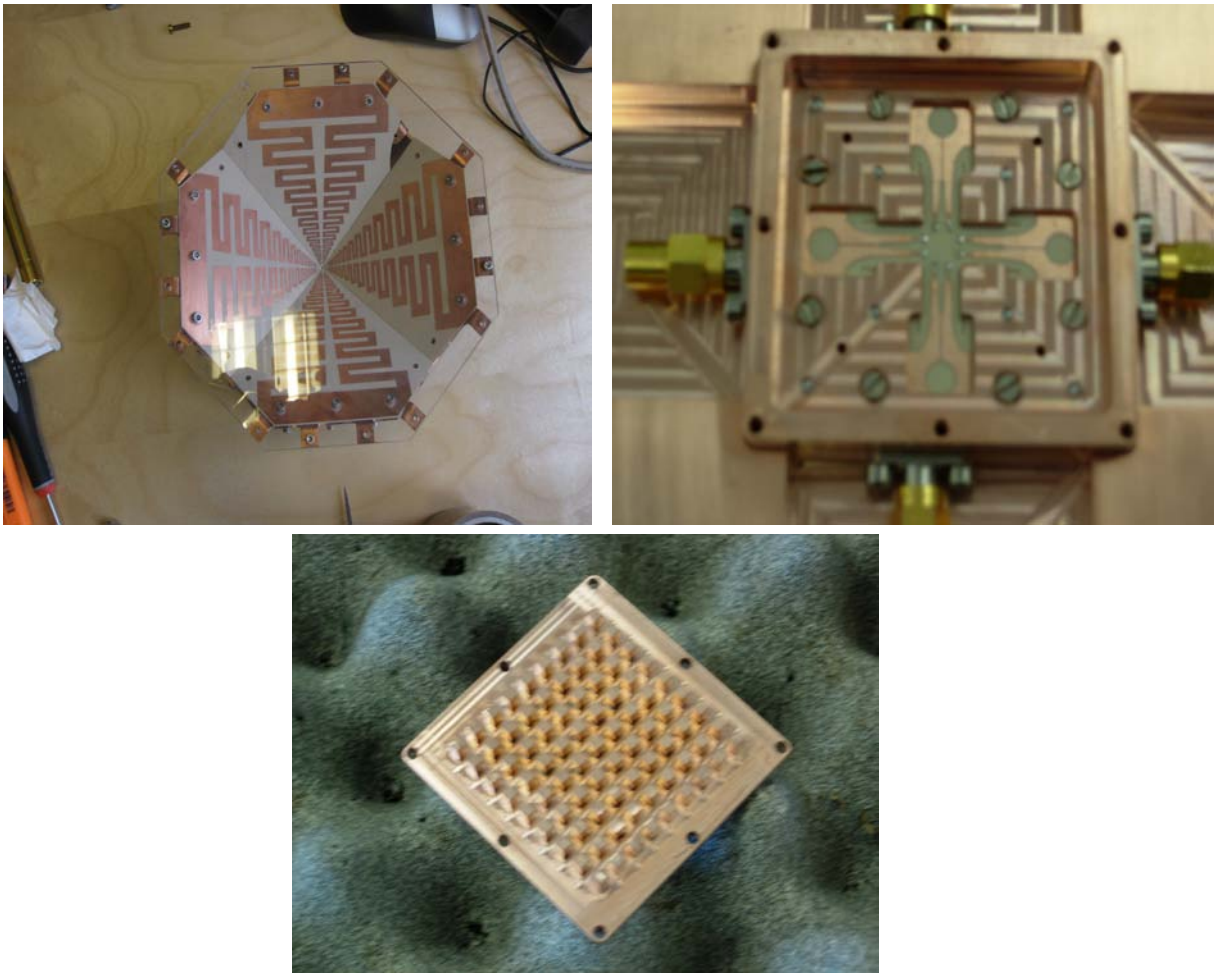

Figure 1- different view of manifactured components

We had two diffrent measurement setup :

Using wideband power divider we can excite one polarization and other polarization will be terminated with match load. figure 2 shows photo of this measurement setup

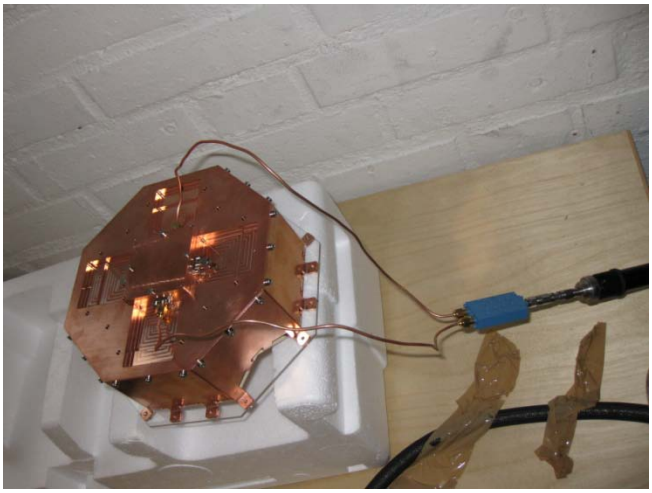

Figure 2: measurement setup using one port of network analyzer

Reflection coefficient can easily be measured by two port network analyzer.

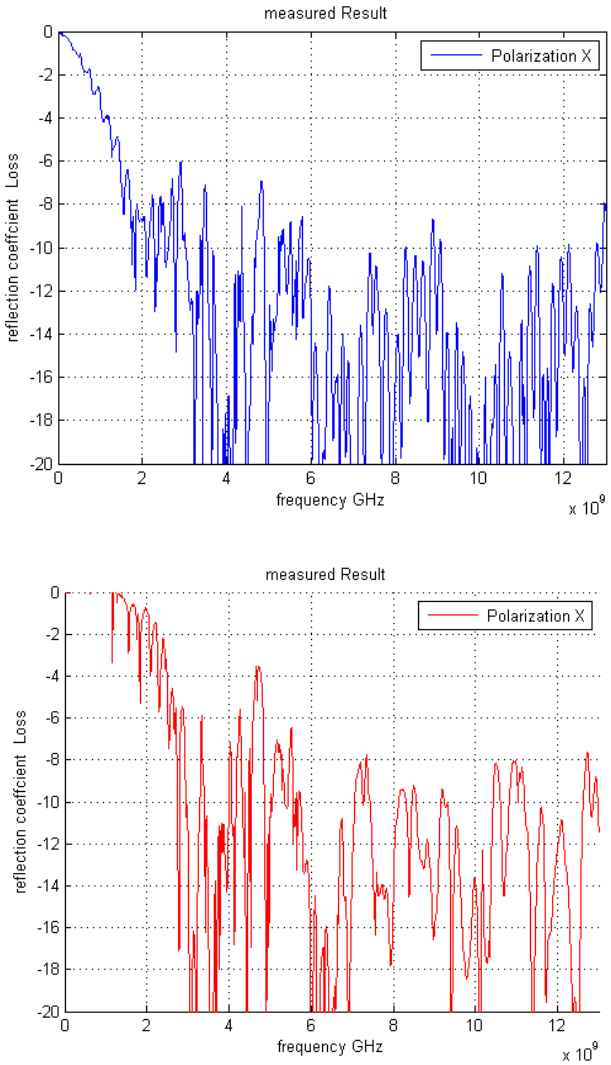

Figure3 : Reflection coefficient for orthogonal polarizations

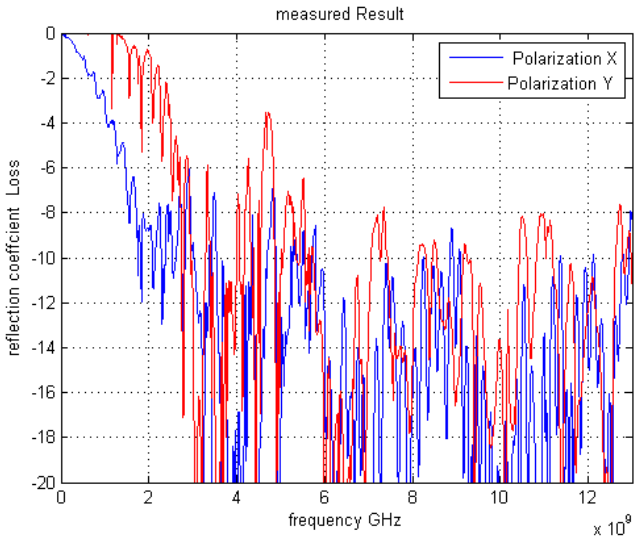

Figure4: Reflection coefficient

In another measurement setup we can use two port measurements and remove the power divider. In this case we should calculate S11 + S21 which is equal to the total reflection coefficient

Figure shows the general view of this setup:

Figure 5: measurement setup using two port of network analyzer

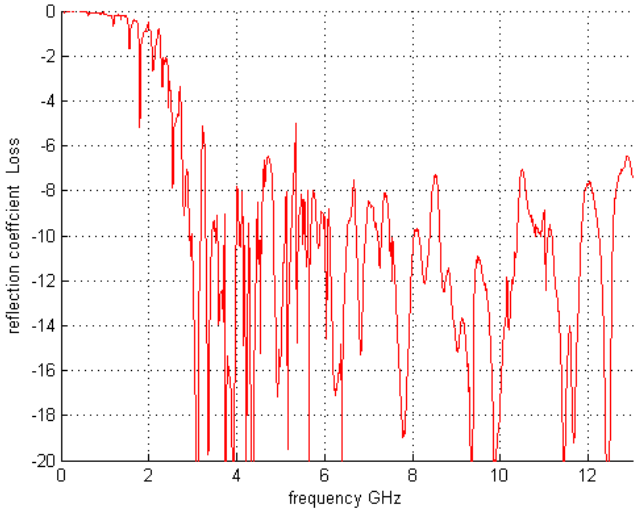

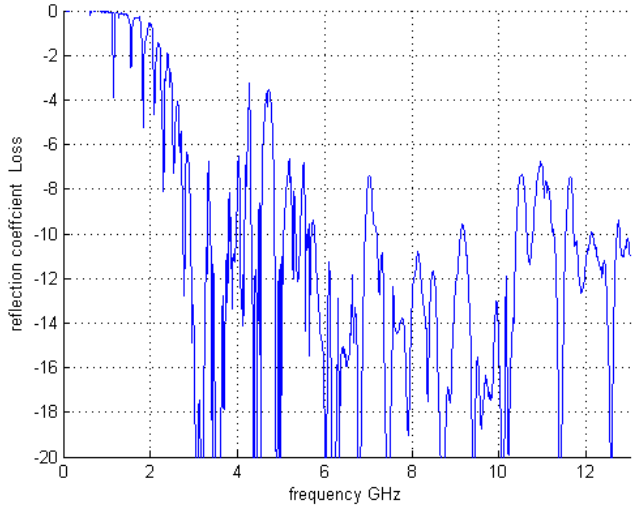

Figure 6: measurement result for different polarization

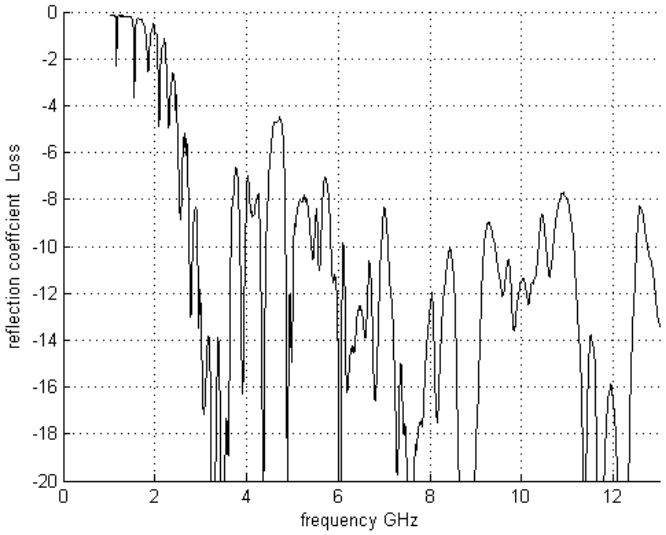

Figure 7: measurement result when pin lid has been removed

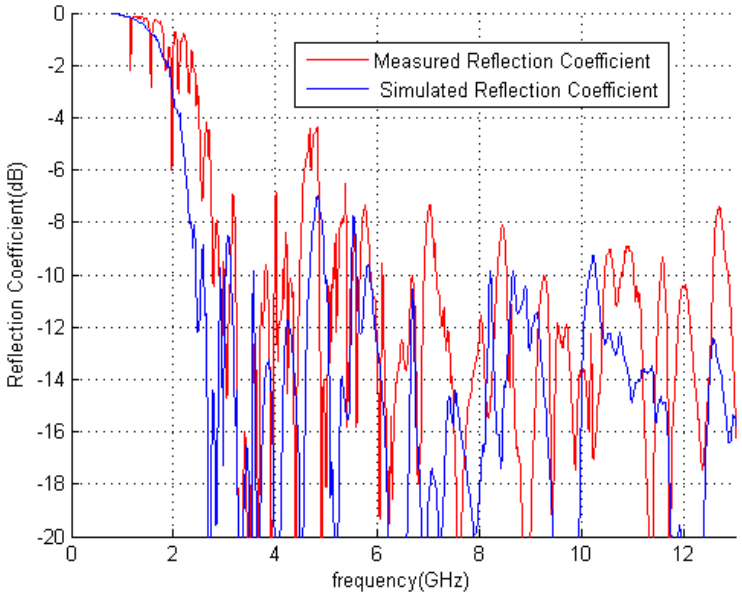

Figure 8: comparison between measured and simulated reflection coeffcients

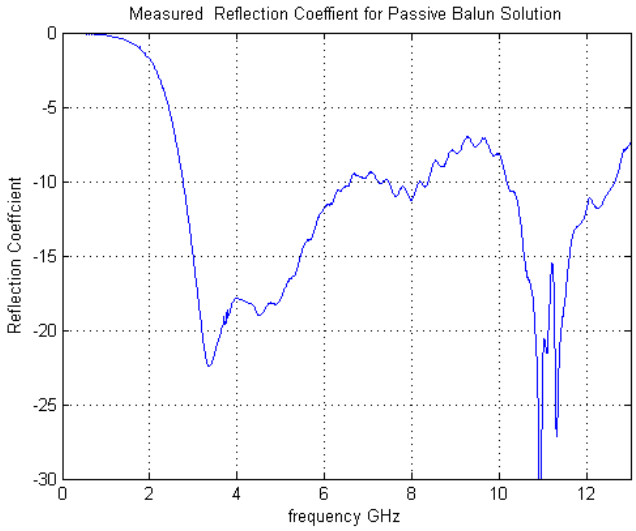

Measured reflection for Balun board alone

Discussion

Measured result for new board shows acceptable performance in operated bandwidth, but generally in both setup performance degraded around 5 GHz. The point is the current result should be evaluated with more measurement and the reason for high reflection coefficient should be investigated with more simulation and measurements. Some basic methods for investigation of this bad performance can be described as below:

- Replacing antenna with 200 ohm resistor to find the contribution of the real impedance of antenna in the performance
- Putting absorber material in the center of antenna to reduce the role of the antenna as much as possible
- Possible manufacturing problems should be studied. It should be mentioned that all the connectors are loose in the current board. There is strong possibility that soldering in connectors have been removed due to the bad installment of connectors.

It should be mentioned that it is ongoing project and we expect more progress for this solution in future.

6.2 Future works

We have studied many subtle ways to find a passive solution for eleven feed antenna and also reducing number of ports from eight to four. The best result that we has covered 3-14 GHz which means that we will miss the lower end of the frequency band. The point is, there is a strong possibility to obtain desired result in lower end by optimizing the following parameters:

- Diameter of the feeding stub
- Diameter of circle slot
- New shape in coupling part
- Use the substrate with high permittivity

According to our study for high frequency, the antenna performance suffer from the increasing loss due to the dielectric thickness, but because of manufacturing difficulties we have used the previous version of the center pick. Future studies can be done to understand how we can realize the modified version of the center puck. Off course modification of this Balun or another wideband passive Balun with lower insertion loss will be an interesting topic for future researches.

Recently a new way for combining ports has been studied. The basic idea is combining one polarization above the ground plane and another polarization below the ground plane. More details are beyond the scope of this thesis.

The final destination for completing this thesis can be one port for one polarization. The basic idea can be combination of wideband passive Balun and wide band unmatched power divider. Figure 6.5 shows the bottom and top view of the simple design.

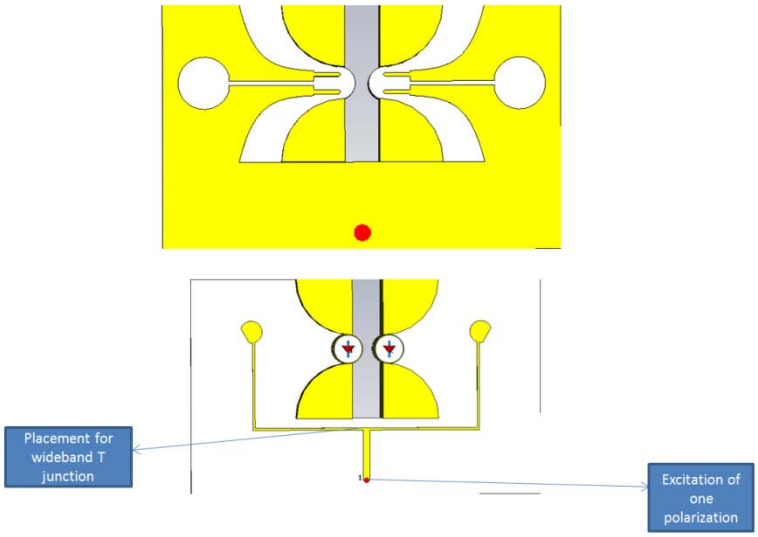

Figure 6.5: simple design for one port per polarization

6.3 Conclusion

In this report, several passive solutions for Eleven feed antenna have been studied. Due to the narrow bandwidth and big size, using the Lange crossover is not possible. The comprehensive study about the microstrip discontinuities has been done. As a result a new ultra wideband T junction has been developed for some different applications. If three ports are matched to 50 ohm, it can be consider as ultra wideband power divider by applications in active balun solution and passive balun solution [9]. If one port matched to 50 ohm and two other ports terminated to 100 ohm it will be used in two layer solution which is also an alternative to reduce the number of the ports to four from previous eight ports. Due to the difficulties that will come with this two layer solution in terms of manufacturing, an ultra wideband one layer solution is highly preferred. So the main task here will be design a structure using wideband baluns. To the best of our knowledge Baluns with 2-14 GHz bandwidth or similar are not commercially available, and they cannot be found in the literature either. In the main parts of this project we have tried to develop a new wideband passive Balun based on the concept of Vivaldi antenna which is member of the class of continuously scaled, gradually curved end fire travelling wave antenna. After an extensive optimization we have designed an ultra wide band Balun which covers 3-14 GHz. Our results have been published in [48]. The main drawback of this passive solution is the performance in the lower end of the bandwidth which is limited by the diameter of the feeding stub and circle slot. In manufacturing point of view, the plus shape of the substrate will be problematic which can be solved by putting via holes in proper distance and period. Another problem in final design was the resonances in operated bandwidth due to the parallel plate cavity modes of the board. Thanks to the new technology which has been developed in Chalmers university of technology resonances could be removed. The idea is to use the lid of nails as the realization of PMC (perfect magnetic conductor). Finally the board has been simulated and results have been validated by measurement.

References

[1] J. Chengalur, Y.Gupta, K.S.Dwarakanath, *Low Frequency Radio Astrophysics*: http://www.gmrt.ncra.tifr.res.in/gmrt_hpage/Users/doc/WEBLF/LFRA/index.html

[2] P. Hall, the SKA: An Engineering Perspective, Springer, 2005.

[3] Niell, A., A. Whitney, W. Petrachenko, W. Schlüter, N.Vandenberg, H. Hase, Y. Koyama, C. Ma, H. Schuh, G. Tuccari (2005) VLBI2010: Current and Future Requirements for Geodetic VLBI Systems, IVS WG3 Report, http://ivscc.gsfc.nasa.gov/about/wg/wg3

[4] G. Cortés, "Wideband Feed Technologies for Arecibo", August 2007

[5] R. Dybdal, "Defocusing loss for a log periodic-fed reflector", IEEE Trans. Antennas Propag. Vol. 33, No. 7, pp. 809 – 812, July 198

[6] V. Rodriguez, "A multi-octave open-boundary quadridge horn antenna for use in the S to Ku-bands," Microwave Journal, March, 2006, pp. 84–92

[7] R. Olsson, P.-S. Kildal, S. Weinreb, "The Eleven antenna: a compact low-profile decade bandwidth dual polarized feed for reflector antennas", IEEE Transactions on Antennas and Propagation, vol. 54, no. 2, pt. 1, pp. 368-375, Feb. 2006

[8] Olsson. R: study of wideband feeds in cylindrical shields for use in large radio telescopes, Chalmers University of technology, 2003.

[9] J.Yang, M.panteleev,P.S. Kildal,Y.Karindikar,L. Helldner,B Klien, N.Waefalk, 'Cryogenic 2-13 GHz Eleven Feed for reflector Antennas in future Wideband Radio Telescope', accepted in Special Issue on Antennas for Next Generation Radio Telescope

[10] Christiansen, W.N. Höbom, J.A.: Radiotelescope, Cambridge university press, 1985

[11] V.H.Rumsey," frequency independent antenna", 1957 IRE National Convention Record, pt. 1,pp 114-118.

[12] R.H.DuHumel and D.E Isbell, 'Broadband logarithmically periodic antenna structures '. 1957 IRE National Convention Record, pt. 1, pp 119-128.

[13] D.E.Isbell, " Log Periodic Dipole Arrays", IRE Trans Antennas Prapagat, Vol. AP-8,pp 260-267,may 1960

[14] Balanis , C.A: Antenna theory- Analyses and design, Harper and Row, 1982

[15] Y. B. Karandikar, P. -S. Kildal, " Comparisons of different descrambler/ power combining boards layout for multi-port, decade bandwidth Eleven feed ", to be presented at The Fourth European Conference on Antennas and Propagation (EuCAP 2010), Barcelona, 12-16 April 2010.

[16] J. Yang, D. Nyberg, J. Yin, "Impedance matrix of a folded dipole pair under Eleven configuration", accepted for publication in IET Microwaves, Antennas & Propagation, Dec. 2009

[17] J. Yang and P.-S. Kildal, "Optimization of reflection coefficient of large log-periodic array by computing only a small part of it," submitted to IEEE Trans. Antennas Propagat, Oct. 2009.

[18] J. Yang, X. Chen, N. Wadefalk, P.-S. Kildal, "Design and realization of a linearly polarized Eleven feed for 1-10 GHz", IEEE Antennas and Wireless Propagation letters (AWPL), Vol. 8, pp. 64-68, 2009

[19] K. REINMUT, HOFFMANN, J. Siegl, "Microstrip-slot Coupler Design- part I S-parameters of uncompensated and compensated Couplers

[20] Pozar.M, 'Microwave Engineering', john Wiley & sons, 2005

[21] T.C.Edwards, 'Founsdations for microstrip circuit design', John Wiley & Sons, 1982

[22] P.-S. Kildal, "Factorization of the feed efficiency of paraboloids and Cassegrain antennas," *IEEE Trans. Antennas Propagat.*, vol. 33, no. 8, pp.903-908, Aug. 1985.

[23] P.S. Kildal, *Foundations of Antennas: A unified Approach*, Student-litteratur, Lund, 2000

[24] M.Traii,M.Nedil,A.GHarsallah,A.Denidni,'A New Design of compact 4*4 Butler Matrix for ISM Applications', international journal of Microwave Science and Technology, December 2008,

[25] Andres.P, Arnedt.F, 'moment method of designing match microstrip bends',1979 European microwave conference, Brighton, England, Digest of papers.430-434

[26] Silvester, P. and P.Benedek,"microstrip discontinuity capacitance for right angle Bends,T junctions and crossings ", IEEE Trans, Vol MTT 21, 1973,pp.341

[27] Thompson, A.F. and A. Gopinath, "calculation of micriostrip discontinuity inductances," IEEE Trans., Vol. MTT-23, 1975, pp.648-655

[28] rag,Ramesh, and I.J.Bahel, "microstrip discontinuties", international Journal of Electronics, Vol 45, July 1978

[29] S.B.Cohen ,"Slot-line- an alternative transmission medium for integrated circuits",1968. G-MTT Symposium Digest, may 1968 ,p 104-109

[30] F.C.de Ronde, "a new class of microstrip directional couplers", in IEEE MTT-S int. microw Symp., Dig., May 1970, pp. 184-189.

[31] j.A.Garcia," a wideband quadrature hybrid coupler", IEEE Trans. Microw. Theory Tech., vol. MTT-19, no 7, pp. 660-661, jul 1971.

[32] A.M.Abbosh," Ultra wideband in phase power divider for multilayer technology", IET microwaves Antenna & Propogation, May 2008

[33] K.C.Gupta, Ramesg Garg,I.J.Bahl,"Microstrip Lines and Slot Lines", Artech House,1979

[34] P.J.Gibson, "The Vivaldi aerial", Proc. 9th European Microwave Conf., 1979, Brighton, UK. pp.101-105.

[35] Ehud Gazit, E., "Improved design of the Vivaldi antenna," *Proceeding Inst. Elect. Eng., pt. H*, Vol. 135, No. 2, 89-92, 1988.

[36] Y. Yang, C. Zhang, and A. E. Fathy, "Development and implementation of ultra-wideband see-through-wall imaging system based on sampling oscilloscope," IEEE Antennas Wireless Propag. Lett., to be published.

[37] Raviprakash Rajaraman," Design of a wideband Vivaldi Antenna Array for The Snow Radar", master thesis, Faculty of the Graduate School of the University of Kansas, February 2004.

[38] D. Sievenpiper, L. Zhang, R. F. J. Broas, N. G. Alexopolous, and E. Yablonovitch, "High-impedance electromagnetic surfaces with a forbidden frequency band," IEEE Trans. Microw. Theory Tech., vol. 47, no. 11, pp. 2059–2074, Nov. 1999

[39] R.Gonzalo,P.Maagt,M.sorolla,"Enhanced Patch antenna performance by suppressing surface waves using photonic bandgap substrates", IEEE Transactions on microwave theory and techniques. Vol. 47, No. 11, November 1999,

[40] Uchimura, H., T. Takenoshita, and M. Fuji, "Development of a laminated waveguide," IEEE Trans. Microwave Theory and Tech., Vol. 46, 2438–2443, Dec. 1998.

[41] P.-S. Kildal, E. Alfonso, A. Valero-Nogueira, E.Rajo-Iglesias, "Local metamaterial-based waveguides in gaps between parallel metal plates". IEEE Antennas and Wireless Propagation letters. 8 p. 84-87

[42] P.-S. Kildal , “Definition of artificially soft and hard surfaces for electromagnetic waves,” Electron. Lett., vol. 24, no. 3, pp. 168–170, Feb. 4th, 1988.

[43] Z.Ying and P.-S. Kildal, “improvement of dipole ,helix,microstrip patch and aperture antennas with ground planes by using corrugated soft surfaces”, IEEE proceeding part H, Vol. 143, No. 3, pp. 244-248,196

[44] Valero-Nogueira, E. Alfonso, J. I. Herranz, and M. Baquero, “Planar slot-array antenna fed by an oversized quasi-TEM waveguide,” *Microw. Opt. Technol. Lett.*, vol. 49, no. 8, pp. 1875–1877, Aug. 2007.

[45] E. Alfonso, P.-S. Kildal, A. Valero, and J. I. Herranz, “Study of local quasi-TEM waves in oversized waveguides with one hard wall for killing higher order global modes,” in *Proc. IEEE Int. Symp. Antennas Propag. (IEEE AP-S)*, San Diego, CA, Jul. 2008, pp. 1–4.

[46] E.Rajo-Iglesias, A. Uz Zaman, P.-S. Kildal, “Parallel plate cavity mode suppression in microstrip circuit packages using a lid of nails”. IEEE Microwave and Wireless Components Letters. 20 (1) p. 31-33.

[47] Rajo-Iglesias, Eva; Quevedo-Teruel, Óscar; Inclan-Sanchez, Luis, “*Planar soft surfaces and their application to mutual coupling reduction”* to appear in IEEE Transaction on Antennas and Propagation, Vol. 57, No. 12, pp. 3852-3859, December 2009

[48] Abolghasem Zamanifekri , Jian Yang , and Per-Simon Kildal ,” A New Decade Bandwidth Passive Balun Solution to Excitation for the Eleven Antenna” , *IEEE Antennas Propag. Soc. Symp., 2010.*

Appendix A

TABLE 11.1 INPUT RESISTANCES (R_{in} IN OHMS) AND DIRECTIVITIES (dB ABOVE ISOTROPIC) FOR LOG-PERIODIC DIPOLE ARRAYS

α	τ = 0.81		τ = 0.89		τ = 0.95	
	R_{in}(ohms)	D_0(dB)	R_{in}(ohms)	D_0(dB)	R_{in}(ohms)	D_0(dB)
10	98	—	82	9.8	77.5	10.7
12.5	—	—	77	—	—	—
15	—	7.2	—	—	—	—
17.5	—	—	76	7.7	62	8.8
20	—	—	74	—	—	—
25	—	—	63	7.2	—	8.0
30	80	—	64	—	54	—
35	—	—	56	6.5	—	—
45	65	5.2	59	6.2	—	—

SOURCE: D. E. Isbell, "Log Periodic Dipole Arrays," *IRE Trans. Antennas Propagat.*, Vol. AP-8, pp 260–267, May 1960. © (1960) IEEE.

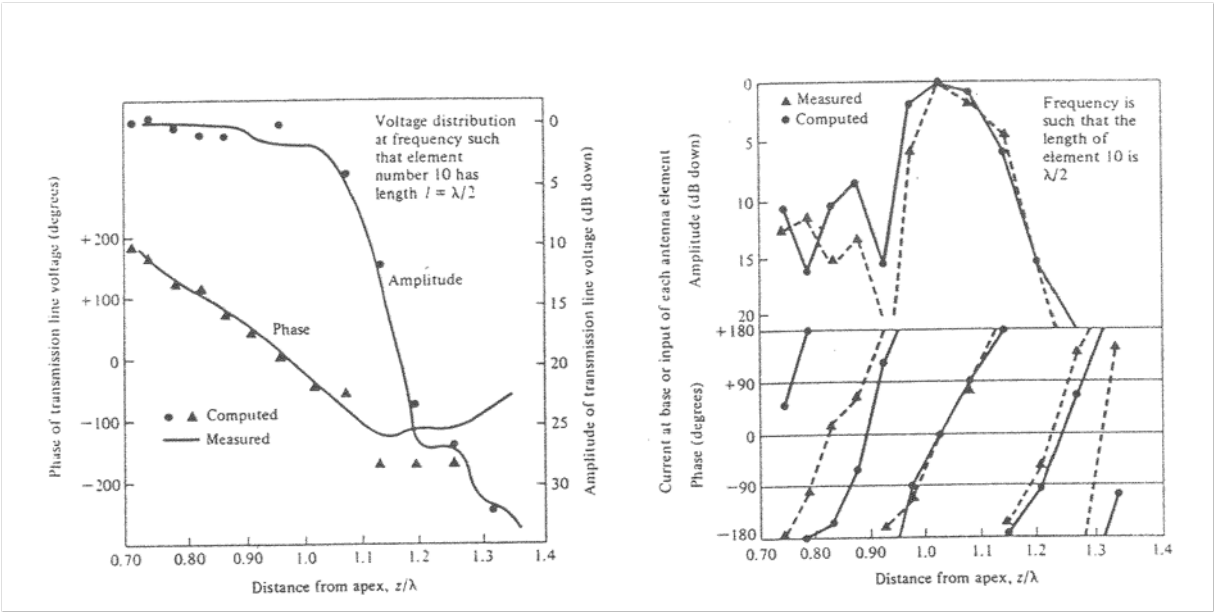

(Up) input resistances (Rin in ohms) and directivities (dB above isotropic) for log-periodic dipole arrays (down) measured and computed voltage and current distributions on log-periodic dipole array of 13 elements with frequency such that $\square_{10} = \frac{\square}{2}$. [10]

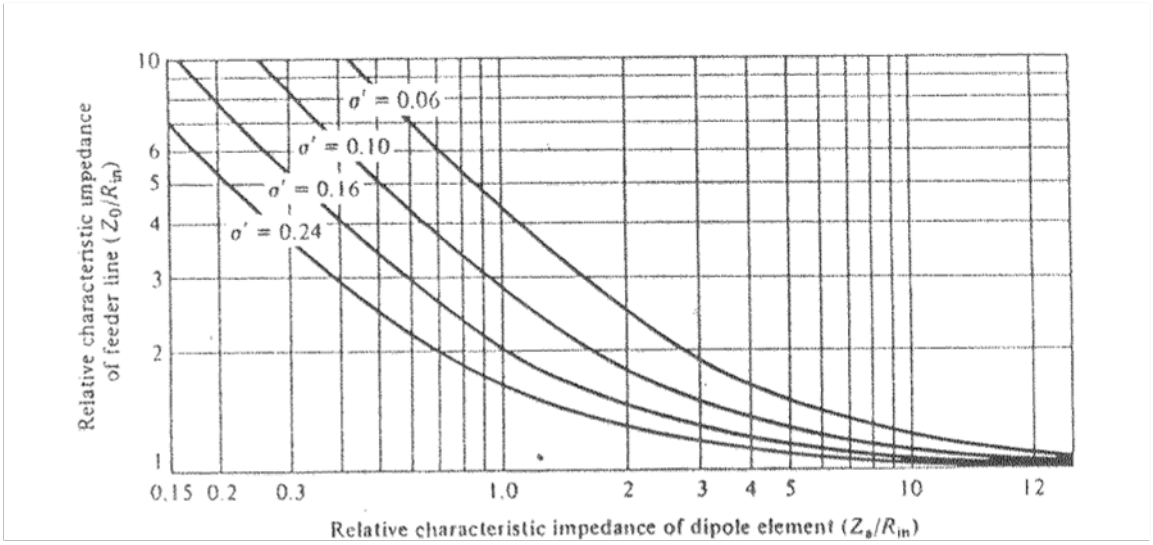

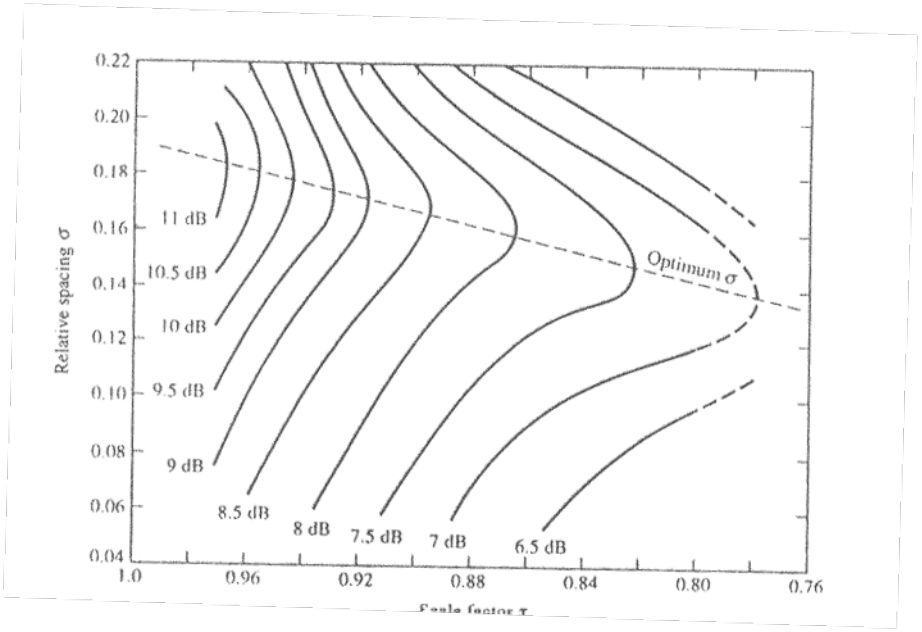

(Up) Relative characteristics impedance of a feeder line as a function of relative impedance of dipole antenna (down) Computed Contours of constant directivity versus σ and τ for log-periodic dipole arrays [10]

Appendix B

ROGERS CORPORATION

Advanced Circuit Materials

Advanced Circuit Materials Division
100 S. Roosevelt Avenue
Chandler, AZ 85226
Tel: 480-961-1382, Fax: 480-961-4533
www.rogerscorporation.com

Data Sheet
TMM

TMM® Thermoset Microwave Materials

Features:

- Wide range of dielectric constants. Ideal for single material systems on a wide variety of applications.
- Excellent mechanical properties. Resists creep and cold flow.
- Exceptionally low thermal coefficient of dielectric constant.
- Coefficient of thermal expansion matched to copper. High reliability of plated through holes.
- Resistant to process chemicals. No damage to material during fabrication and assembly processes.
- Thermoset resin for reliable wirebonding. No specialized production techniques required. TMM 10 and 10i laminates can replace alumina substrates.

Some Typical Applications:

- RF and Microwave Circuitry
- Global Positioning Systems Antennas
- Power Amplifiers and Combiners
- Patch Antennas
- Filters and Coupler
- Dielectric Polarizers and Lenses
- Satellite Communication Systems
- Chip Testers

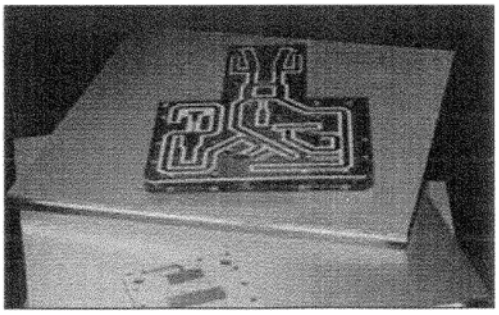

TMM® thermoset microwave materials are ceramic thermoset polymer composites designed for high plated-thru-hole reliability stripline and microstrip applications. TMM laminates are available in a wide range of dielectric constants and claddings.

The electrical and mechanical properties of TMM laminates combine many of the benefits of both ceramic and traditional PTFE microwave circuit laminates, without requiring the specialized production techniques common to these materials. TMM laminates do not require a sodium napthanate treatment prior to electroless plating.

TMM laminates have an exceptionally low thermal coefficient of dielectric constant, typically less than 30 ppm/°C. The material's isotropic coefficients of thermal expansion, very closely matched to copper, allow for production of high reliability plated through holes, and low etch shrinkage values. Furthermore, the thermal conductivity of TMM laminates is approximately twice that of traditional PTFE/ceramic laminates, facilitating heat removal.

TMM laminates are based on thermoset resins, and do not soften when heated. As a result, wire bonding of component leads to circuit traces can be performed without concerns of pad lifting or substrate deformation.

TMM laminates combine many of the desirable features of ceramic substrates with the ease of soft substrate processing techniques. TMM laminates are available clad with 1/2 oz/ft² to 2 oz/ ft² electrodeposited copper foil, or bonded directly to brass or aluminum plates. Substrate thicknesses of 0.015" to 0.500" and greater are available. The base substrate is resistant to etchants and solvents used in printed circuit production. Consequently, all common PWB processes can be used to produce TMM thermoset microwave materials.

Typical Values — **TMM® Thermoset Microwave Materials**

PROPERTIES	TYPICAL VALUES					DIRECTION	UNITS	CONDITIONS	TEST METHOD
	TMM3	TMM4	TMM6	TMM10	TMM10I				
[1] Dielectric Constant, ε_r	3.27 ± 0.032	4.50 ± 0.045	6.00 ± 0.060	9.20 ± 0.230	9.80 ± 0.245	Z		10 GHz	IPC-TM-650 method 2.5.5.5
[1] Dissipation Factor, tan δ	0.0020	0.0020	0.0023	0.0022	0.0020	Z		10 GHz	IPC-TM-650 method 2.5.5.5
Thermal Coefficient of ε_r	+37	+15	-11	-38	-43*		ppm/K	-55 to +125°C	IPC-TM-650 method 2.5.5.5
Insulation Resistance	>2000	>2000	>2000	>2000	>2000		Gohm	C/96/60/95	ASTM D257
Volume Resistivity	$3X10^8$	$6X10^8$	$1X10^8$	$2X10^8$	$2X10^8$		Mohm cm		ASTM D257
Surface Resistivity	$>9X10^8$	$1X10^9$	$1X10^9$	$4X10^7$	$4X10^7$		Mohm		ASTM D257
Flexural Strength	16.53	15.91	15.02	13.62	-	X,Y	kpsi	A	ASTM D790
Flexural Modulus	1.72	1.76	1.75	1.79	1.80*	X,Y	Mpsi	A	ASTM D790
Impact, Notch Izod	0.33	0.36	0.42	0.43	-	X,Y	ft-lb/in		ASTM D256A
Water Absorption (2X2)							%	D/48/50	ASTM D570
1.27mm (0.050" thk)	0.06	0.07	0.06	0.09	0.16				
3.18mm (0.125" thk)	0.12	0.18	0.20	0.20	0.13				
Specific Gravity	1.78	2.07	2.37	2.77	2.77			A	ASTM D792
Specific Heat	0.87	0.83	0.78	0.74	0.72*		J/g/K	A	Calculated
Thermal Conductivity	0.70	0.70	0.72	0.76	0.76	Z	W/m/K	80°C	ASTM C518
Thermal Expansion	15	16	18	21	19	X,Y	ppm/K	0 to 140°C	ASTM D3386
	23	21	26	20	20	Z			
Td	425	425	425	425	425		°C TGA		ASTM D3850
Copper Peel Strength	5.7 (1.0)	5.7 (1.0)	5.7 (1.0)	5.0 (0.9)	5.0 (0.9)	X,Y	lb/inch (N/mm)	after solder float 1 oz. EDC	IPC-TM-650 Method 2.4.8
Lead-Free Process Capatible	YES	YES	YES	YES	YES				

Notes: ASTM D3386 corresponds to IPC-TM-650, method 2.4.4.1
* estimated

Typical values are a representation of an average value for the population of the property. For specification values contact Rogers Corporation.

(1) Prolonged exposure in an oxidative environment may cause changes to the dielectric properties of hydrocarbon based materials. The rate of change increases at higher temperatures and is highly dependent on the circuit design. Although Rogers' high frequency materials have been used successfully in innumerable applications and reports of oxidation resulting in performance problems are extremely rare, Rogers recommends that the customer evaluate each material and design combination to determine fitness for use over the entire life of the end product.

AVAILABLE THICKNESS:		STANDARD PANEL SIZE:	STANDARD COPPER CLADDING:
0.015" (0.381mm)	0.125" (3.175mm)	18" X 12" (457 X 305mm)	½ (17µm), 1 oz (35µm), 2 oz. (70µm) electrodeposited copper foil. Heavy metal cladding available. Contact Rogers customer service.
0.020" (0.508mm)	0.150" (3.810mm)	18" X 24" (457 X 610mm)	
0.025" (0.635mm)	0.200" (5.080mm)		
0.030" (0.762mm)	0.250" (6.350mm)		
0.050" (1.270mm)	0.275" (6.985mm)		
0.060" (1.524mm)	0.300" (7.620mm)		
0.075" (1.905mm)	0.500" (12.70mm)		
0.100" (2.540mm)			

The information in this data sheet is intended to assist you in designing with Rogers' circuit material laminates. It is not intended to and does not create any warranties express or implied, including any warranty of merchantability or fitness for a particular purpose or that the results shown on this data sheet will be achieved by a user for a particular purpose. The user should determine the suitability of Rogers' circuit material laminates for each application.

These commodities, technology and software are exported from the United States in accordance with the Export Administration regulations. Diversion contrary to U.S. law prohibited.

TMM is a licensed trademark of Rogers Corporation.
©1991, 2002, 2005, 2006, 2008 Rogers Corporation, Printed in U.S.A. All rights reserved.
Revised 05/2008 0797-0508-0.5CC Publication #92-108